MICROSPHERE-MEDIATED CONTROL OF EMBRYOID BODY MICROENVIRONMENTS

A Dissertation
Presented to
The Academic Faculty

by

Richard L. Carpenedo

In Partial Fulfillment
of the Requirements for the Degree
Doctor of Philosophy in Bioengineering in the
Wallace H. Coulter Department of Biomedical Engineering

Georgia Institute of Technology
May 2010

MICROSPHERE-MEDIATED CONTROL OF EMBRYOID BODY MICROENVIRONMENTS

Approved by:

Dr. Todd McDevitt, Advisor
Department of Biomedical Engineering
Georgia Institute of Technology

Dr. Niren Murthy
Department of Biomedical Engineering
Georgia Institute of Technology

Dr. Ravi Bellamkonda
Department of Biomedical Engineering
Georgia Institute of Technology

Dr. Andrew Lyon
School of Chemistry
Georgia Institute of Technology

Dr. Michelle LaPlaca
Department of Biomedical Engineering
Georgia Institute of Technology

Dr. Steven Stice
Regenerative Bioscience Center
University of Georgia

Date Approved: March 25, 2010

To my family - Don, Ellen, Carolyn and Marilyn.

ACKNOWLEDGEMENTS

During the nearly six years I have spent in the Bioengineering program at Georgia Tech, I have learned an immeasurable amount about science, research, Atlanta, bacon and life. I have many people to thank for these numerous lessons.

First, I would like to thank the members of my committee – Dr. Todd McDevitt (my advisor), Dr. Ravi Bellamkonda, Dr. Michelle LaPlaca, Dr. Niren Murthy, Dr. Andrew Lyon, and Dr. Steve Stice. I owe the successes of my project as well as my development as a researcher in large part to their guidance and advice. I've known Dr. Bellamkonda the longest of anyone on my committee (including Todd). I first met Ravi when I was an undergraduate at Case Western Reserve University, where he was a professor at the time. I had Ravi as a professor for multiple courses and did undergrad research with a collaborator of his at Cleveland State. In the early days of the McDevitt lab, we relied strongly on the Bellamkonda lab (our next-door neighbors) for equipment and technical expertise, which reflects strongly on Ravi's generosity and sense of community. I think Ravi held me to a high standard because of how long he has known me, and for this I am truly grateful. Dr. LaPlaca has pushed me to work outside of my comfort zone and I thank her for helping me improve my project. Dr. Murthy and Todd have been trying to collaborate on a project since I started at Georgia Tech, with Niren's polymers and probes always working their way into my experiments. I'm sure one of these collaborations will be successful. I thank Niren for forcing me to look at the big picture of my project, and for letting me borrow his books. Dr. Lyon has helped me think about my work from the standpoint of a chemist rather than an engineer or biologist. For

this I am thankful, and I am sure Andrew's novel materials will be useful for future McDevitt lab research. Dr. Stice, from cross-state rival UGA, has been extremely gracious in serving on my committee. His vast knowledge of all things stem cells has been extremely helpful and I am appreciative of his input. While each member of my committee has been helpful and supportive, none has contributed as much to my development as my advisor, Todd.

When I started at Georgia Tech, I had a vague idea of the type of research I wanted to do, but nothing concrete. I had a list of faculty members that I wanted to meet and talk about projects with, but no one whose lab seemed like a perfect fit. During orientation, there were two new professors who were allowed to talk about their research interests in order to recruit grad students, one of whom was Todd. Todd's ideas struck me as interesting, so I decided to meet with him. Despite my misgivings about joining a start-up lab, Todd's enthusiasm and the novelty of his ideas were enough to sell me on joining his lab. While the process of building a lab from the ground up seemed like a hassle at the time, I am extremely glad that I joined Todd's lab. Todd has always put his students first, making time to meet with us no matter how busy he is. He was extremely patient during the first year or two, when we were all naïve and just getting acquainted with the field and academia in general. But he pushed us to work hard, critically assess our results, and publish our data. And his goading would have been moot had we not seen how hard he worked to make his lab what it is today. I cannot thank Todd enough for his support, encouragement and guidance throughout my entire time at Georgia Tech.

There are many individuals in the BME department, IBB and bioengineering program who deserve many thanks. The IBB core facility staff has been instrumental in

training and support for histology and microscopy equipment. In particular, Tracy Couse and Sha'Aqua Asberry in the histology lab, and Johnafel Crowe and Steve Woodard in the confocal labs have been extremely helpful and I owe them many thanks. Chris Ruffin has been tremendously supportive as an academic advisor in the bioengineering program. I would also like to thank the biomedical engineering academic advisors and financial staff, including Shannon Sullivan, Paul Fincannon, Penelope Pollard, and Sandra Wilson. Filling out paperwork accurately and punctually have never been strengths of mine, and these individuals have been very supportive and patient.

I would also like to acknowledge various professors and post-docs who contributed to my project. Dr. John McDonald was immensely generous in offering the use of equipment and expertise of his lab in the microarray studies performed in the course of my project. Dr. Nathan Bowen and Dr. Lilya Matyunina in the McDonald lab were very kind to assist in performing and analyzing this experiment. Dr. Taby Ahsan provided very helpful feedback during her time at Georgia Tech. As a new lab with no senior grad studies, it was greatly appreciated that Taby was kind enough to share her experience and perspective with us. Dr. Brani Vidakovic provided useful assistance in statistical analysis for various aspects of my research. Drs. Manu Platt, Evan Zamir, and Valeria Milam each provided useful comments through discussion or email exchanges during various stages of my project, and I am thankful for this input.

I recall hearing grad school described once as chronic, nagging pain – I believe it was being contrasted with medical school, which is more like acute pain. While I admit this seems like an apt analogy, the members of the McDevitt lab made the pain of grad school much more tolerable. Ima Ebong and I were the first students to officially join the

lab; Carolyn and Rekha (Dr. Rekha Nair, that is) joined shortly thereafter. Though Ima left after about three years, I am thankful for the time we spent together in lab, and for the enthusiasm and excitement she added to the lab. I have always been impressed with Rekha's work ethic. I think I could count the number of times I've gotten into lab before her on one hand (maybe two). Rekha's extensive knowledge of French has proven very useful for crossword puzzle purposes, and her excursions to India have provided the lab with a steady supply of Fenney. I admire Carolyn's ability to balance her lab work with other activities, like teaching at the CRC, training for triathlons, and commuting OTP. Carolyn has a penchant for being on the receiving end of my sarcastic comments but handles it very well, hopefully because she knows I'm kidding. Rekha and Carolyn have been instrumental in shaping the environment of the McDevitt lab; it is impossible to imagine what it would be like without them. Alyssa joined the lab during my second year and has proven to be a worthy addition, both on a scientific and social level. Alyssa has been a frequent golf partner for me over the years. I always get a little nervous when the men's and lady's tees are right next to each other, because then I have no excuse when she out-drives me. Alyssa and I also share an interest in Boston sports teams, particularly the Red Sox. I owe Alyssa many thanks for the occasional ride to or from lab, when it's either too cold, too rainy, or I've had one too many beers to bike. Andres joined the lab the following year when he became the second male graduate student in the lab. Andres and I have many common interests, including sports, the Sports Guy, crosswords, mustaches and follicle quantification. Andres brought a level of excitement to the lab, both socially and with respect to research. He is always willing to help out, learn a new technique, or share interesting articles. Barbara and Ken joined the lab after

Andres – I cannot recall if one joined before the other. When Ken first joined the lab, we went out to lunch at Nuevo Laredo, where Ken ate a rather ordinary size taco plate and proceeded to complain about being extremely full. I promptly told Ken he would not make it in the McDevitt lab. Ken has repeatedly proven me wrong by successfully completing eating challenges, including El Gigante (beef was a bad choice). Ken's not as fast an eater as Andres or me, but he makes up for it in heart. It is fitting that while Ken succumbed to the pressure to finish his enormous burrito, Barbara could not be pressured into even ordering a burrito. I admire Barbara's forthrightness as well as her ability to come up with nicknames that antagonize Alyssa. Melissa joined the lab next, and in doing so added to the tally of Boston sports fans. Melissa has displayed a strong work ethic during her time in the McDevitt lab, as well as a commitment to lab social events. Kirsten was the most recent grad student addition, and though her time in the lab will be brief, I am sure she will accomplish a great deal.

I would also like to thank Dr. Priya Baraniak, who was the first post-doc to join the lab. Priya has provided me with valuable feedback during group meetings, and though I cannot condone her loyalty to Duke and coach K, I am appreciative of her help. I am also thankful to the technicians in the McDevitt lab – Marissa Cooke and Jesse McClellan. In addition to being a skilled technician, Marissa has brought tremendous energy to the lab, as well as a sense of sarcasm that rivals (and potentially surpasses) my own. Jesse (aka 'W') has made valuable contributions in his brief time here as the McDevitt lab continues to expand. I would also like to thank Beth Krauth, who was the first technician to join the lab. Though Beth left the lab to take another job, she made many important contributions toward my project and to the lab in general.

Undergraduates have always played an important role in the McDevitt lab, and I would be remiss not to thank many of them here. Ross Marklein was the first undergrad I was charged with mentoring. Ross was there at the ground level, when I was still trying to figure out if my project would ever work. Ross helped me define my project, helped develop the techniques and analyses, and somehow left right as everything was starting to fall into place. Ross also contributed strongly to the social dynamic of the lab. You could not leave your laptop unattended while Ross was around, or else you were likely to have a new desktop background when you returned. Ross also instigated a number of eating contests, including the pickle challenge and the infamous eggnog chug. I owe Ross many thanks, and I wish him luck as he continues his education. I was fortunate to work with other talented undergraduates, including Scott Seaman. Scott continued in Ross's footsteps by conducting research that complimented my own project. Scott is also a talented baseball player who made a great ringer for our IM softball team. Scott was also a frequent golf partner – in fact, when Scott was in the lab, we could have put together a formidable team for a scramble. Other undergrads that I owe thanks include Courtney Scott, Ranni Tewfik, and Jonathan Kent, who was actually a high school student when I mentored him. Undergrads who I did not mentor were also memorable members of the McDevitt lab. Shreya Shukla was the first undergrad to join the lab, followed by Geoffrey Berguig, James Waring, and Luke Hiatt. I thank these undergrads for making the lab a fun environment in which to work. I also thank Geoff for letting me borrow his bike while he was in Spain.

While work has made up a significant portion of my time at Georgia Tech and in Atlanta, I have many friends to thank for distracting me from work. I have known Tom

Rafferty since my first week as an undergraduate. We moved to Atlanta at the same time, as he was staring at Emory when I started at Tech. We've been through a lot together, and I owe Tom a huge thank you for all his support. Many friends from my first few years at Georgia Tech have graduated and moved on, including Blaine Zern, Craig Duvall, Matt Rhyner, Sean Sullivan, Torrence Welch, John Wilson, the Baras, Katie Rafferty, and Tim Petrie. I am thankful for all the good times we've had in Atlanta, and will continue to have through fantasy sports, long email strings, conferences, etc. There are also many who have remained in Atlanta, or haven't quite graduated yet, including Scott Robinson, Angela Lin, Neal Weinrich, Brock Wester, Dave Dumbauld, Nick Willet, Jeremy Lim, Sean Coyer, Ed Phelps, Jay Sy, and Seth Gazes, and those who seem like they're just getting started, like Vince Fiore, Brent Uhrig, and Ted Lee. I am particularly thankful to my roommate (and landlord, I suppose) Scott. The bikes rides, Falcons games, scotch and sci-fi nights have been great distractions from the grind of research. You'll graduate someday, Scott. And also our Kirkwood neighbor Angela, with whom we organize various deep-fryer, lobster boil, or 5K events. Dave Dumbauld, who has been my workout partner for nearly a year now and golf partner for longer than that, has forced me to push myself or risk being surpassed. The fact that we cannot do cleans at the CRC anymore has really hurt Dave's chances of beating me in a Crossfit workout. I'd like to thank Vince for reminding me to look both ways before crossing the street, and Brent for reminding me that it's just a game.

Finally and most importantly, I'd like to thank my family for their unwavering support. My parents have always encouraged me to work hard and receive a strong education, and for this I am grateful. I would not have completed this dissertation were it

not for the values instilled in me by my parents, including patience, self-discipline, and inquisitiveness. My older sister Carolyn has always set a high standard to live up to. From Carolyn I've learned to push myself to do the best that I can. My Aunt Marilyn has always been an important part of my life, and I thank her for teaching me many lessons, including that dark chocolate and red wine are health foods. I owe many thanks to my extended family, including aunts, uncles and cousins, whose support and love have not been overlooked. Finally, I thank my grandparents, Sil, Cleo, Mario and Cassy, who I know would have been proud to read this dissertation.

TABLE OF CONTENTS

LIST OF FIGURES

LIST OF ABBREVIATIONS

BMP	Bone morphogenetic protein
CTR	CellTracker Red^{TM}
EB	Embryoid body
ECM	Extracellular matrix
ESC	Embryonic stem cell
HD	Hanging drop
ITS	Insulin, transferrin, and selenium-supplemented media
LIF	Leukemia inhibitory factor
MAD	Mode absolute deviation
MP	Microparticle
MS	Microsphere
PCR	Polymerase chain reaction
PLL	Poly(l-lysine)
RA	Retinoic acid
SAM	Significance analysis of microarrays
SEM	Scanning electron microscopy

SUMMARY

Embryonic stem cells (ESCs) hold great promise for treatment of degenerative disorders such as Parkinson's and Alzheimer's disease, diabetes, and cardiovascular disease. The ability of ESCs to differentiate to all somatic cell types suggests that they may serve as a robust cell source for production of differentiated cells for regenerative medicine and other cell-based therapeutics. In order for ESCs to be used effectively in clinical settings, efficient and reproducible differentiation to targeted cell types must be demonstrated. Methods to induce differentiation of ESCs typically involve culture in monolayer or formation of spheroids termed embryoid bodies (EBs). Monolayer culture is advantageous for the relatively uniform microenvironment that is presented to cells, but is limited in scalability, as surface attachment of cells is required. EB culture is performed in suspension, making it easily amenable to large-scale production. However, the complex and dynamic microenvironment inherent in EBs limits the efficiency of directed differentiation using this approach. A system capable of synergizing the uniformity of 2D culture with the scalability of 3D suspension culture is of great interest for the translation of stem cells into realizable therapies. The *overall objective* of this project was to engineer microenvironmental control over differentiating ESCs through the formation of EBs uniform in size and shape, and through the incorporation of morphogen-containing polymer microspheres within the interior of EBs. The *central hypothesis* was that morphogen delivery through incorporated polymer microspheres within a uniform population of EBs will induce controlled and uniform differentiation of ESCs.

Rotary suspension culture was developed in order to efficiently produce uniform EBs in high yield. ESCs aggregated into EBs with faster kinetics in rotary culture than in static suspension. Compared to static suspension culture, rotary suspension also significantly improved the production of differentiating cells and EBs over the course of 7 days, while simultaneously improving the homogeneity of EB size and shape compared to both hanging drop and static EBs. Differentiation assessment using quantitative PCR indicated that differentiation could be modulated through the use of rotary EB culture.

The diffusive transport properties of EBs formed via rotary suspension were investigated. The diffusion of a fluorescent, cell permeable dye was used to model the movement of small morphogenic molecules within EBs. Confocal microscopy demonstrated that the dye was not able to fully penetrate EB, and that the larger EBs at later time points (7 days) retarded dye movement to a greater extent than earlier EBs (days 2 and 4). Dye diffusion was further assessed by imaging cryosections of labeled EBs, which confirmed that dye is preferentially sequestered by cells at the periphery of EBs. Analysis of the fluorescence of dissociated EBs fortified the observed trend that later EBs (7 day) were labeled less efficiently than earlier EBs (2 or 4 days). Calculation of the percentage of cells at a given depth in EBs as a function of spheroid radius was performed, and matched well with experimental data.

Polymer microspheres capable of encapsulating morphogenic factors were incorporated into EBs in order to overcome the diffusional limitations of traditional soluble delivery. First, control over microsphere integration within EBs was demonstrated. The size of poly (lactic-co-glycolic acid) (PLGA) microspheres was observed to have an impact on incorporation, with smaller microspheres promoting

greater incorporation. The coating of microspheres with an adhesive protein also promoted incorporation, while coating with poly(lysine) did not encourage microsphere incorporation. Additionally, microsphere to cell ratio and rotary mixing speed were observed to impact integration of microspheres, with higher microsphere ratios and slower rotary speeds resulting in greater numbers of incorporated particles. Analysis of EB morphology as well as cell viability and differentiation demonstrated that the presence of microspheres did not significantly affect cells within EBs.

The use of microsphere-mediated delivery within EBs to direct cell differentiation was examined. Retinoic acid (RA), a small molecule morphogen commonly employed in ESC differentiation, was encapsulated in PLGA microspheres. The morphology of EBs containing RA microspheres (RA MS EBs) was assessed and compared to untreated EBs, EBs containing unloaded microspheres, and soluble RA treated EBs. RA MS EBs formed uniquely cystic spheroids with a visceral endoderm layer enveloping a pseudo-stratified columnar epithelium. Transcriptional analysis using microarrays indicated that RA MS EBs cultured for 10 days were in a differentiation state similar to the early primitive streak stage of mouse development. The organization of epiblast and endoderm cells was examined using immunostaining, and RA MS EB ultrastructure was analyzed with scanning electron microscopy; both of these analyses confirmed the primitive streak-like differentiation state of the EBs.

Finally, the continued differentiation of RA MS EBs in defined media conditions was assessed. RA MS EBs were transferred to regular serum, low serum, or serum-free media after 10 days of differentiation in regular serum media. The choice of media appeared to influence the germ lineage differentiation of the epiblast-like cells in RA MS

EBs. Gene expression demonstrated that regular serum enhanced endoderm induction, serum-free media supported ectoderm differentiation, while mesoderm was most prominent in untreated EBs in full serum.

In summary, this work has realized a unique approach for stem cell differentiation through modification of the internal microenvironment of ESC spheroids. This novel inside-out method toward engineering EBs demonstrated that the mode of morphogen delivery (soluble or microsphere-mediated) significantly affected the course of differentiation. These studies provide the basis for ongoing work, which will utilize the choice of microsphere material, coating, and morphogen in order to uniquely study mechanisms of ESC differentiation and achieve unparalleled engineering of the EB microenvironment.

CHAPTER 1

INTRODUCTION

Embryonic stem cells (ESCs) are derived from the inner cell mass during the blastocyst stage of development [1-4]. These cells are pluripotent, meaning they have the ability to differentiate into all somatic cell types from the three germ lineages (endoderm, mesoderm and ectoderm) as well as germ cells [1,5]. Because they are derived from one of the earliest developmental states, ESCs are commonly used to study embryology *in vitro*, particularly with human ESCs, as direct examination of human embryos is not possible [6,7]. The pluripotent nature of ESCs has also garnered attention as a potential cell source for tissue engineering and regenerative medicine [8], which seek to restore function of damaged cells and tissue through controlled assembly of cells, scaffolds, and/or growth factors [9-11]. A renewable source of cells, either terminally differentiated or multipotent progenitors, is required for successful implementation of cell-based therapeutics. The unique ability of ESCs to self-renew indefinitely *in vitro* and differentiate into all somatic cell types has made ESCs a potential cell-sourcing solution for tissue engineers. However, to be used successfully in therapeutic applications, particularly at a large scale, the differentiation of ESCs to desirable cell types must be controlled and efficient.

Differentiation of ESCs can be induced through a variety of techniques. The simplest differentiation protocols involve removal of serum and Leukemia inhibitory factor (LIF), a cytokine known to be essential for maintenance of mouse ESC pluripotency [12,13], from ESCs grown in monolayer. While this approach has been

shown to induce spontaneous ESC differentiation, particularly to neural cell types, cell survival is low and production of terminally differentiated cells is inefficient [14]. The addition of growth factors, cytokines, and other morphogens to ESCs in monolayer has been described in order to more efficiently direct ESC differentiation [15,16]. Co-culture of ESCs with stromal cells has also been reported in efforts to mimic specific cell niches and thereby induce specific differentiation events [17-19]. While both of these methods have been successful in improving the efficiency of differentiation to a given cell type, the scale of monolayer based approaches is inherently limited by surface area, as cell attachment is required.

Alternatively, ESCs can be induced to differentiate as three-dimensional spheroids termed embryoid bodies (EBs) [20]. Because EBs are cultured under suspension conditions, they are suitable for scalable production via large volume bioreactors. Additionally, the microenvironment within EBs more closely mimics the cell environment *in vivo*, which consists of complex interactions with cells, extracellular matrix (ECM), and secreted factors [21]. When grown in non-adhesive conditions, ESCs spontaneously aggregate into EBs; however, spontaneous aggregation of ESCs results in inefficient, heterogeneous EB formation as well as agglomeration of individual EBs into large, irregular masses. The lack of microenvironmental control over EBs grown under such conditions may contribute to the heterogeneity that is typically observed between EBs. Additionally, the three-dimensional nature of EBs suggests that gradients of oxygen, nutrients, and morphogenic factors may develop with EBs [22,23]. Compared to monolayer culture, in which all cells are exposed to the same environment and are in direct contact with the media, spheroid culture presents cells with a complex, dynamic

milieu which may hinder the effectiveness of directed differentiation strategies that rely on solely on supplementation of exogenous factors.

Strategies for ESC differentiation that utilize the scalability of EB culture while simultaneously harnessing the control and uniformity of monolayer culture are of great interest in filling a gap between basic stem cell science and translation to clinical applicability. Therefore, the *overall objective* of this project was to engineer microenvironmental control over differentiating ESCs through the formation of EBs uniform in size and shape, and through the incorporation of morphogen-containing polymer microspheres within the interior of EBs. The *central hypothesis* was that morphogen delivery through incorporated polymer microspheres within a uniform population of EBs will induce controlled and uniform differentiation of ESCs. The objective was accomplished by testing the central hypothesis through the following specific aims:

Specific Aim 1. Develop a system for promotion of homogeneous embryoid body production that can be utilized for the incorporation of polymer microspheres within EBs.

The working hypothesis was that gentle mixing conditions provided by rotary orbital culture would promote aggregation of ESCs as well as incorporation of microspheres within cell aggregates. This hypothesis was examined by first comparing rotary EB culture to hanging drop and static suspension culture, two established EB formation methods. The efficiency of formation, uniformity of size and shape, yield, and differentiation of rotary EBs were assessed and compared to static suspension and

hanging drop EBs. The incorporation of fluorescently-labeled polymer microspheres within EBs using rotary mixing was analyzed by fluorescent microscopy and spectroscopy. Control over incorporation was assessed as a function of adhesive coating, microsphere size, microsphere to cell seeding ratio, and orbital mixing speed. The effects of microsphere incorporation on EB morphology, viability, and differentiation were assessed for different size microspheres as well as different mixing ratios.

Specific Aim 2. Examine the diffusion of small, hydrophobic molecules into EBs formed under rotary suspension conditions.

The working hypothesis was that the diffusion of molecules into EBs would be limited by inherent barriers and that diffusion would decrease as a function of time. This hypothesis was examined by incubating EBs formed via rotary suspension in a fluorescent, cell permeable dye after 2, 4 and 7 days of differentiation. The diffusion of dye into EBs was analyzed using confocal imaging of whole EBs, fluorescent imaging of frozen EB sections, and fluorescent quantification of dissociated EBs. The diffusion in EBs was further assessed by creating an algorithm to calculate the percentage of cells at each radial distance within EBs as a function of EB size.

Specific Aim 3. Determine the *in vitro* differentiation of ESCs within EBs in response to microsphere mediated delivery of a morphogenic factor relative to soluble treatment.

The working hypothesis was that microsphere-mediated delivery of retinoic acid would enhance the uniformity of differentiation relative to soluble retinoic acid treatment. This

hypothesis was examined by incorporating RA-loaded microspheres within EBs using rotary mixing. Untreated EBs, EBs containing unloaded microspheres, and EBs treated with soluble RA were produced and compared to the RA-loaded microsphere EBs. Microspheres containing different levels of RA were examined, and EBs were treated with different concentrations of soluble RA. The morphology of differentiating EBs was assessed using hematoxylin and eosin staining. Gene expression in EBs was assessed using quantitative PCR as well as whole genome genechip microarrays. Embryoid body ultrastructure was examined using scanning electron microscopy, and protein expression was examined using immunostaining of whole, permeabilized EBs as well as EB sections.

Specific Aim 4. Evaluate the ability to direct differentiation of ESCs in EBs after treatment with retinoic acid microspheres into specific cell lineages using defined media and soluble morphogen treatment.

The working hypothesis was that EBs treated with RA microspheres would differentiate in a controlled manner in response to culture in defined media and exogenous morphogen supplementation. The rationale was that the cystic spheroids formed from RA microsphere treatment after 10 days of differentiation would be more susceptible to morphogen permeation than regular EBs. The hypothesis was examined by culturing RA microsphere EBs for 10 days in regular differentiation media prior to culture in either low serum or serum-free media supplemented with BMP4. Differentiation was assessed through quantitative PCR for analysis of gene expression, and immunostaining of whole EBs for protein expression.

This work is *significant* because it created a novel strategy to direct differentiation within EBs using controlled-release polymer microspheres. The use of rotary culture for production of uniform EBs in high yield and for incorporation of microspheres within EBs was established, providing a highly efficient and translatable system for EB formation. Diffusional limitations characterized within EBs demonstrated the need for engineered spatial control over morphogen presentation to cells within EBs. The ability to induce uniform differentiation within EBs through microsphere-mediated morphogen delivery demonstrated the effectiveness of inside-out engineering approach. This work is *innovative* because it utilized the scalability of 3D culture while seeking to impart the homogeneity of 2D culture conditions. This work was a unique fusion of the fields of stem cell biology and drug delivery that will have broader implications in fields such as biomaterials, tissue engineering and regenerative medicine.

CHAPTER 2

BACKGROUND

Embryonic Stem Cells

Embryonic stem cells (ESCs) are derived from the inner cell mass (ICM) of the pre-implantation blastocyst (embryonic day 3.5 in mice, 5-8 in humans) and have the unique ability to both self-renew indefinitely and differentiate into all somatic cells types [1-4]. The pluripotency, or ability to give rise to all three germ layers, of ESCs has made them an attractive source for cells that cannot easily be isolated or expanded *in vitro*. The capacity for ESCs to differentiate into cardiomyocytes, neurons, pancreatic β-cells, endothelial cells, chondrocytes and osteocytes has made these cells of interest to scientists and engineers studying and seeking to cure a breadth of diseases and disorders [1-5,24]. Applications such as cell-based therapeutics, *in vitro* drug screening and toxicology testing also require cells that can be provided via ESC differentiation [8,25,26]. Additionally, ESCs can be utilized to model embryonic development and processes such as gastrulation, tissue formation, and cell patterning [6,27-29]. The more recent derivation of induced pluripotent stem cells (iPS) from adult cell sources [30-32] provides intriguing new opportunities for these embryonic-like cells, such as studying mechanisms of various disorders at the cellular and molecular levels using iPS cells derived from afflicted donors [33-35].

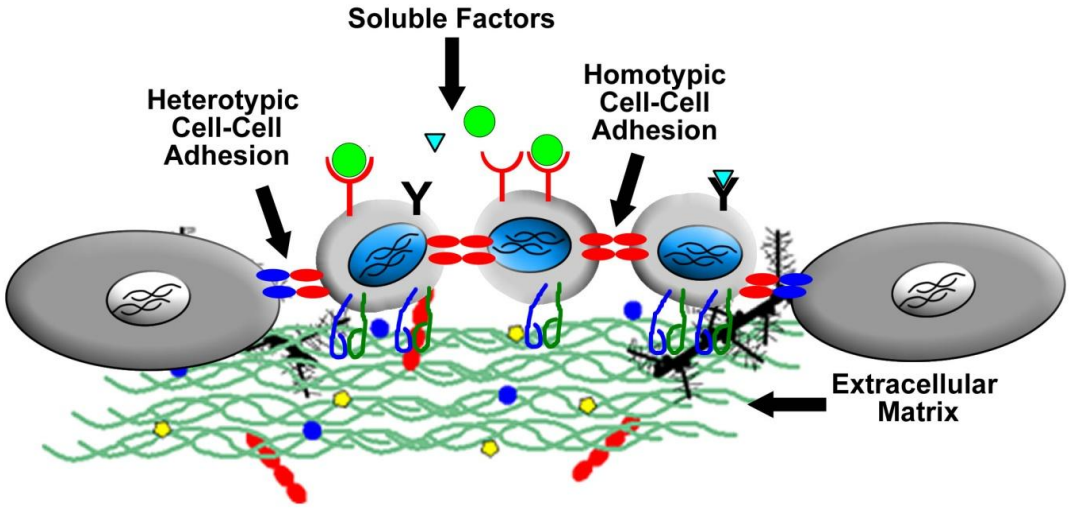

Figure 2.1. Microenvironmental factors affecting embryonic stem cell fate. Embryonic stem cell self-renewal and differentiation are influenced by homotypic and heterotypic cell-cell adhesions, soluble factors and the extracellular matrix. Modified from Carpenedo and McDevitt [36].

A variety of environmental factors contribute to cell fate decisions made by ESCs, including soluble factors, cell-cell adhesions (both homotypic and heterotypic), cell-extracellular matrix (ECM) adhesions, and mechanical forces (Figure 2.1) [37]. The integration of all these components determines whether an ESC self-renews to maintain pluripotency or differentiates. The specific pathways along which ESCs differentiate are also governed by these environmental influences. The exquisite sensitivity of ESCs to their microenvironment has made controlling their behavior a challenging endeavor. Typically, murine ESCs are maintained in a pluripotent state on mouse embryonic fibroblast (MEF) feeder cells or on gelatin-coated tissue culture plates supplemented with Leukemia inhibitory factor (LIF) [1,12,13,38,39]. Human ESCs cannot be maintained as pluripotent cells through LIF supplementation alone and are generally grown on MEFs [4,40]. Feeder-free hESC cultures can be maintained on Matrigel-coated surfaces grown in MEF-conditioned or bFGF-supplemented media [4,41]. Differentiation of ESCs can

be induced using a variety of methods, including monolayer culture [42], monolayer co-culture with various cell types [43], or through aggregation of ESCs into spheroids known as embryoid bodies (EBs) [20]. In the most basic differentiation protocols, LIF is removed from murine ESCs, and cells spontaneously differentiate [42]. Serum can be removed in order to induce cells to differentiate down what was termed the "default pathway" which is generally considered neuroectoderm differentiation [44], though it is unclear whether this notion is applicable in mouse or only in chick and Xenopus embryos[45]. The addition of growth factors, small molecules, and other morphogens to ESC monolayers has been studied in order to direct ESC differentiation toward specific cell types [15,16,46]. Co-cultures have been utilized in an attempt to recreate specific niches *in vitro* to provide instructive cues for ESC differentiation. Cells such as bone marrow stromal cells (including S17 [43,47] and PA6 [19,48] OP9 [17,18]) and END-2 cells (an embryonic carcinoma-derived visceral endoderm-like cell line) [49] have been shown to promote differentiation to hematopoietic cells, dopaminergic neurons, and osteoblasts, among others [17-19,43,47-49]. While monoculture and co-culture are frequently used for ESC differentiation, the aggregation of ESCs into EBs is a particularly common technique for the differentiation of mouse and human ESCs.

Embryoid bodies

Embryoid bodies are named for their likeness to post-implantation embryos. The morphogenic events in EBs mimic multiple aspects of the post-implantation mouse embryo, including primitive endoderm formation [38,50], germ layer differentiation [5,24], and epithelial to mesenchymal transition [51]. The process of cavitation in mouse

embryogenesis has also been examined using EBs [52-59]. The specific mechanism of cavitation in developing embryos and EBs is thought to be regulated by programmed cell death induced by factors secreted by visceral endoderm, and survival of cells based on basement membrane attachment [52,59]. The involvement of endoderm in cystic EB formation was implicated in studies in which EBs grown in HepG2 (a hepatocarcinoma-derived endoderm cell line) conditioned media formed cystic EBs that lacked an outer visceral endoderm layer [53,54,60]. Additionally, hedgehog [57,58] and FGF [55,56] signaling have been linked to EB cavitation.

Because EBs are grown in suspension, they are more suitable for large-scale culture than 2D cultures, which require surface attachment. EBs can be formed using a variety of techniques, including hanging drop [61], static suspension [1], semi-solid methylcellulose culture [62,63], and stirred-culture bioreactors [64-66]. Each system has specific advantages and disadvantages [20,62,67]; for example, hanging drop is relatively controlled, but not suitable for scale-up, while static suspension is simple and scalable, but not well controlled. Rotary suspension culture provides a middle ground between hanging drop and static suspension, in that it produces EBs uniform in size and shape, yet at a high yield [68]. Recently, forced aggregation methods using micropatterned well-inserts have been developed to efficiently produce uniform EBs in large quantities [69]. However, maintenance of such EBs may be problematic, as agglomeration can occur when EBs are transferred to large-batch suspension cultures [70].

The microenvironmental factors that dictate cell fate in EBs are similar to those for ESCs in general. Control of EB size, interactions with ECM, cell-cell interactions, and soluble factors all can be used to direct differentiation within EBs [21] (Figure 2.2).

EB size control has been accomplished through a variety of methods, including stirred suspension [68,71,72], utilization of patterned microwells [73,74], and forced aggregation [69,75]. The size of EBs has been reported to play a role in specifying differentiation trajectory [72,76]. Encapsulation of EBs in ECM hydrogels has been performed in order to manipulate cell-ECM interactions [77-79]. Cell-cell interactions are critical for EB differentiation, as E-Cadherin mutants are unable to form EBs [80]. Directed differentiation of EBs is most commonly accomplished through addition of soluble factors to the culture media. Growth factors such vascular endothelial growth factor (VEGF) [81,82], brain derived neurotrophic factor (BDNF) [83], basic fibroblast growth factor (bFGF) [84], epidermal growth factor (EGF) [85], and platelet derived growth factor (PDGF) [85] have been studied in the context of EB differentiation. Other morphogens such as bone morphogenetic proteins (BMPs) [86], Wnts [87] and retinoic acid [88-90] have also been assessed for directed EB differentiation. Due to its potenct effects on ESC differentiation, retinoic acid is one of the more commonly employed morphogens for induction of ESC differentiation.

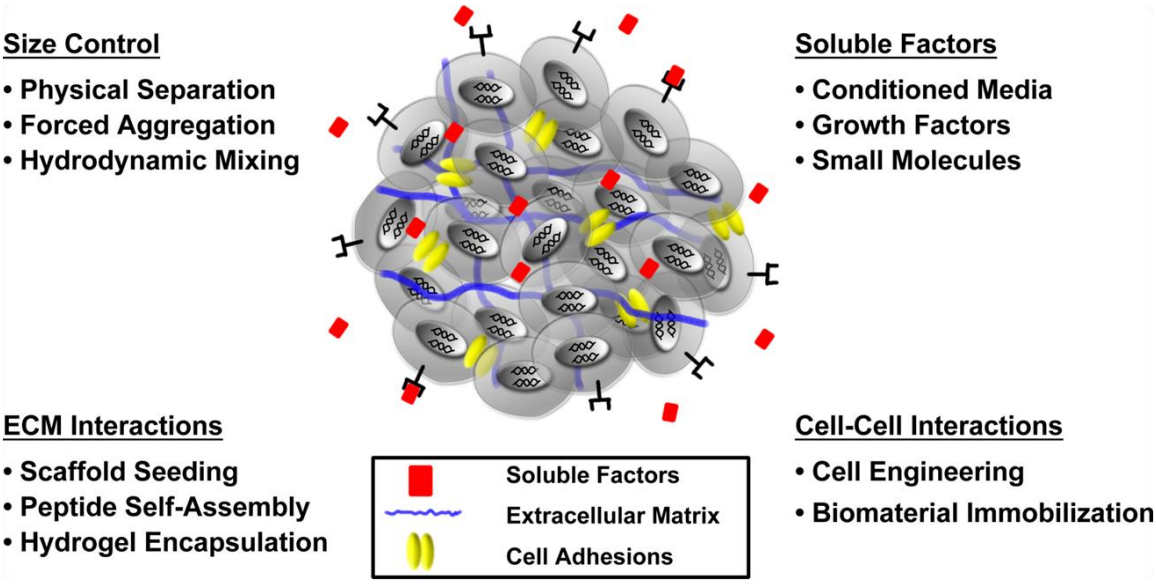

Figure 2.2. Environmental factors that influence EB differentiation. Embryoid body differentiation is influenced by variety of factors comprising the intercellular cell microenvironment. The size of the EB, soluble factor signaling, ECM interactions and cell-cell interactions can all influence ESC commitment. General strategies to control the different elements of the EB microenvironment are listed for each. Adapted from Bratt-Leal, Carpenedo, and McDevitt [21].

Retinoic acid effects on ESC differentiation

Retinoic acid (RA) is a derivative of retinol (vitamin A) capable of inducing potent morphogenic activity during embryological development and adult tissue regeneration [91-95]. All-*trans* RA is trafficked from the cytoplasm to the nucleus by cellular retinoic acid binding protein 2 (CRABP2) [96], and once it enters the nucleus, all-*trans* RA binds to the retinoic acid receptor (RAR), which then forms a heterodimer with the retinoid X receptor (RXR). The RAR/RXR complex binds specifically to retinoic acid response elements (RAREs) within promoter regions to regulate gene expression [97]. RA signaling has been reported to target over 500 genes [98], some of which are critical in the early stages of the developing embryo, including the Oct4 promoter [99] and the Hox family of homeobox genes [100-103]. Responsiveness to RA

in the developing embryo is controlled by precise localization of the ligand [104]. The majority of reports indicate that RA treatment induces neural differentiation when introduced to differentiating EBs at early time points and in high concentrations [88,89,105,106]. High RA concentration (0.5 μM) has been shown to increase expression of neural markers (Wnt-1, Mash-1) and decrease mesodermal marker (brachyury, zeta globin) expression [88]. Expression of neural markers appears to be concentration dependant, with high RA concentration inducing a more caudal phenotype, while lower RA concentrations produce cells with rostral identity [89,107]. Timing is also important for neural development from retinoid signaling, as the order of RAR activation in the signaling pathway influences the type of neural cells produced from neural progenitors [108]. While RA induced neurogenesis is common, heterogeneity of differentiation is still high, as neural yields are typically 40% [109] and mesoderm and endoderm markers are still expressed [88,89], and in some cases, upregulated [106]. In addition, a few reports have shown that when introduced in low concentrations after day 4, cardiomyocyte differentiation can be induced [110,111]. Retinoic acid has also been shown to increase the frequency of EBs containing adipocytes [112] as well as pancreatic β-cells [46,113]. Treatment of human ESCs with RA has been reported to induce formation of polarized, non-neural ectoderm [114-116]. The RA induced differentiation to keratin 14 and 18 positive epithelium was dependent on the presence of BMP signaling. The effect of RA on differentiation is further complicated when co-factors such as serum [106,117] and beta-catenin signaling [118] are taken into account. Thus, RA appears to be important in early embryonic development and the timing and

concentration of its delivery to differentiating ESCs are critical in controlling the fate of the cells.

Transport in Multicellular Spheroids

Multicellular spheroids have often been investigated *in vitro* to determine the efficacy of cancer tumor therapies, as developmental biology models for embryogenesis, and as engineered tissue constructs [6,119,120]. Multicellular spheroids, such as EBs, pose unique challenges for uniform delivery of signaling molecules to cells *in vitro* due to their inherent 3D structure. Depending on transport conditions, such as the physical-chemical characteristics and diffusion properties of the molecule(s) being examined and spheroid size and permeability, severe limitations may be imposed on the soluble delivery of factors from the outside of cellular aggregates [121-125]. This can create a non-uniform distribution of molecules within the multicellular spheroid environment, which in turn can result in divergent cellular behaviors. For example, 3D aggregation of cancer cells confers a difference in drug resistance depending on the spatial location of cells within the spheroid [126,127]. Previous work analyzing the tight junctions of cells within differentiating EBs has demonstrated that the epithelial layer that typically forms on the outer surface of the EB can act as a barrier to the diffusion of small molecules (10^{2-3} Da) from the extracellular environment to the inner microenvironment of the EB [128,129]. Studies using EBs as a model for angiogenesis indicate that the diffusion of small molecules in EBs is limited in non-vascularized EBs compared to EBs containing primitive vasculature [23,130]. This suggests that studies examining the effects of soluble biomolecules on differentiating EBs are limited by the fact that not all of the cells

within the cellular aggregate are exposed to treatment in a consistent or uniform fashion. The permeability barrier at the surface of the EBs likely results in a radial gradient of biomolecule delivery such that cells may be exposed to heterogeneous concentrations of a soluble differentiation factor depending on their spatial location within an EB. The heterogeneity in molecular presentation to the cells may contribute to the heterogeneous cell differentiation commonly observed.

Engineering Stem Cell Environments

Recently, biomaterials have attracted considerable attention as a means to engineer control of the stem cell microenvironment in order to manipulate stem cell self-renewal and differentiation [131-134]. High-throughput fabrication of acrylate-based polymers co-polymerized from 25 different monomers deposited on glass slides were used to screen substrates capable of supporting ESC adhesion and directing differentiation [135]. Polymer compositions differed in their ability to support cell growth and attachment, as well as ESC differentiation to various phenotypes, demonstrating that material properties alone can influence stem cell fate decisions. Phage display technology has been applied to screen peptide sequences that support cell adhesion and growth [136]. Similarly, arrays of complex extracellular matrices composed of various mixtures of collagen I, collagen III, collagen IV, fibronectin, and laminin and various soluble morphogenic factors (Wnt3a, BMP4, Activin A, Fgf4), have been used to screen the differentiated phenotypes of ESCs in a high-throughput manner in 2D [137,138]. Although planar high-throughput assays enable efficient screening of numerous, combinatorial environments, they fail to adequately recapitulate the native structure of developing

tissues. The influence of biomaterials on stem cell differentiation has also been extended into 3D environments. Simply varying the functional group chemistry of small molecules tethered to hydrogels was shown to induce various differentiation responses of encapsulated human mesenchymal stem cells (hMSCs) [139], though the mechanism remains unclear. Environments that support hMSC viability and differentiation have been studied as a function of degradability, cell adhesion ligand, and ligand density [140]. Embryonic stem cell self-renewal has been shown to be supported in alginic acid/gelatin hydrogels [141], as well as hydrogels composed of poly(N-isopropylacrylamide-co-acrylic acid) semi-interpenetrating polymer networks [142]. Differentiation of ESCs encapsulated in a variety of hydrogels has also been reported. PEG-based hydrogels, in combination with soluble factors, have been utilized to induce chrondrogenic differentiation of ESCs [143,144], as have alginate-based scaffolds [145]. Alginate hydrogels have been shown to support differentiation of ESCs in a concentration dependent manner, with higher concentrations inhibiting the formation of cystic EBs [146]. Hyaluronic acid (HA) hydrogels have also been used to support both self-renewal and differentiation of human ESCs [78]. hESCs were maintained in an undifferentiated state in HA hydrogels cultured in mouse embryonic fibroblast (MEF) conditioned media, whereas culture in media containing VEGF was shown to induce differentiation suggestive of angiogenesis. Altogether, this literature suggests that biomaterials can be used to support the growth and differentiation of ESCs and that material properties may play a key role in directing stem cell fate.

Degradable Microsphere-mediated Drug Delivery

Degradable polymer microspheres are a well-established means to safely deliver encapsulated molecules to cells and tissues in a controlled manner [147]. The release profile characteristics of the materials can be controlled by parameters such as the type of polymer(s) and formulation methods used, the size, morphology and crystallinity of the particles, and the amount and distribution of the encapsulated molecule(s) to be delivered by the microspheres. The physical-chemical properties of polymeric microspheres related to release characteristics and the biocompatibility of such materials have been thoroughly studied [147,148]. Microsphere delivery vehicles have frequently been employed *in vivo* as an alternative to systemic drug therapies to treat diseases such as cancers of the head and neck, brain tumors and retinopathies by releasing a therapeutic compound, such as retinoic acid (RA) [149-151]; for cancer treatments, RA delivery is referred to as differentiation therapy. Microspheres engineered to be roughly the same size as cells (1-10 μm) can be physically mixed with cells and incorporated into cellular microenvironments. For example, PLGA microspheres have been investigated as degradable transplantation vehicles for a number of different cell types, including various stem cells, for *in situ* tissue engineering applications [152-155]. Not only can the particles serve as a temporary adhesive substrate to promote cell survival *in vivo*, but they can also simultaneously deliver encapsulated molecules, such as morphogens, in the immediate vicinity of the transplanted cells [156-159]. These studies show that degradable microspheres incorporating instructive cues can be integrated directly into 3D cell environments to control cell function and perhaps differentiation.

CHAPTER 3
ROTARY SUSPENSION CULTURE FOR PRODUCTION OF UNIFORM EMBRYOID BODIES*

Introduction

Embryonic stem (ES) cells have the ability to differentiate into all somatic cell types [2-4], enabling them to serve as a potent cell source for tissue engineering and regenerative medicine applications, as well as an *in vitro* model system to study early embryonic development. Differentiation of mouse and human ES cells can be induced in a variety of manners, but the most common technique is via formation of cell aggregates in non-adherent spheroids referred to as embryoid bodies (EBs) [1,5,20]. The molecular and cellular morphogenic signals and events within EBs recapitulate many aspects of the developing embryo, including differentiation to cells of endoderm, mesoderm, and ectoderm lineages, similar to gastrulation in vivo [24,52]. Embryoid bodies generally develop an outer layer of primitive endoderm that envelops a core of differentiating cells that take on a cystic appearance [52]. The precise number and spatial coordination of the various cell-cell interactions involved in EB formation are thought to influence the course of ES cell differentiation, and as a result, controlling cell number and size of EBs may be an important step in directed differentiation strategies [69,74].

Two techniques typically employed for EB formation are hanging drop and static suspension culture [20]. The hanging drop method, in which cells are dispersed in 15-20

---

*Modified from:
RL Carpenedo, CY Sargent, TC McDevitt. *Rotary Suspension Culture Enhances the Efficiency, Yield, and Homogeneity of Embryoid Body Differentiation.*. Stem Cells, 2007, 25(9): 2224-2232.

μL drops suspended from the lid of a Petri dish, has been used to more precisely control the microenvironment for EB formation and differentiation [61,160,161]. Since EBs formed in each drop are physically separated, individual EBs are not able to agglomerate, allowing production of a fairly homogeneous final population of EBs. This method, however, is not practical for large-scale applications, as each drop generally yields only one EB, and a typical 100 mm Petri dish can only accommodate approximately 100 drops. Suspension culture, on the other hand, can be used to produce EBs in larger quantities (100's-1000's) by simply inoculating ES cells in differentiation media at a density of $10^{4\text{-}6}$ cells/mL on a non-adherent surface, whereupon the cells spontaneously aggregate into spheroids. While this method can be used to produce a larger number of EBs and differentiated cells than hanging drops, it offers little control over the size and shape of EBs, and often results in agglomeration of EBs into large, irregular masses. Currently, there are no techniques for laboratory-scale production of EBs that offer a satisfactory compromise between the controlled environment of hanging drops and the ease of producing large quantities of EBs by suspension culture methods.

Recently, spinner-flask, slow turning lateral vessel (STLV), and high aspect rotating vessel (HARV) bioreactors have been used for larger-scale production of EBs [64-66,162-165]. The agitation provided by bioreactors improves circulation of nutrients and cell waste products, but can also be manipulated to control cell aggregation [166-168]. As a result, certain bioreactors have been shown to produce a controlled environment for EB formation and differentiation. While such approaches may provide a more uniform differentiation environment capable of sustaining increased EB and differentiated cell yield, bioreactors may not be practical solutions for many researchers

examining multiple experimental samples in parallel. For example, the relatively large volume of even the smallest common bioreactors (typically > 100 mL / bioreactor) makes conducting screening studies of various media compositions much more laborious and expensive for researchers studying basic mechanisms of ES cell differentiation. Thus, an improved method for simple, laboratory-scale EB differentiation capable of mimicking the beneficial attributes of larger volume bioreactors would be useful to many stem cell researchers.

Orbital rotary shakers have been used to create spheroids from cell types such as tumor cells [169,170], hepatocytes [171], neural stem cells [156], and fetal brain cells [172] since the constant circular motion provided by this simple system generally increases the efficiency of spheroid formation. Multiple cell culture dishes can be accommodated on the rotary platform, easily allowing production of numerous parallel samples and comparison of different experimental parameters. Although horizontal rotation of mouse ES cells has been noted qualitatively to improve the homogeneity and reproducibility of EB formation [173], a quantitative characterization of the effects of rotary culture in comparison to hanging drop and static suspension EB culture methods has not been previously described. In this study, differences in the formation efficiency, homogeneity, yield and differentiation of suspension EBs formed by hanging drop, static and rotary conditions were directly compared. EBs initiated on a rotary orbital shaker formed more efficiently, demonstrated higher cell and EB yield, and exhibited improved homogeneity of size and shape compared to EBs formed in static suspension conditions. In addition, rotary EBs appeared to differentiate more efficiently than static suspension cultures based on morphological appearance and gene expression profile patterns. These

results suggest that rotary suspension culture is a simple, yet significantly better method than hanging drop and static suspension culture for EB formation and differentiation.

Methods

Embryonic stem cell culture

Murine embryonic stem cells (D3) [1] (passages 23-32) were maintained in an undifferentiated state on tissue culture dishes coated with 0.67% gelatin in Dulbecco's modified Eagle's medium (DMEM) (Mediatech Inc., Herndon, VA, http://www.cellgro.com), supplemented with 15 % fetal bovine serum (FBS) (Hyclone, Logan, UT, http://www.hyclone.com), 2mM L-glutamine (Mediatech), 100 U/mL penicillin, 100 μg/mL streptomyocin, and 0.25 μg/mL amphotericin (Mediatech), 1x MEM nonessential amino acid solution (Mediatech), 0.1 mM 2-mercaptoethanol (Fisher Chemical, Fairlawn, NJ, http://www.fishersci.com), and 10^3 U/mL leukemia inhibitory factor (LIF, Chemicon International, Temecula, CA, http://www.chemicon.com). Cells were routinely passaged every 2-3 days prior to reaching 70% confluence.

Embryoid body formation

Undifferentiated ES cells were dissociated from monolayer culture with a 0.05% trypsin-EDTA solution (Mediatech) to obtain a single cell suspension. Suspension cultures of embryoid bodies were initiated by resuspending 4 x 10^5 cells/mL in differentiation media, consisting of undifferentiated growth media without LIF. Static and rotary suspension cultures were cultivated in sterile 100x15 mm non-tissue culture treated polystyrene (i.e. bacteriological grade) Petri dishes (Becton Dickinson

Biosciences, San Jose, CA, http://www.bdbiosciences.com) with a final volume of 10 mL of differentiation media. Rotary suspension culture EBs were initiated by placing dishes on an orbital rotary shaker (Lab-Line Lab Rotator, Barnstead International, Dubuque, IA, http://www.barnsteadthermolyne.com) set at approximately 40 rotations per minute, except during studies in which rotary speeds of 25 and 55 rpm were also examined. Embryoid bodies were maintained for up to 7 days in suspension, with media changed every one to two days by allowing EBs to sediment in 15 mL centrifuge tubes, aspirating the old media, and resuspending in fresh media. Hanging drop EBs were prepared by suspending $4x10^4$ cells/mL in differentiation media in 15 µl drops on the lids of a 100x15 mm square Petri dishes, with ~72 drops/plate. This concentration and volume (resulting in ~600 cells/drop) were chosen because lower concentrations resulted in inefficient production of EBs (i.e. many drops do not produce an EB) and higher concentrations often resulted in formation of multiple EBs per drop.

Efficiency of embryoid body formation

The efficiency of formation for static and rotary EBs was determined by quantifying the percent of total cells that incorporated into EBs, as opposed to cells that remained free in suspension, or adhered to the culture dish. After 6 and 12 hours, static and rotary suspension cultures were passed through a 40 µm cell strainer in order to separate cell aggregates constituting primitive EBs from individual cells. The cell strainer was rinsed 5 times with 1.0 mL of PBS and the suspension of individual cells that readily passed through the cell strainer was centrifuged at 1000 rpm for 5 minutes to pellet the cells. The supernatant was aspirated and the cells were re-suspended in 1.0 mL

of PBS. EBs trapped in the cell strainer were collected by inverting the strainer over a 50 mL centrifuge tube and rinsing thoroughly with PBS to dislodge the EBs. The EBs were allowed to sediment by gravity, and the supernatant was aspirated. The EB pellet was rinsed once with 5.0 mL PBS and the supernatant was again aspirated after the EBs settled. The EBs were trypsinized for 5 minutes at 37 °C in 0.05% trypsin-EDTA and neutralized with an equal volume of culture media. In addition, the cells attached to the culture dish were rinsed with PBS and trypsinized. The three fractions of cells (cells incorporated into EBs, individual cells in suspension, and adherent cells attached to the culture dish) were quantified using a Coulter Multisizer III with a 100 μm aperture (Beckman Coulter Inc., Fullerton, CA, http://www.beckmancoulter.com). The total number of cells was calculated from the sum of the three cell fractions and used to determine the percentage of cells in each fraction.

Yield of embryoid bodies and cells

Embryoid body and differentiating cell yield were assessed by directly counting individual EBs and dissociated cells from EBs in separate parallel samples. Static and rotary EBs were collected by gravity sedimentation, the excess media was aspirated and EBs were suspended in 2.0 mL of a 60:40 solution of Isoton II (Beckman Coulter):glycerol (Fisher Chemical). Triplicate samples of this solution were each added to 150 mL of Isoton/glycerol solution and counted using a Coulter Multisizer III equipped with a 2000 μm aperture. The total number of EBs present was calculated based on this count, taking the appropriate dilution factor into account. The total number of cells within EBs was determined by dissociating the EBs with 0.25% trypsin-EDTA

(Mediatech) and counting the cells present with a 100 μm aperture Coulter counter, as described above (higher trypsin concentration was used in this study than in previous studies to more efficiently dissociate EBs).

Live/Dead assay

Static and rotary EBs were formed as described above, and after 2, 4, and 7 days of differentiation, cell viability was assessed using LIVE/DEAD® staining (Molecular Probes Inc., Eugene, OR, http://probes.invitrogen.com). Samples were incubated in serum-free, phenol red free media containing 1μM calcein AM and 2μM ethidium homodimer I at room temperature for 30 minutes. EBs were then washed three times with PBS, resuspended in fresh PBS, transferred to 6-well plates and immediately imaged using fluorescent microscopy.

BrdU assay

Cell proliferation was assessed using immunostaining for 5-bromo-2'-deoxyuridine (BrdU) incorporated into cells synthesizing DNA. After 2 and 5 days of suspension culture, static and rotary EBs were pulsed with 10 μM BrdU (Molecular Probes) for 6 hours. EBs were then washed twice with PBS, fixed in 10% formalin for 30 minutes, washed three times in PBS, and resuspended in HistoGel (Richard-Allan Scientific, Kalamazoo, MI, http://www.rallansci.com). Fixed samples were dehydrated in a series of graduated alcohol solutions (70-100%) and xylene, embedded in paraffin, and 5 μm paraffin sections were cut using a rotary microtome. Sections were deparaffinized, and antigen retrieval was performed by incubating slides in 1.5 N HCl for

15 minutes at 37°C followed by two 5 minute rinses in 0.1 M Borax buffer (pH 8.5). Slides were incubated for 30 minutes in blocking buffer (2% goat serum, 0.05% Triton X in PBS), followed by a two hour incubation with peroxidase-conjugated anti-BrdU antibody (1:50 dilution, Roche Applied Science, Indianapolis, IN, http://www.roche-applied-sceince.com). Slides were then washed three times in PBS prior to colorimetric development of diaminobenzidine (DAB, Vector Laboratories, Burlingame, CA, http://www.vectorlabs.com). Nuclei were counterstained with hematoxylin and slides were coverslipped.

TUNEL assay

Apoptotic cells in static and rotary EBs were detected using a terminal transferase dUTP nick end labeling (TUNEL) assay. After 4 and 7 days of suspension culture, static and rotary EBs were fixed in 10% formalin for 30 minutes, washed three times with PBS, and resuspended in HistoGel. Fixed samples were processed and embedded as described above, and 5 μm paraffin sections were cut using a rotary microtome. Apoptotic cells were identified using the DeadEnd™ colorimetric TUNEL system (Promega Corporation, Madison, WI, http://www.promega.com). Briefly, sections were deparaffinized in xylene, rehydrated in graded ethanol washes and rinsed in PBS. Sections were permeabilized in proteinase K solution and then incubated in buffer containing biotinylated nucleotide mix and recombinant terminal deoxynucleotidyl transferase (rTNT). A streptavidin horseradish peroxidase solution was then added to bind to biotinylated nucleotides incorporated into the DNA of apoptotic cells. The DAB

substrate was then added for colorimetric development to stain apoptotic cell nuclei brown, and cell nuclei were counterstained blue with hematoxylin.

Morphometric analysis

Phase images of EBs were acquired daily during the course of hanging drop, static and rotary culture with a Nikon TE 2000 (Nikon Inc., Melville, NY, http://www.nikonusa.com) inverted microscope with a SpotFLEX camera (Diagnostic Instruments, Inc., Sterling Heights, MI, http://www.diaginc.com). EBs were analyzed using ImageJ image analysis software (http://rsb.info.nih.gov/ij) to measure cross-sectional area and perimeter and calculate circularity (defined as 4π x [Area/Perimeter^2]) of static and rotary EB samples for at least 100 EBs from each sample (n=3). Hanging drop EBs were analyzed by transferring 2 plates of hanging drop EBs (roughly 100 EBs) into suspension immediately before imaging. Histogram plots of area and circularity values were generated with equal numbers of static and rotary EBs divided into 30 equally sized bins (due to the lower number of hanging drop EBs present, only 12 bins were used for hanging drop area analysis). The fraction of EBs within each bin was plotted versus the upper bin limit for both area and circularity. Mode absolute deviation (MAD) for area plot analysis was calculated for static and rotary EBs at each day as the sum of the absolute difference between each area value and modal area value divided by the total number of data points for the 95% least deviant values.

Histology

Embryoid bodies were formed as described above, and after 2, 4, and 7 days of culture, samples were harvested for histological examination. Samples were fixed in 10% formalin for 30 minutes, and were processed, embedded and sectioned as described above. Slides were then stained with hematoxylin and eosin (H&E) and imaged with a Nikon Eclipse 80i microscope equipped with a SpotFLEX camera (Diagnostic Instruments).

Reverse-transcription polymerase chain reaction analysis

RNA was extracted from undifferentiated ES cells on day 0 and from hanging drop, static and rotary EBs on days 2, 4, and 7 using the RNeasy Mini kit (Qiagen Incorporated, Valencia, CA, http://www.qiagen.com). Reverse transcription for complementary DNA synthesis was performed with 1 μg of RNA per sample using the iScript cDNA synthesis kit (Bio-Rad, Hercules, CA, http://www.bio-rad.com), and real-time PCR was performed with SYBR green technology on the MyiQ cycler (Bio-Rad). Forward and reverse primers for Oct-4, Nanog, Brachyury-T (B-T), nestin, α-fetoprotein (AFP), and glyceraldhyde-3-phosphate-dehydrogenase (GAPDH) were designed with Beacon Designer software, purchased from Invitrogen and validated with appropriate controls. Oct-4 and Nanog relative gene expression were quantified as compared to undifferentiated ES cell expression levels using the Pfaffl method of quantification [174]. Brachyury-T, nestin, and AFP concentrations were calculated using standard curves and normalized to GAPDH expression levels.

Statistical analysis

All experimental samples were analyzed in triplicate, with data presented as mean ± standard deviation. Statistical significance was determined using Student's t-tests with a significance level of $p<0.05$.

Results

Time course of embryoid body formation

Static and rotary suspension cultures were initiated with equal numbers of cells ($4x10^5$ cells/mL), and hanging drop EBs were formed with ~600 cells/drop ($4x10^4$ cells/mL). Rotary cultures formed regular, spherical EBs after 2 days, whereas static EBs appeared smaller and formed less defined cell aggregates (Figure 3.1A). At the same time point, EBs formed in hanging drops appeared similar in shape to rotary EBs, yet slightly larger in diameter (~250 μm diameter for hanging drop, compared to ~190 μm diameter for rotary). By day 4, hanging drop EBs increased in size (~500 μm diameter) and remained largely uniform in shape, though some irregularly shaped EBs were present. Static cultures formed small, spherical EBs, as well as larger, irregularly shaped aggregates of individual EBs. Rotary EBs at day 4 were larger than at day 2 (~250 μm), but remained regular and spherical with no appearance of agglomeration. Day 7 hanging drop EBs increased slightly in size from day 4 (~625 μm), and static cultures showed fewer small spherical EBs than at day 4, as well as many more large agglomerates of

multiple EBs. Rotary EBs at day 7 were larger in size than at day 4 (~290 μm) and remained largely spherical and uniform in appearance. Higher magnification of EBs revealed that hanging drop and rotary EBs at 4 and 7 days of suspension culture exhibited a smooth, primitive endoderm-looking cell layer at the periphery of most EBs, whereas static EBs displayed a more irregular layer of cells at the edges of the EBs (Figure 3.1A, insets).

Influence of rotary speed on embryoid body size

To study the effect of rotary speed on EB formation, $4x10^5$ cells/mL were inoculated in dishes placed on orbital shakers at 25, 40 or 55 rpm and observed using phase contrast microscopy (Figure 3.1C). By day 2, EBs formed on rotary shakers at 25 rpm were quite large, roughly 400 μm in diameter (406 ± 64 μm). In addition, fewer total EBs were present in 25 rpm EBs than at 40 or 55 rpm, as counts of EBs sampled from each population indicated that roughly 10x more EBs were present at 40 rpm than 25 rpm. After 2 days, EBs formed at 55 rpm were smaller and appeared to have more free cells not incorporated into EBs than either 25 or 40 rpm samples (Figure 3.1C). These trends persisted throughout 7 days of suspension culture, with 25 rpm rotary motion producing the largest and fewest EBs, and the 55 rpm shaker yielding the smallest EBs and a higher proportion of free cells in suspension. Because of the relatively large number of EBs obtained compared to 25 rpm, and the more efficient formation of EBs (indicated by fewer individual cells remaining in suspension) compared to 55 rpm, 40 rpm was used as the rotary speed for all of the subsequent characterization experiments for this study.

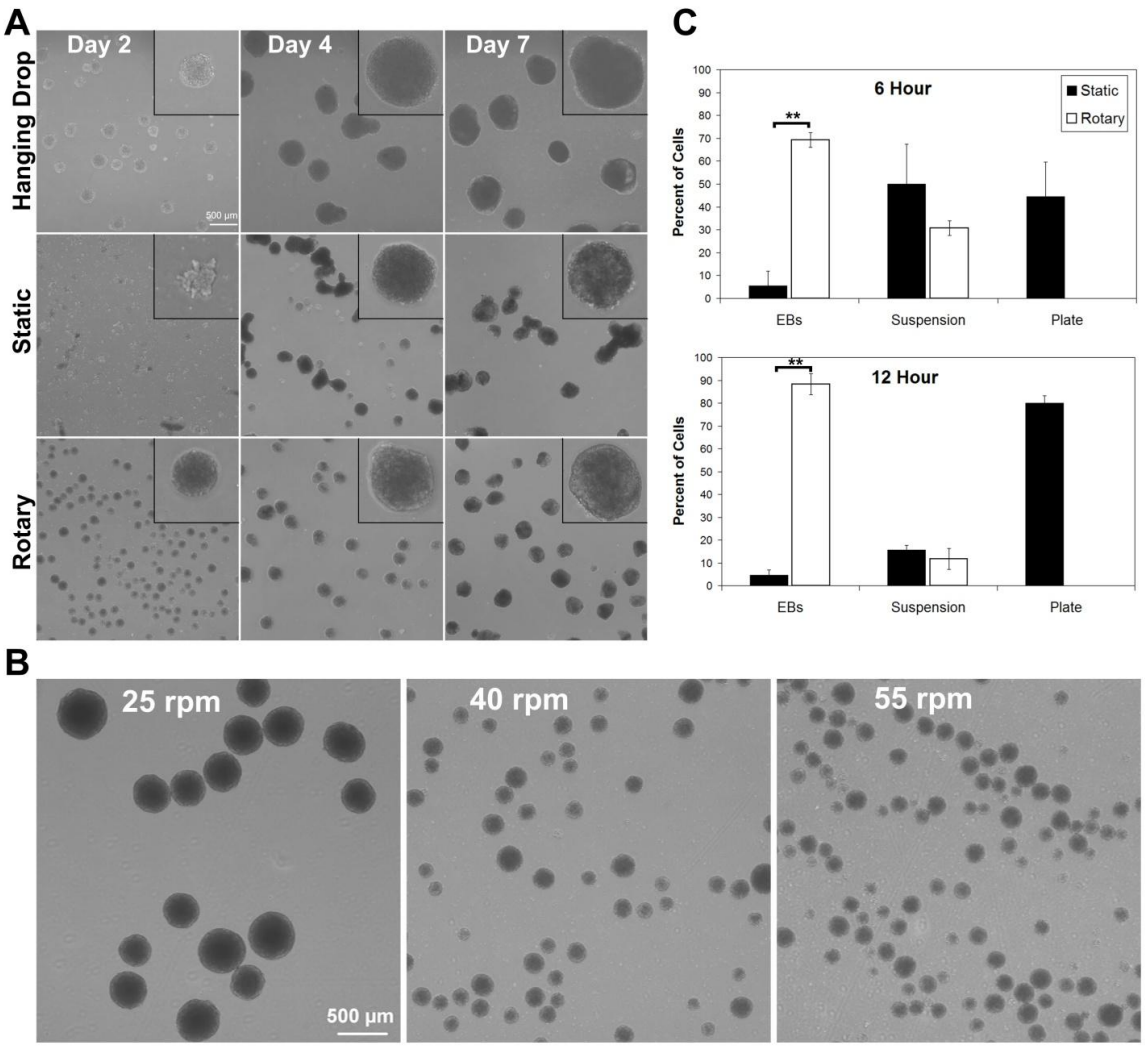

Figure 3.1. Time course of embryoid body formation for hanging drop, static and rotary suspension conditions. A) Hanging drop and rotary EBs formed by day 2 and increased in size at days 4 and 7 while showing minimal signs of agglomeration. Static cultures formed small, irregular cell aggregates at day 2. By day 4, both small, spherical EBs and large agglomerates were present and by day 7, the majority of static EBs were large, irregular clusters. B) The number of cells contained in embryoid bodies (EBs), free in suspension (Suspension), and adhered to the plate (Plate) was assessed at 6 and 12 hours, with significantly more cells found in EBs in rotary culture than in static after both 6 and 12 hours. Static cultures exhibited increased tendency for free cells to begin to adhere to the surface of the plate. C) Rotary EBs initiated at 25 rpm formed large EBs by day 2, while EBs at 40 and 55 rpm rotary conditions formed a greater number of smaller EBs. ** represents $p<0.01$, compared with static at the same time point, bar = 500 µm.

Efficiency of embryoid body formation

From the preliminary time course studies, it appeared that rotary EBs formed more efficiently than static cultures within the first 1-2 days of suspension. To quantify this more specifically, the fractions of cells incorporated within EBs, remaining in suspension, or attached to the polystyrene dish surface were counted using a Coulter counter after 6 and 12 hours of EB formation. By 6 hours, 69.3 ± 3.2% of cells were forming putative EBs in rotary cultures (40 rpm) compared to only 5.6 ± 3.4% for static EBs (Figure 3.1B). After an additional 6 hours of suspension culture (12 hours total), 88.4 ± 4.6% of cells were incorporated into primitive EBs for rotary samples, whereas in static cultures, only 4.5 ± 2.6% of cells were contained within floating EBs. In addition, 79.9 ± 3.3% of the cells adhered to the culture dish under static conditions, whereas no adherent cells could be obtained from the rotary samples. This suggested that while free cells in rotary suspension continued to incorporate into EBs during the first 12 hours of culture, static suspension cells became increasingly adherent to the polystyrene surface, thereby delaying or reducing overall EB formation.

Embryoid body and cell yield

In addition to an increase in the efficiency of EB formation, the number of cells and EBs formed under rotary conditions also increased compared to static. This was initially observed in preliminary studies by a considerably larger pellet of rotary EBs collected during re-feedings, as well as the need for more frequent media changes to sustain the rotary cultures properly. In order to quantify the yield of EBs and total differentiating cells, static and rotary EBs were collected at days 2, 4 and 7 and counted

directly or enzymatically dissociated with trypsin to obtain a single cell suspension prior to counting. The number of EBs present was greater for rotary than static cultures at each of the time points examined (Figure 3.2A, inset). At day 2, 8118 ± 1183 rotary EBs were present, compared to only 3459 ± 1088 static EBs. However, because of the detection limits of the instrument used, cell aggregates less than 50 μm in diameter could not be counted. As a result, many of the small clusters of cells formed by day 2 in static suspension, seen in Figure 3.1A, were not counted. By day 7, the number of rotary EBs decreased to 6724 ± 430, and static decreased slightly to 3255 ± 671. While EB yield revealed significant differences between the static and rotary cultures, the total number of differentiating cells is a more accurate and meaningful metric of overall yield. At days 2 and 4 of differentiation, modest increases in cell yield were observed in rotary cultures relative to static (Figure 3.2A), but by day 7, rotary cultures contained an average of 95.9 ± 5.0 x 10^6 cells, compared to only 24.4 ± 1.2 x 10^6 cells for static culture.

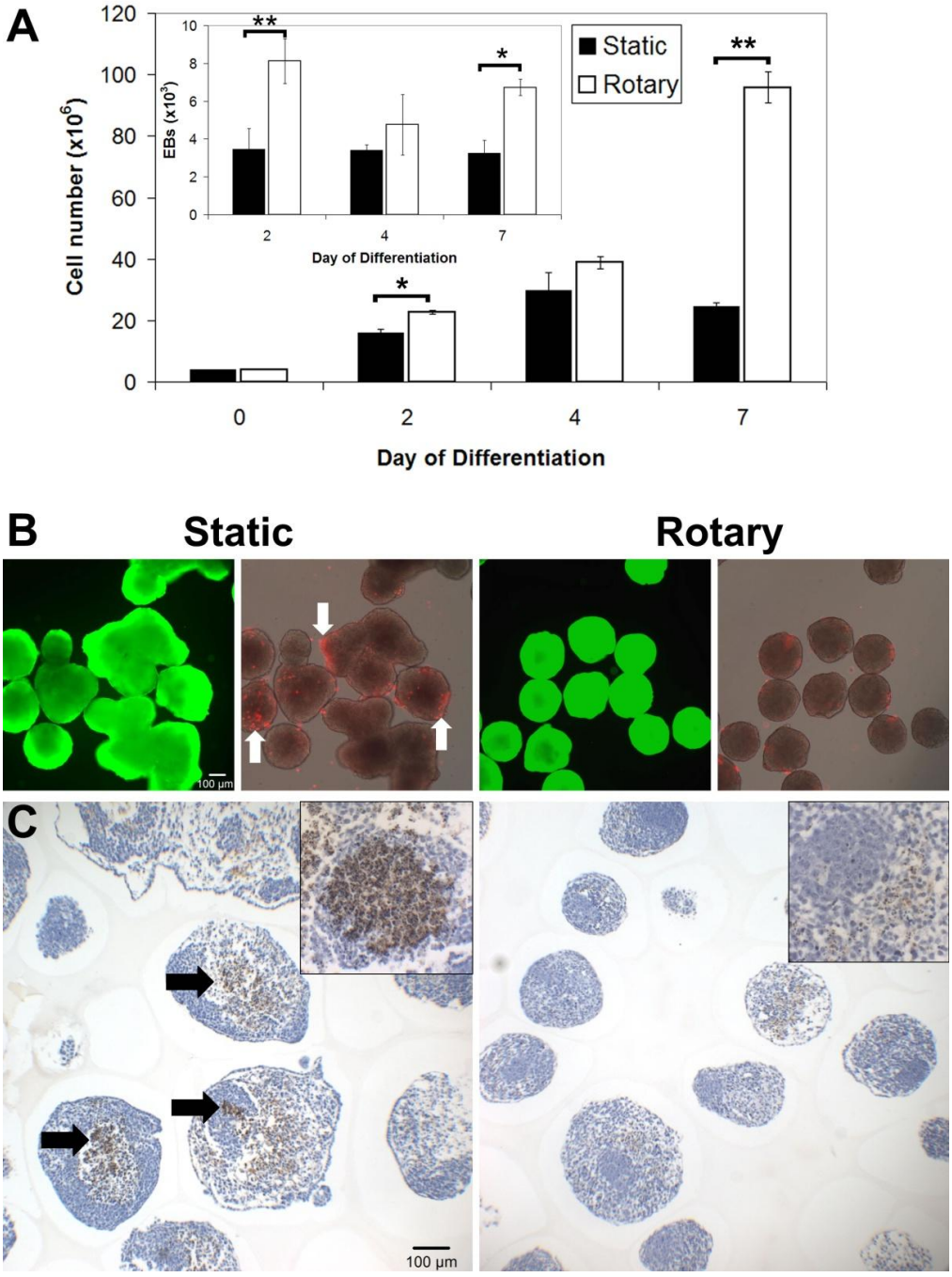

Figure 3.2. Time course comparison of cell and embryoid body yield in static and rotary conditions. A) Total cell yield counted from dissociated EBs indicated that rotary culture yielded significantly more cells than static at days 2 and 7 of differentiation. Additionally, whole EBs were counted at day 2, 4, and 7, revealing significantly more EBs produced by rotary culture than static at days 2 and 7 (inset). *=$p<0.05$, ** = $p<0.01$. B) LIVE/DEAD staining revealed that majority of cells within EBs were viable (green stain) for both static and rotary EBs, while static EBs appeared to contain more dead cells (red stain) than rotary EBs (white arrows indicate clusters of dead cells). C) Apototic cells in EBs were labeled brown using a TUNEL assay and revealed the presence of apoptotic cores at the center of static EBs (black arrows).

Viability of cells within embryoid bodies

In order to elucidate the cause of differences in cell yield between static and rotary EBs at later time points, cell viability, proliferation and apoptosis assays were preformed. Live/Dead staining performed at days 2, 4 and 7 indicated that at all three points, both static and rotary EBs contained mostly viable cells, as indicated by prevalent green staining. Staining of day 2 EBs revealed no difference in the presence of dead cells between static and rotary EBs (data not shown), but by day 4, static EBs appeared to contain more clusters of dead cells (red stain, clusters indicated by white arrows) than rotary EBs, which contained sparse, individual dead cells (Figure 3.2B). This trend appeared to continue throughout EB differentiation, with dead cells found more prevalently in static EBs than rotary at day 7 (data not shown). BrdU staining was performed to detect proliferating cells within static and rotary EBs after 2 and 5 days of differentiation. Low levels of proliferating cells were detected at each time point, likely due to the relatively long doubling time of cells within EBs, and no differences were noted between static and rotary EBs (data not shown). TUNEL staining for the detection of apoptotic cells revealed no differences between static and rotary EBs at day 4 of suspension culture; however, at day 7, more static EBs contained apoptotic cells than rotary EBs (Figure 3.2C). In addition, dense cores of apoptotic cells were found within static EBs (indicated by black arrows), while positive staining within rotary EBs was sparser and appeared to constitute less of the total EB area. This data indicates that static EBs show reduced cell viability, perhaps due to a greater number of cells undergoing programmed cell death compared to rotary EBs, potentially due to transport limitations in

agglomerated EBs or other morphogenic events associated with associated with agglomeration.

Homogeneity of embryoid body formation

In an attempt to quantify the homogeneity of EB formation, the area and circularity of EBs formed in hanging drop, static and rotary cultures were assessed by image analysis methods. Hanging drop culture resulted in EBs with a fairly narrow area distribution at day 2, followed by considerable increase in cross-sectional area and dramatic broadening of the area distribution at days 4 and 7, indicating deviation over time from an initially homogeneous size distribution (Figure 3.4A). Static cultures formed small putative EBs at day 2 and increased in size at days 4 and 7 as shown in Figure 3.4B. As with hanging drop EBs, static EBs showed broadening of the area distribution curve over the course of differentiation. By day 7 the distribution exhibited no clear peak, as EBs varied widely from very small cell clusters to giant agglomerates of EBs. Rotary cultures showed an increase in size with time, yet the peak broadening was much less pronounced than for hanging drop or static EBs (Figure 3.4C). Distribution broadening was quantified by calculating the mode absolute deviation (MAD) for each histogram for static and rotary EBs (Figure 3.4D). The MAD index was larger in static cultures than in rotary at all time points studied, with differences approaching significant levels by day 4 ($p<0.06$), and statistical significance achieved by day 7 ($p<0.05$).

Circularity (4π x (Area/Perimeter^2)) was used to indicate the degree to which irregular clusters of EBs formed as opposed to regular, spherical EBs. Hanging drop EBs showed narrow distributions with sharps peaks close to 0.9 at days 2, 4 and 7, indicating

formation and maintenance of spherical EBs (Figure 3.4E). Static cultures displayed a very broad circularity distribution at day 2, with no discernable peak present (Figure 3.4F). In contrast, day 2 rotary cultures exhibited a sharp peak around 0.9, similar to hanging drop (Figure 3.4G). This was in agreement with the observation that rotary EBs formed earlier (Figure 3.1C) and were regular in shape at day 2 whereas static cultures showed irregular multi-cell aggregates at the same time point (Figure 3.1A). By day 4, static EBs showed an increase in circularity, with a small peak present around 0.9. This coincided with the appearance of EBs by day 4 (Figure 3.1A). Rotary cultures still displayed a peak around 0.9 that was slightly broadened compared to day 2, indicating slightly less uniform EB circularity. Day 7 distributions appeared similar to day 4 for both rotary and static cultures, but were slightly broader and negatively shifted, indicating decreased homogeneity of circularity. The fraction of EBs with circularity values greater than 0.8 was calculated for both rotary and static EBs since 0.8 falls exactly in between circularity values associated with round, individual EBs (0.9) and the merger of two distinct EBs into a larger agglomerate (0.7) (Figure 3.3). The fraction of rotary EBs with circularity values > 0.8 was significantly greater than static cultures at 2 ($p<0.01$), 4 ($p<0.05$) and 7 days ($p<0.01$) (Figure 3.4H).

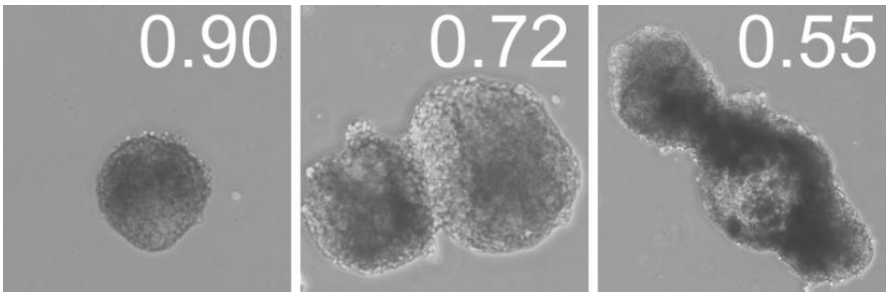

Figure 3.3. Circularity values of selected embryoid bodies. Circularity, defined as 4π x Area/Perimeter2, was determined for EBs using ImageJ. Individual EBs with circular cross sections had circularities close to 0.9, whereas agglomerates of two EBs gave values around 0.7, and agglomerates of multiple EBs showed circularity less than 0.6.

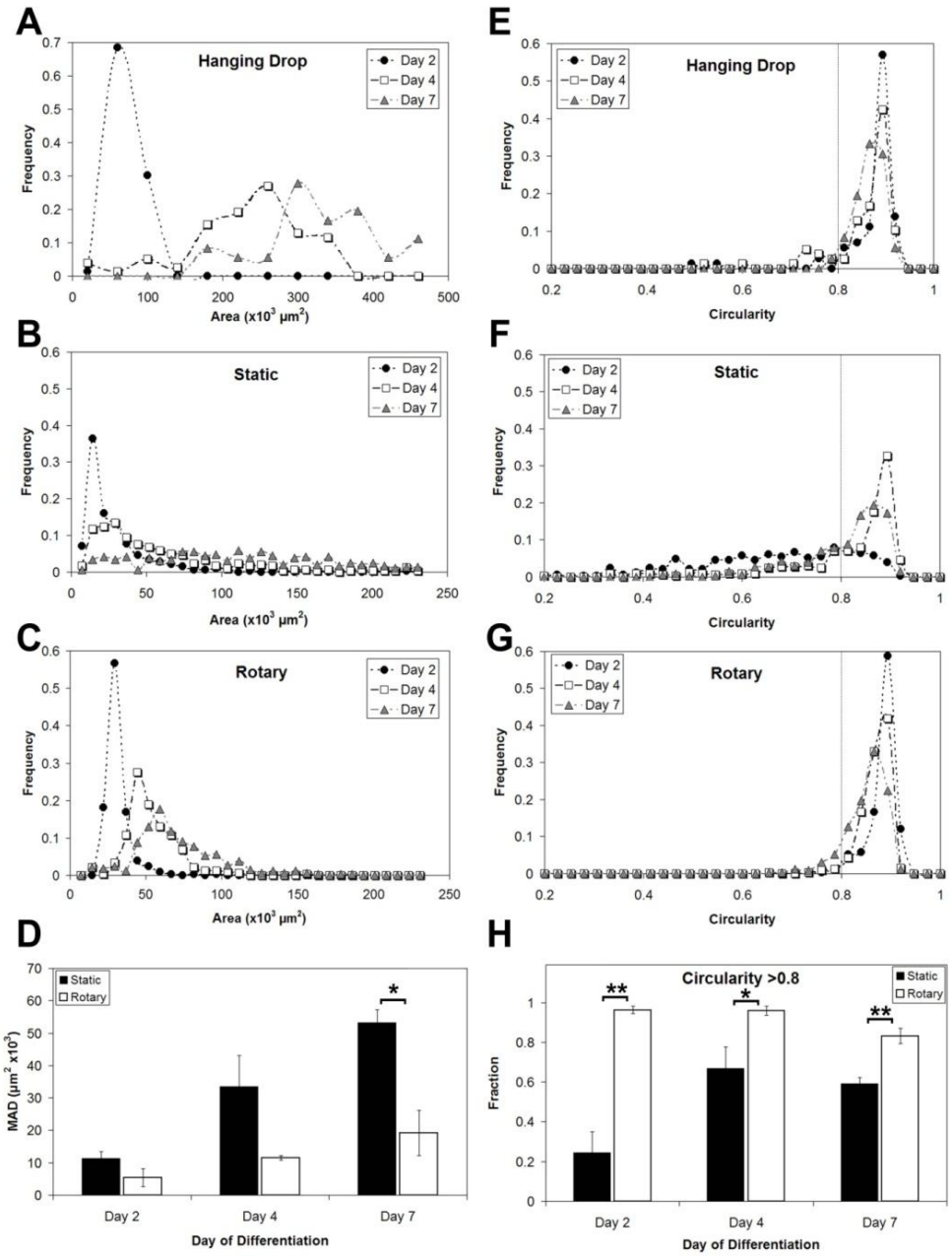

Figure 3.4. Homogeneity of embryoid body formation. Embryoid bodies formed by hanging drop, static and rotary cultures were imaged at days 2, 4, and 7 of suspension culture, and the area (A-D) and circularity (E-H) of EBs were examined. A-D: Area values for hanging drop (A), static (B) and rotary (C) EBs were sorted into 30 bins (12 for hanging drop), and the number of values in each bin was plotted versus upper bin limit (note scale differences for hanging drop). Rotary EBs showed more uniform distribution than hanging drop and static EBs, indicated by larger peak values and smaller peak widths. Mode absolute deviation showed greater deviance in static culture than in rotary (C). E-H: Circularity was more uniform for hanging drop (E) and rotary (G) EBs than static (F) , and a significantly higher fraction of rotary EBs having a circularity value greater than 0.8 at all time points studied (H). * represents $p<0.05$, ** represents $p<0.01$.

Histology of embryoid bodies

Embryoid bodies were collected from hanging drop, static and rotary cultures at days 2, 4 and 7 of suspension culture and visually assessed by H&E staining. At day 2, static EBs were small and irregular, in agreement with live phase images in Figure 3.1A, and appeared to be largely undifferentiated, indicated by a lack of organized cellular structures (Figure 3.5). Hanging drop and rotary EBs appeared slightly larger than static EBs at day 2, but exhibited a similar undifferentiated morphology. By day 4, hanging drop EBs increased in size compared to day 2 and appeared to increase in packing density. Static EBs began to agglomerate at day 4, in agreement with phase images (Figure 3.1), and showed little sign of differentiated cell morphologies. In contrast, rotary EBs did not appear to agglomerate, and contained multiple small cystic structures (denoted by black arrows in Figure 3.5) in a majority of the EBs. At day 4, over 70% of rotary EBs contained at least one cyst, compared with less than 8% in static EBs. Day 7 hanging drop EBs continued to increase in size, and also began to display cysts, similar to rotary EBs. By day 7, static EBs began to display cystic structures, with 50% of EBs containing at least one cyst, compared to 56% in rotary. Additionally, some EBs contained very large cysts (denoted by red arrow in Figure 3.5) constituting a majority of the EB cross-sectional area. These structures were more apparent in day 4 rotary EBs than static samples; however, by day 7, static cultures exhibited a similar percentage of large cystic EBs as the rotary cultures. Large day 4 and day 7 static EBs began to exhibit necrotic core areas, suggesting possible diffusion limitations negatively impacting cell viability. This morphology was in agreement with cell yield data, which demonstrated diminished cell yield in static EBs, and also previous reports which suggest that EB

agglomeration results in a reduction in viable cells [64,66]. Rotary EBs, on the other hand, did not possess necrotic regions, consistent with results of the viability studies, and

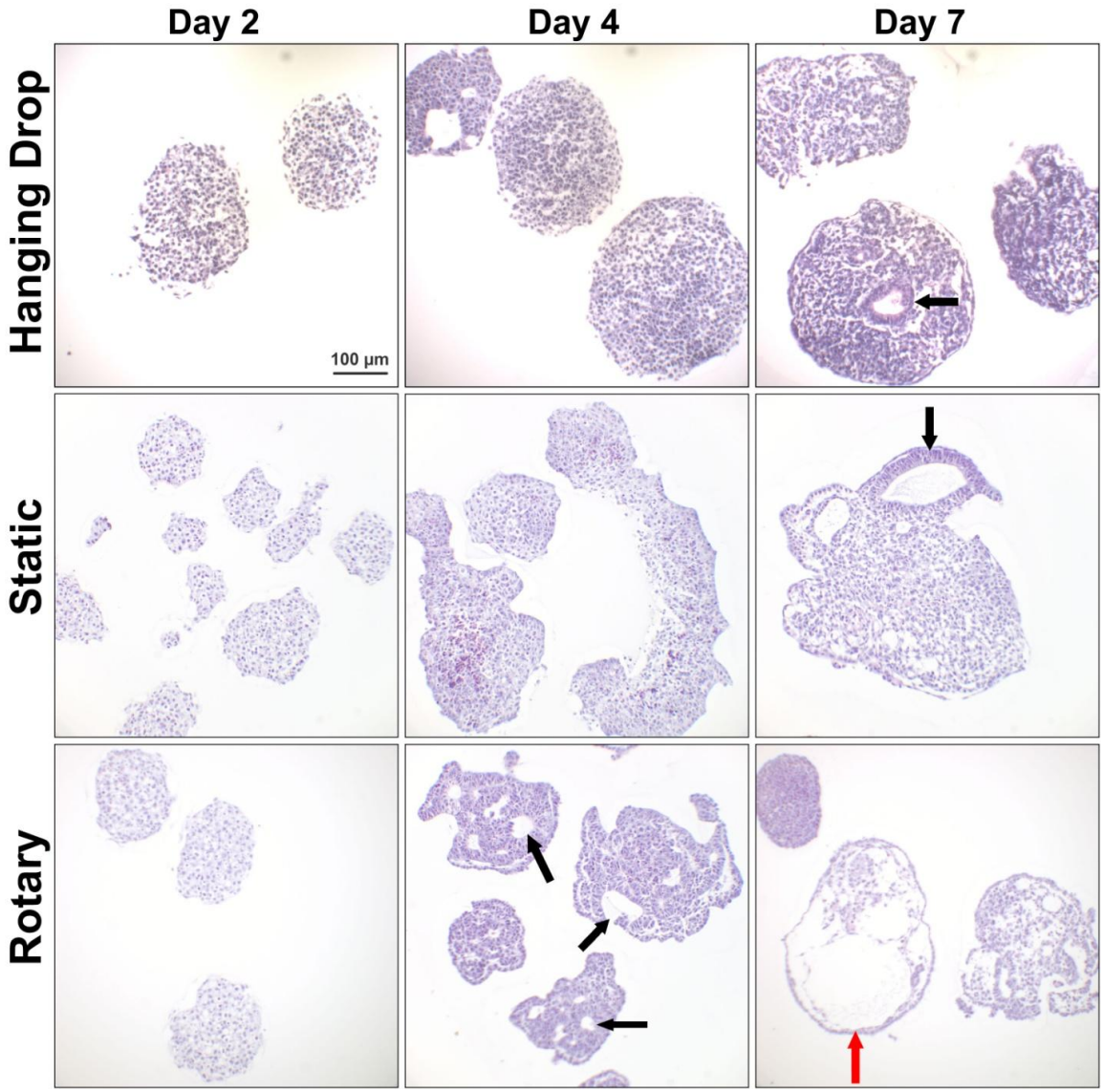

Figure 3.5. Histology of embryoid bodies formed by hanging drop, static and rotary culture. Day 2 static EBs were small, irregular and lacked internal cellular organization, while day 2 hanging drop and rotary EBs appeared to be similar to static, but slightly larger and more regularly shaped. Day 4 hanging drop EBs increased in size, while static EBs showed signs of agglomeration as indicated by large irregularly shaped EBs. Day 4 rotary EBs showed more differentiated appearance with small cysts forming (black arrows). By day 7, hanging drop EBs were larger and formed cysts, static EBs displayed small cystic cavities as well as large cysts occupying much of the EB, and rotary EBs exhibited large, completely cystic EBs (red arrow). 20x magnification, bar = 100 µm.

the majority of the cells distributed throughout rotary EBs appeared viable.

Quantitative gene expression analysis

Expression of the pluripotent genes Oct-4 and Nanog, the early mesoderm marker Brachyury-T, the ectoderm marker nestin and the endoderm marker α-fetoprotein were assessed quantitatively using PCR. The expression of Oct-4 (Figure 3.6A) and Nanog (Figure 3.7) relative to undifferentiated ES cells was similar among hanging drop, static and rotary EBs, indicating that rotary culture did not inhibit or delay normal ES cell differentiation. Brachyury-T expression was also similar between static and rotary EBs, with a transient increase in expression at day 4 that subsided by day 7, while hanging drop EBs showed insignificantly higher expression levels at day 4 with similar downregulation by day 7 (Figure 3.6B). Nestin expression was similar in EBs under all conditions, with no significant differences noted between groups for a given time point (Figure 3.6C). α-fetoprotein showed minimal expression prior to day 7, at which point hanging drop, static and rotary EBs displayed increased levels of the gene (Figure 3.6D). The higher levels of AFP expressed by hanging drop and rotary EBs correlated with the smooth, primitive endoderm layer seen in phase images (Figure 3.1A, insets). This data suggests a possible enhancement of differentiation in rotary cultures relative to static. Additionally, the expression of genes from all three germ layers indicates that EBs formed by rotary suspension retain their pluripotent differentiation capacity. The pluripotent capacity of rotary EBs is further supported by the observation of beating foci, neurite extensions, and other mature phenotypes after plating EBs on gelatin-coated substrates, similar to that seen in hanging drop and static suspension EBs.

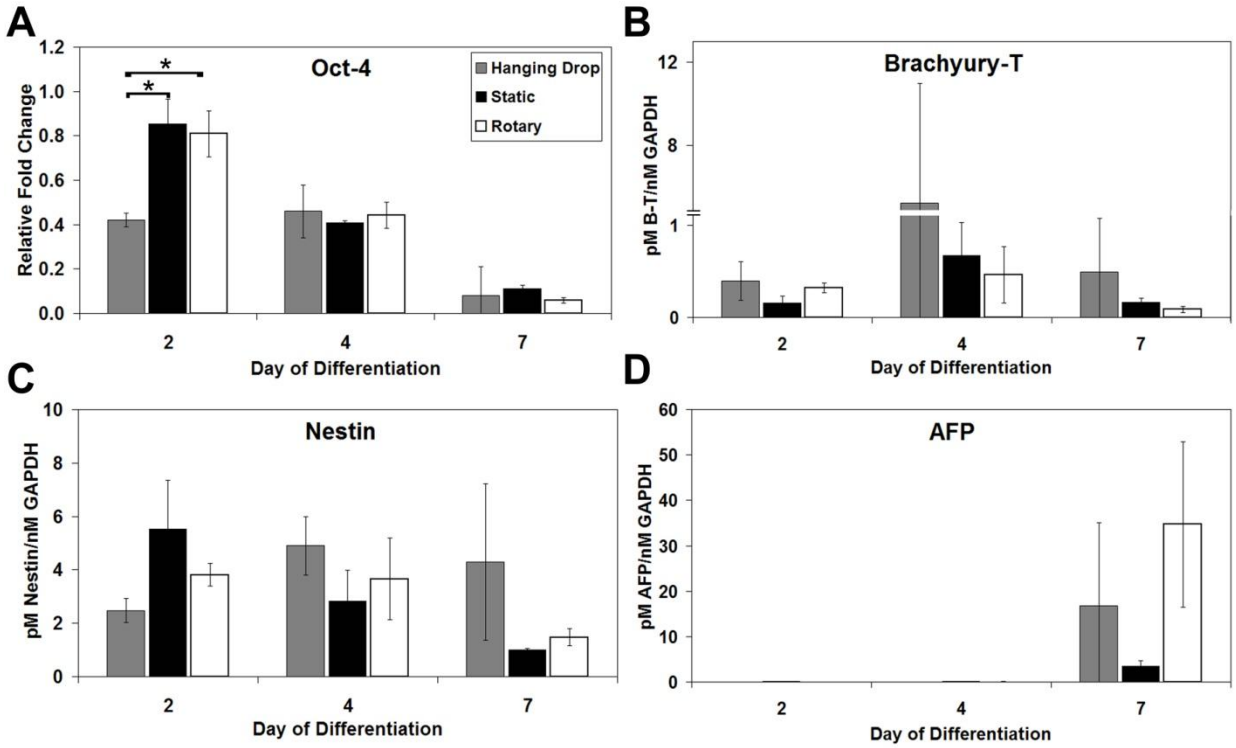

Figure 3.6. Quantitative PCR analysis of gene expression in hanging drop, static and rotary EBs. RNA extracted from EBs at day 2, 4 and 7 was compared for hanging drop, rotary and static cultures using quantitative PCR. Similar gene expression patterns were found for pluripotent marker Oct-4(A), and the mesoderm marker Brachyury-T (B), with hanging drop EBs showing increased expression at day 4. Expression of the ectoderm marker nestin was similar for all groups (C), while cells from rotary EBs showed higher AFP expression than static at day 7 (D), suggesting enhanced endoderm differentiation. * represents $p<0.05$

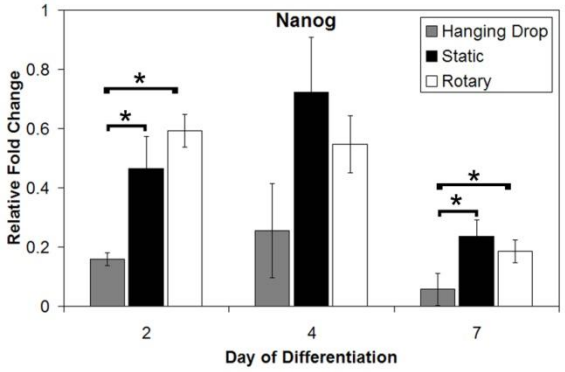

Figure 3.7. Quantitative gene expression analysis of Nanog in hanging drop, rotary, and static EBs. Similar gene expression patterns of the undifferentiated ES cell marker Nanog were observed in static and rotary EBs. Hanging drop EBs showed significantly lower expression of Nanog and day 2 and 7 of differentiation. * represents $p<0.05$

Discussion

In this study, the effects of orbital rotary culture on the efficiency of EB formation, yield and viability of differentiating cells and EBs, homogeneity of size and shape of EBs, and differentiation were investigated relative to hanging drop and static suspension culture. Rotary culture increased the efficiency of EB formation, resulting in a 20-fold increase in the number of ES cells incorporated into EBs compared to static culture after 12 hours, and rotary culture also significantly increased the yield of EBs and cells formed after 7 days of differentiation in suspension. EBs formed from rotary suspension also appeared to contain fewer dead and apoptotic cells than those from static suspension culture. Rotary culture produced EBs with greater homogeneity in size than either hanging drop or static suspension culture, and also produced an EB population with a homogenous shape similar to hanging drop and greater than static suspension culture. Additionally, EBs formed by the rotary process showed increased levels of endoderm expression compared to static EBs, but comparable induction of mesoderm and ectoderm markers and down-regulation of pluripotent markers during the course of differentiation. These results indicate that the rotary method of EB formation is an effective means for producing a controlled, uniform population of EBs in bulk suspension while simultaneously increasing the efficiency and yield of differentiating ES cells.

Physical separation techniques, such as hanging drop cultures, provide a route to control the size and efficiency of initial EB formation and prevent EB agglomeration [175]. Similarly, EBs have been formed in individual conical tubes [176] or 96-well round-bottom plates [62,177] with or without centrifugation to promote cell aggregation for EB formation. Although each approach can effectively produce distinct EBs of

similar size, individual formation and maintenance of EBs is laborious and inefficient. Thus, physical separation methods may be useful for small scale studies of EB differentiation, but they are not feasible for larger-scale production of EBs in bulk suspension culture. As an alternative approach, EB formation in agarose [65,70] and alginate [146] beads has been investigated as a means to "shield" EBs from one another in suspension and thereby prevent agglomeration. However, cell encapsulation methods require additional materials and equipment that may complicate EB production and affect the overall homogeneity of the EB population. In this study, consistent rotary motion alone during suspension culture enabled EBs to form rapidly, efficiently and homogeneously during the first 2 days of culture. In addition, after EB formation, persistent rotary motion appeared to inhibit EB agglomeration, resulting in a more homogeneous population of EBs throughout the duration of suspension culture.

Continuously mixed culture methods have been used successfully with many cell types such as hepatocytes [178], tumor cells [179], and neural stem cells [156,167] to enhance the formation of cell aggregates. Similar strategies to increase the efficiency and scale of EB production from both mouse and human ES cells have been examined more recently with various bioreactors, such as spinner flasks, slow turning lateral vessels (STLVs), and high aspect rotating vessels (HARVs) [23,64,66,162,164,165]. HARVs have been shown to promote formation of large aggregates of EBs and induce cell death, thereby reducing the overall yield of viable cells and creating a more heterogeneous population of EBs [66]. Certain spinner flasks and STLVs, however, have been shown to reduce aggregation of EBs and thus sustain larger numbers of EBs. Interestingly, spinner flasks with bulb-shaped impellers are capable of forming EBs from single-cell

suspensions, whereas spinner flasks with paddle-type impellers merely induce massive cell aggregation and EB agglomeration [164]. These observations, along with the efficient EB formation and reduced agglomeration seen in the present study, imply that the specific fluid mechanics profile of mixed culture systems may need to balance the induction of early cell aggregation required to form EBs with inhibition of EB agglomeration once individual EBs have formed.

Imposing flow on cells, particularly in 3D culture systems, provides a number of beneficial *in vitro* effects, such as increased diffusion of nutrients and oxygen, that promote cell viability. Increasing the yield of viable differentiated cells relative to the starting number of ES cells is important, since fewer input cells needed to produce EBs reduces the labor and cost of ES cell expansion prior to initiating differentiation protocols. In addition, reduction of EB agglomeration can also increase the yield of viable cells by preventing oversized EB formation [64,66]. However, the benefits of dynamic culture systems only exist up to a certain threshold, whereupon relatively large shear stresses begin to exert a detrimental effect on cells. For example, as higher rotation speeds such as 55 rpm were examined, the cultures contained more free cells in suspension than slower speeds, though it was not clear whether free cells were being sheared off EBs or simply incorporating less into EBs originally. Furthermore, lower rotary speeds may have negative effects on EB viability and yield as well, as massive cell agglomerates have been observed at rotary speeds below 20 rpm, while 25 rpm produces roughly one-tenth the number of EBs as 40 rpm. In contrast, rotary speeds close to 40 rpm appear to produce a population of EBs that both form efficiently, with few free cells

remaining in suspension, and in high yield. Thus, it is likely that a range of values for rotational speed exists which benefit cell viability and overall differentiated cell yield.

The ability to control the size of EBs may be necessary for creating robust, reproducible strategies for ES cell differentiation because cell differentiation is influenced by spatial and temporal patterns of cell-cell interactions, and thus the size of individual EBs formed may affect their differentiation profiles. Hanging drop size as a function of initial ES cell number has been integrated into differentiation protocols for different cell lineages [160]; however, this method is limited in its ability to effectively control EB size, as small differences in initial cell number within drops may result in large differences in EB size after just 2-3 population doublings, potentially accounting for the broad distributions observed in hanging drop area at days 4 and 7 in this study (Figure 3.4A). Rotation speed and cell density of larger volume, stirred culture systems have been shown to influence the size and shape of EBs, but differences in cell differentiation were not described [23,66,164]. Using rotary orbital culture, lower rotary speeds, such as 25 rpm, produced larger EBs (Figure 3.1B) while higher speeds, such as 55 rpm, yielded much smaller EBs, indicating that an inverse relationship between rotary speed and initial EB formation size exists. Such observations warranted more rigorous characterization of EB size and rotary speed [72]. These studies also suggested that modulation of rotary speed influenced gene expression and differentiation kinetics within EBs [72]. Additionally, the use of rotary culture at a single speed (40 rpm) was demonstrated to enhance cardiomyocyte differentiation relative to static suspension EBs [71]. Ongoing studies seek to assess whether modulated differentiation in rotary EBs at different speeds

is a consequence of EB size or the hydrodynamic environment, or a synergistic relationship between the two.

In addition to creating a more homogeneous and larger population of EBs in bulk suspension, rotary culture may induce differentiation of ES cells more efficiently than static suspension culture. Mature embryoid bodies are generally considered to be formed from an outer layer of primitive endoderm surrounding an interior of differentiating cells, with the endoderm providing molecular signals necessary for proper differentiation [52,57]. The morphological appearance of a primitive endoderm surface layer and increased levels of AFP gene expression in rotary EBs appears to indicate enhanced endoderm formation. Furthermore, formation of cystic structures in the interior of EBs is generally considered to be a positive indication of ES cell differentiation. The earlier and more pronounced appearance of cystic structures in rotary EBs than in static suggests that differentiation is induced sooner and could lead to more rapid and efficient differentiation of subsequent cell types dependent on endoderm-derived morphogenic cues for proper differentiation.

CHAPTER 4

DIFFUSION WITHIN EMBRYOID BODIES

Introduction

Embryonic stem cells (ESCs) are pluripotent cells derived from the inner cell mass of the blastocyst that are capable of infinite self-renewal and differentiating into cells from all three germ layers (ectoderm, mesoderm and endoderm), as well as germ cells. Embryonic stem cells have been derived from mouse [1,2,180], non-human primate [181,182] and human embryos [4,183]. More recently, pluripotent cells have been created from adult cell sources using a variety of viral and non-viral techniques [30-32,184,185] and are collectively known as induced pluripotent stem cells (iPSCs). The plasticity of pluripotent cells has made them applicable in studies of developmental biology *in vitro* and as a potential cell source for regenerative cell therapies as well as *in vitro* pharmacological drug screening and toxicity testing. Differentiation of ESCs can be induced by a variety of methods, including adherent monoculture [186], co-culture with differentiated cell types [187], and via formation of spheroids called embryoid bodies (EBs) [1]. Differentiation of ESCs as EBs is particularly common due to the similarities of these 3D spheroids to developing embryos with respect to morphogenesis and differentiation. Additionally, EB culture provides ESCs with a microenvironment rich in cell-cell and cell-extracellular matrix (ECM) contacts that cannot be easily replicated in monolayer culture.

Spheroid culture is not limited to ESCs, but rather is utilized for a number of cell types, including hepatocytes [171,178,188,189], embryonic carcinoma cells [190-192],

and adult stem cells (mesenchymal [193,194] and neural [195-197]). A variety of cancer cell types are also commonly grown as spheroids [198-203] (and reviewed by [119,204,205]) and are typically referred to as multicellular tumor spheroids (MCTS). The use of MCTS for *in vitro* studies of cancer biology is preferred over monolayer culture as MCTS more closely mimics solid tumors *in vivo* in regard to cell morphology, cell growth, drug resistance, and cell death [119,200,204]. Additionally, MCTS culture more accurately replicates the heterogeneity inherent to the solid tumor microenvironment than monolayer culture, as regions of oxygen and nutrient depletion and necrosis develop, whereas cells in monolayer are exposed to more homogeneous conditions [124]. Because of these similarities to solid tumors, MCTS are often employed for modeling of growth kinetics [203,206], angiogenesis [199,207], immune cell interactions [205], and diffusivity within solid tumors [121,123,125]. Diffusive properties are of particular importance in cancer research as incomplete drug diffusion, particularly deep within tumor tissue, can result in ineffective cancer therapeutics [208]. Incomplete vasculature, extracellular matrix production, increased interstitial fluid pressure, and tight cell junctions all contribute to the resistance solid tumors and tumor spheroids pose toward complete drug penetration [208,209].

EBs also present obstacles for solute diffusion and uniform uptake by cells comprising EBs. Studies have been performed on the diffusive properties of EBs as a function of differentiation time course and anti-angiogenic drug treatment [23]. Interestingly, these studies suggested that vascular differentiation occurring within EBs facilitated transport, resulting in later stage EBs displaying a higher diffusion coefficient than early EBs, while anti-angiogenic agents reduced this difference. However, other

studies have reported that ECM and basement membrane are produced within EBs, and that later stage EBs display more developed and organized basement membrane [51,55,56]. Studies investigating the role of basement membrane in diffusion within EBs demonstrate that disruption of membrane formation, via modulation of nitogen interactions with laminin, resulted in enhanced EB permeability [210]. Additionally, studies with human EBs have shown that EBs progress from a primitive cluster of cells at early time points (3 days) to spheroids with smooth, matrix-rich exteriors at later time points (7 and 10 days) [22]. Diffusive transport studies demonstrate that methylene blue uptake by the shell-like EB exterior decreases significantly between 3 and 7 days of differentiation, suggesting that ultrastructural changes within differentiating EBs restrict molecular diffusion [22]. The discrepancies observed between these studies as well as the species and culture system-specific differences common in EBs warranted further investigation into the diffusional properties of EBs.

In this study, the diffusive transport characteristics of murine EBs formed via rotary suspension culture were assessed. Scanning electron microscopy was used to examine the ultrastructure of differentiating EBs, particularly at the EB periphery. Fluorescent dye uptake by cells in EBs was assessed both *in situ* by microscopy, and by dissociating EBs and quantifying cell labeling. A simple model of EB geometry was used to determine the percentage of cells at a given depth from the EB exterior as a function of spheroid radius. Finally, a diffusion model based on Fick's laws was constructed to demonstrate that experimental results are in agreement with governing transport equations. These results indicate that significant barriers to solute diffusion exist within EBs that should be taken into account in directed differentiation protocols.

Methods

Embryonic stem cell culture

Murine embryonic stem cells (D3) [1] (passages 23-32) were maintained in an undifferentiated state on tissue culture dishes coated with 0.1% gelatin in Dulbecco's modified Eagle's medium (DMEM) (Mediatech Inc., Herndon, VA), supplemented with 15 % fetal bovine serum (FBS) (Hyclone, Logan, UT), 2mM L-glutamine (Mediatech), 100 U/mL penicillin, 100 μg/mL streptomyocin, 0.25 μg/mL amphotericin (Mediatech), 1x MEM nonessential amino acid solution (Mediatech), 0.1 mM 2-mercaptoethanol (Fisher Chemical, Fairlawn, NJ), and 10^3 U/mL leukemia inhibitory factor (LIF, Chemicon International, Temecula, CA). Cells were routinely passaged every 2-3 days prior to reaching 70% confluence.

Embryoid body formation

Undifferentiated ESCs were dissociated from monolayer culture with a 0.05% trypsin-EDTA solution (Mediatech) to obtain a single cell suspension. Suspension cultures of EBs were initiated by resuspending 4 x 10^5 cells/mL in differentiation media (undifferentiated growth media without LIF) on bacteriological grade Petri dishes. Rotary suspension culture EBs were initiated by placing dishes on an orbital rotary shaker (Lab-Line Lab Rotator, Barnstead International, Dubuque, IA) set at 40 revolutions per minute (RPM). Embryoid bodies were maintained for up to 10 days in

suspension, with media changed every one to two days by allowing EBs to sediment in 15 mL centrifuge tubes, aspirating the old media, and resuspending in fresh media

Scanning electron microscopy

Embryoid bodies were collected after 10 days of rotary culture and were fixed in 2.5% gluteraldehyde (Electron Microscopy Sciences) diluted in sodium cacodylate buffer (Electron Microscopy Sciences) for 1 hour. After rinsing, EBs were further treated with 1% osmium tetroxide (Electron Microscopy Sciences) for 1 hour. Samples were dehydrated in graded acetone dilutions and critically point dried using a Polaron E3000 critical point dryer (Quorum Technologies Inc, Guelph, ON, Canada). Finally, EBs were sputter coated for 120 seconds at 2.2 kV using a Polaron SC7640 sputter coater and imaged using a Hitachi S-800 scanning electron microscope (Hitachi High Technologies, Pleasanton, CA).

CellTracker labeling

After 2, 4, and 7 days of rotary culture, EB samples were collected and labeled with CellTracker Red^{TM} (CTR; Molecular Probes). EBs were incubated for 30 minutes in 24 well plates containing 1.0 mL of 2.5 μM CTR solution. The CTR solution was then replaced with regular differentiation media, and EBs were incubated for an additional 30 minutes. EBs were then rinsed with PBS and then dissociated into single cells via trypsin-EDTA digestion. Trypsin was neutralized using differentiation media and cells were collected via centrifugation, resuspended in PBS, loaded into a hemocytometer, and counted. Fluorescent images of CTR labeled digested EBs were acquired on a Nikon

Eclipse 80i microscope equipped with a Spot RT3 Slider camera (Diagnostic Instruments), and the percentage of labeled cells was calculated for each time point.

Confocal microscopy

Embryoid bodies were labeled with CTR as described above. Prior to the trypsinization step, samples of labeled EBs were collected for imaging via confocal microscopy. Images were acquired on a Zeiss LSM/NLO Multi-Photon microscope. Labeled EBs were imaged at a range of Z-depths with 4.66 μm between optical sections. ImageJ software was used to generate plot profiles as well as to calculate the fraction of labeled pixels within EBs. Briefly, fluorescent intensity profiles were generated using the rectangular selection tool in order to create intensities averaged in the vertical direction across the horizontal length of the rectangle. Distance values were transformed such that the center of the EB corresponded to zero on the x-axis. The fraction of labeled pixels in each EB section was also calculated using ImageJ. The threshold and analyze particles features were used to quantify the number of fluorescent pixels in each section, and the number of pixels corresponding to the entire EB area was also calculated. The fraction of labeled pixels at each Z-depth was determined and values were normalized to the maximum labeling fraction for each EB.

Cryosectioning

EBs fluorescently labeled with CTR (as described) were collected, rinsed in PBS, and embedded in optimal cutting temperature (OCT) solution. The OCT blocks containing EBs were frozen over dry ice until completely solid and stored at -20°C prior

to sectioning. Ten µm sections were taken using a cryostat (Micron Cryo-Star HM 560MV), with at least 100 µm between sections to minimize repeated sectioning of the same EBs. OCT was washed from the sections using PBS followed by two washes in deionized water. To counterstain cell nuclei, slides were incubated in Hoechst (diluted 1:100) solution for 5 minutes, washed in PBS and water, and coverslipped using aqueous mounting medium (Gel/Mount, Biomedia Corp.). Slides were imaged on a Nikon 80i microscope. Cell labeling in cryosections was quantified using ImageJ software. Each EB was divided into four equi-radial regions (i.e. the length of each region in the radial direction was equal). The percentage of CTR-labeled pixels was quantified by using the analyze particles tool to calculate the number of fluorescent pixels, and the selection tool and measure feature to determine the total pixels within the specified region.

Geometric model

An algorithm to calculate the percentage of cells at a given radius within an EB as a function of EB size was constructed using Matlab (The MathWorks Inc.). EBs were assumed to be solidly packed spheroids consisting of concentric cell layers, each 10 µm (the average diameter of an ESC) thick. The volume of a layer at radius r=r1 was determined by calculating the volume at r=r1 and then subtracting the volume of a sphere at r=r1 - 10µm (i.e. volume of a shell calculation). The number of cells in a given layer was calculated as the quotient of layer volume and the volume of a single cell. The percentage of total cells at a given depth from the EB exterior was plotted for multiple spheroid radii.

Diffusion model

Concentration as a function of radial distance from the center of a spheroid was modeled using Fick's second law as the governing equation. The system was assumed to be in steady state with a constant consumption rate. Calculation of the constants based on the different boundary conditions can be found in Appendix A. Concentration was plotted as a function of radial distance from the EB center using Matlab.

Statistical analysis

Values are reported as mean ± standard deviation. Statistical significance was determined using one or two way ANOVA coupled with Tukey's post hoc analysis using Systat (v12, Systat Software Inc.).

Results

Embryoid body ultrastructure

Embryoid bodies were cultured for 10 days under rotary suspension conditions prior to imaging via scanning electron microscopy (SEM). The EB surfaces contained regions in which individual cells protruded, though the majority of the surface area was smooth with individual cells less discernable (Figure 4.1A). This suggests that cells predominantly have a flattened, epithelial morphology, and that ECM is deposited between cells. Bisection of EBs revealed the formation of a dense, shell-like layer approximately 10 μm thick enveloping the EB (Figure 4.1B, C). This layer was similar in appearance to the collagen IV-containing shell structure reportedly formed in human

EBs [22]. Formation of EBs with smooth surfaces, matrix-rich peripheries and epithelial-like cells motivated further investigation into molecular diffusion within EBs.

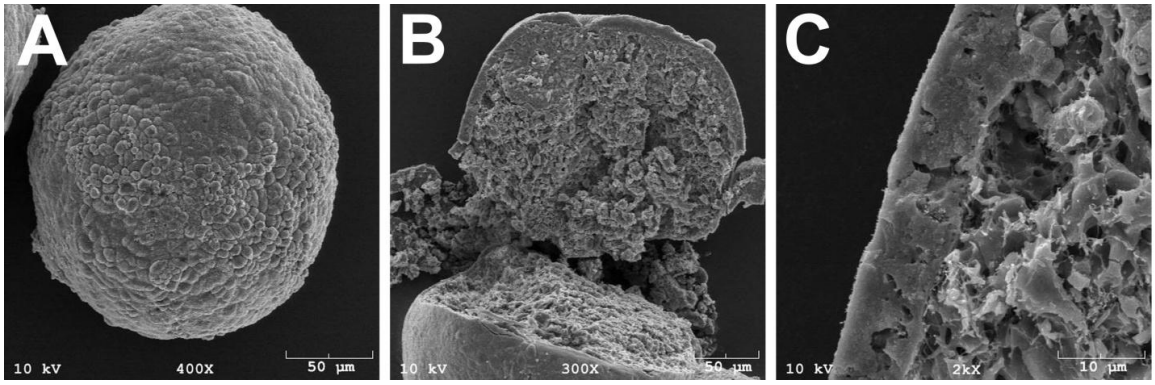

Figure 4.1. Ultrastructure of embryoid bodies. EBs were imaged with scanning electron microscopy after 10 days. EBs had smooth surfaces (A), and bisected EBs had a shell-like exterior (B) approximately 10 µm thick (C).

CellTracker Red diffusion in embryoid bodies

Embryoid bodies were formed via rotary suspension culture, and phase images confirmed formulation of relatively uniform, spherical EBs by 2 days and continued EB growth after both 4 and 7 days (Figure 4.2). Diameters for the EBs were 155 ± 28, 192 ± 29, and 250 ± 35 µm for day 2, 4 and 7 EBs, respectively. In order to investigate molecular diffusion within EBs as a function of time, EBs formed via rotary suspension culture were collected and assessed after 2, 4, and 7 days using confocal microscopy, cryosectioning of OCT-embedded EBs, and quantification of dissociated EBs.

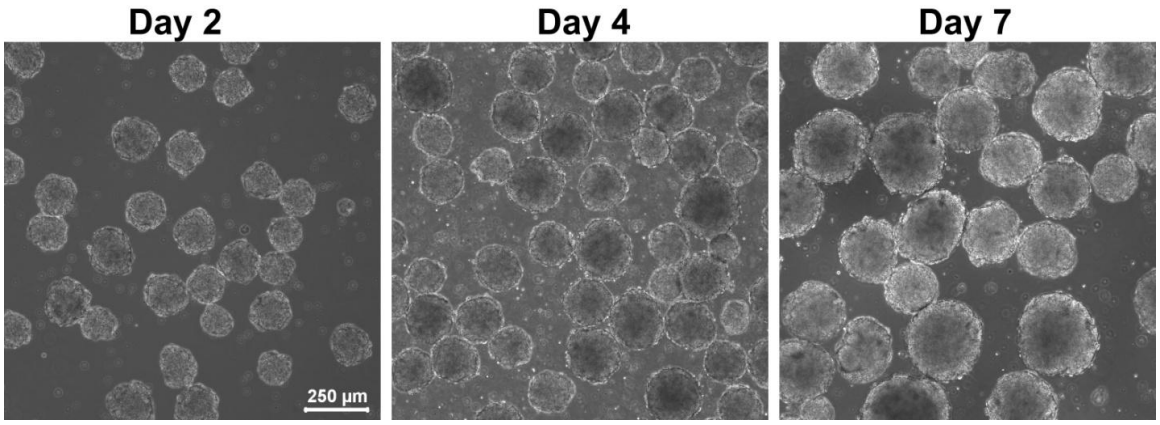

Figure 4.2. Temporal analysis of EB appearance. EBs formed via rotary suspension culture were spherical and uniform, and EB size increased over time.

Confocal microscopy

After 2, 4, and 7 days of rotary culture, EBs labeled with CTR displayed intense fluorescent staining on their exterior surface (Figure 4.3, 0 µm column). At deeper optical sections, temporal differences were noted in EBs. Day 2 EBs remained relatively uniform in CTR staining at deeper sections, whereas day 4 and day 7 EBs displayed ring-like staining patterns (Figure 4.3, 18.6 and 37.3 µm columns). Cells at the exterior were intensely stained while EB interiors were unlabeled. This phenomenon was quantified using the Plot Profile feature of ImageJ. Averaged intensity profiles were generated across three depths of EBs for each time point (Figure 4.3, right column). Fluorescent signal was maintained in day 2 EBs across the entire EB diameter, even at the deepest optical section. In contrast, both day 4 and day 7 EBs produced profiles with signal spanning the EB at the superficial layer, but signal was lost at the EB center at depths of both 18 and 37 µm. In the deepest sections, fluorescent signal was only detected 20-30 µm into day 4 and day 7 EBs, suggesting that at these time points, CTR is only able to penetrate through 2-3 cell layers.

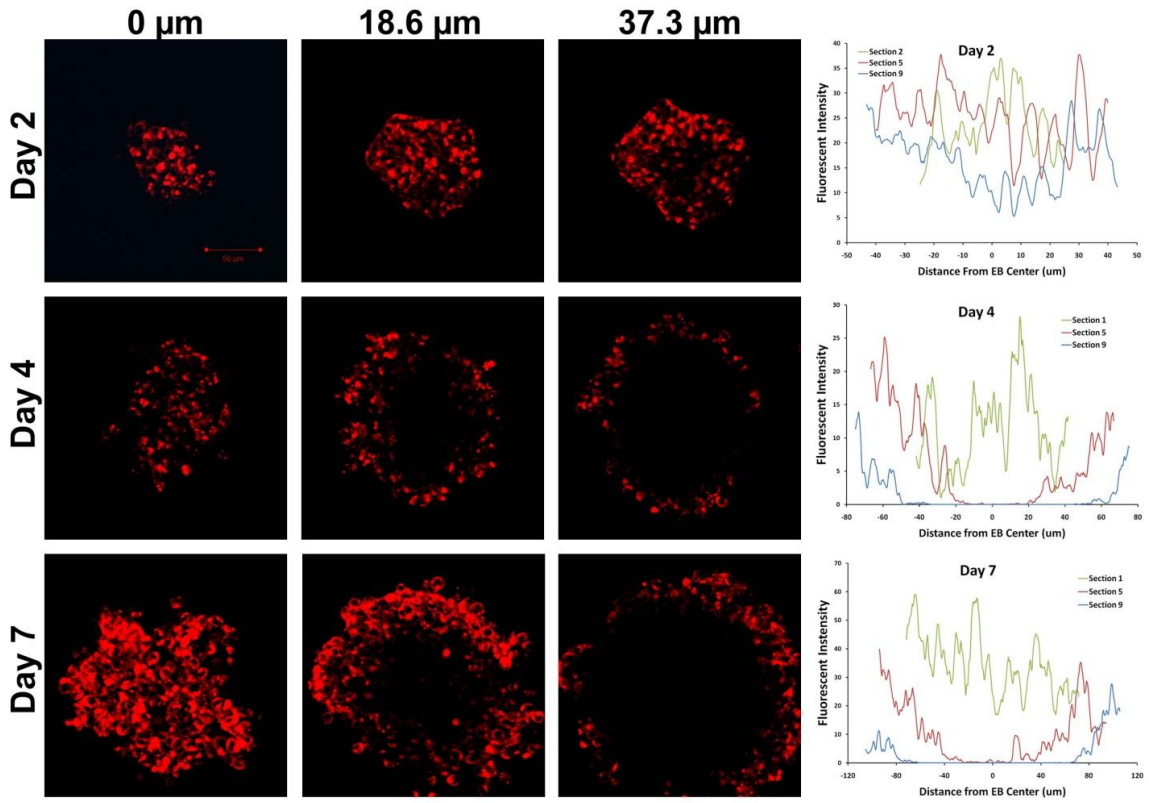

Figure 4.3. Confocal imaging and analysis of CellTracker Red labeling. EBs stained with CTR were imaged after 2, 4 and 7 days, and representative images at three Z-depths (0, 18.6, and 37.3 µm) are shown. Plot profiles were constructed across the EB diameters for three depths at each time point, demonstrating the ring-like staining profile in day 4 and 7 EBs.

Cell labeling in confocal images was also quantified on an area basis. The percentage of fluorescent pixels was quantified within optical sections of EBs. Due to variations in the absolute percentages obtained, attributed in part to photobleaching, values were normalized to the maximum percentage for each EB analyzed. Plots of normalized labeling as a function of Z-depth demonstrate that early EBs (day 2) display relatively uniform profiles, whereas later EBs (days 4 and 7) show a gradual decrease in staining at deeper sections (Figure 4.4). However, statistical significance was only observed at 28 µm sections between day 2 and day 7 EBs ($p = 0.046$). These results are

in agreement with the plot profiles described above and suggest that diffusion within EBs is restricted in a time-sensitive fashion.

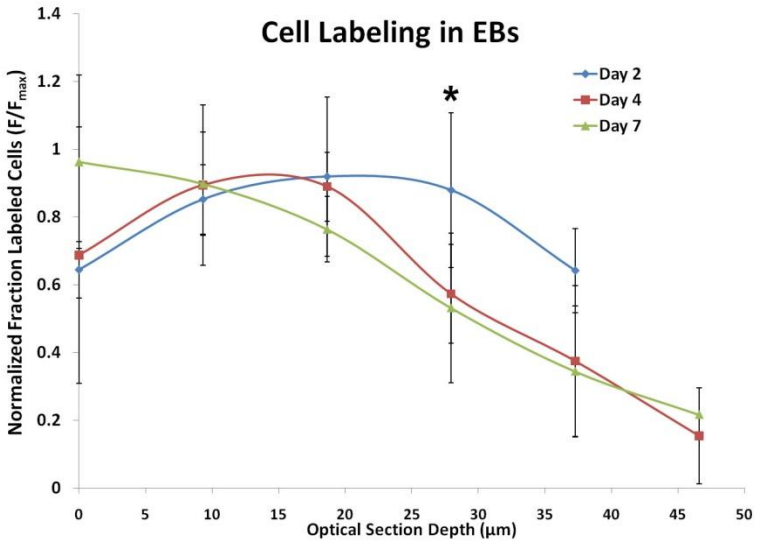

Figure 4.4. Fraction of labeled cells in EBs. Confocal images were analyzed for the percentage of labeled pixels within EBs as a function of both time and Z-depth. Values are normalized to the maximum labeling fraction for a given EB. * denotes $p < 0.05$ for Day 2 vs. Day 7.

Cryosections of labeled EBs.

To further characterize CTR diffusion in EBs, labeled EBs were embedded in OCT, frozen over dry ice, and sectioned with a cryostat. Quantification of fluorescence as a function of radial distance once again indicated that staining was most prevalent around the EB exterior (denoted region R1 in Figure 4.5), and that staining progressively decreased toward that EB center. Interestingly, the centermost region (R4) did not follow this pattern, and instead showed staining most similar to an intermediate (R2) region. The cause of this discrepancy is not entirely clear, though sectioning artifact and background fluorescence may be factors.

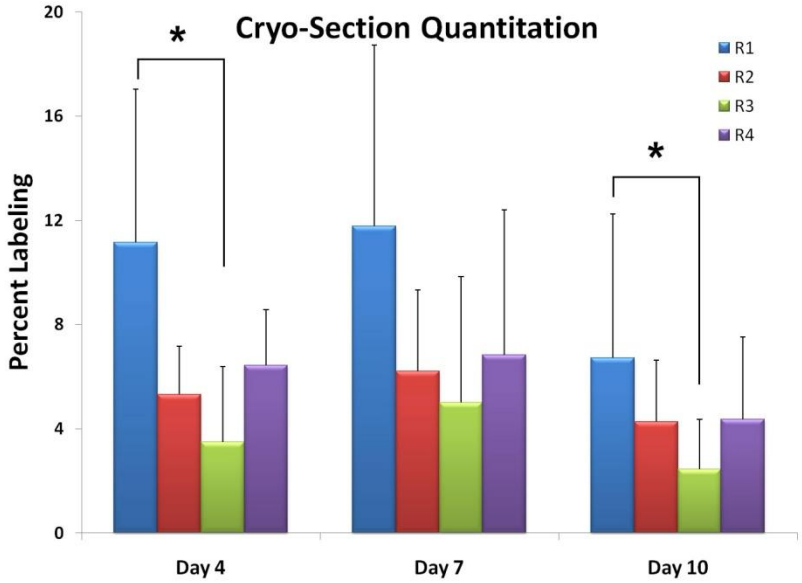

Figure 4.5. Analysis of frozen EB sections. The percentage of labeled pixels in frozen sections was quantified in 4 radial regions (R1 is the outermost region, R4 is the interior). Staining was most prevalent at the EB exterior (R1 region). *denotes $p < 0.02$.

EB dissociation

Cell labeling within EBs was further assessed via quantification of fluorescence in dissociated EBs. As described above, EBs were labeled with CTR prior to trypsin digestion and reduction to single-cell suspensions. Cells were then loaded in a hemocytometer, and the total number of cells as well as the number of fluorescent cells was counted under a fluorescent microscope. This method of quantification resulted in comparatively high percentages of labeled cells (Figure 4.6). As expected, day 2 EBs had the highest level of cell labeling (94.7 ± 3.7 %) while later EBs had progressively fewer labeled cells (78.5 ± 5.4 and 59.8 ± 8.4 % for days 4 and 7). All time points had significantly different labeling percentages ($p < 0.05$). In previous quantification methods (analysis of confocal and frozen section images), labeling was assessed through quantitation of fluorescent pixels rather than the number of positive cells. The binary

nature of dissociative quantitation (i.e. either CTR positive or negative) means that a cell with low fluorescent intensity, translating to few fluorescent pixels, is counted the same as a cell with intense fluorescence and many positive pixels. As such, these data appear to be in agreement with results obtained from *in situ* imaging and frozen sections.

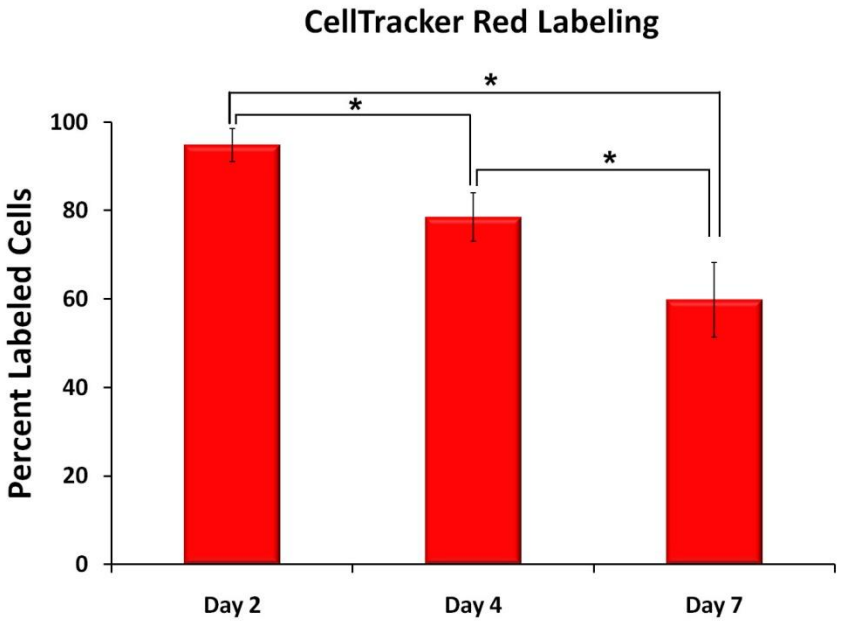

Figure 4.6. CellTracker labeling in dissociated EBs. EBs were labeling with CellTracker Red and the percentage of labeled cells was quantified by dissociating EBs and counting fluorescent cells using microscopy. The percentage of labeled cells progressively decreased with time. * denotes $p < 0.05$.

A model of embryoid body geometry

In the above analyses, CTR labeling within EBs was generally observed to decrease as EBs matured, and staining was less prevalent in the interior than exterior cell layers. A significant amount of EB growth takes place between each of the time points examined, suggesting that EB growth may play a role in determining the fraction of cells that are exposed to media solutes. A graphical representation of the percentage of cells at

a given distance from the EB surface was created for various EB radii (Figure 4.7). EBs were assumed to consist of concentric cell layers of equal thickness (10 μm, the approximate diameter of a single ESC). The volume of each cell layer was calculated, and the number of cells in the layer was calculated as this volume divided by the volume of a single cell. This figure illustrates that in spheroids with very small radii, nearly all cells are in contact with the media, suggesting that transport limitations do not exist. However, for spheroids with radii greater than 100 μm, less than 25% of cells are in contact with the surrounding media. Confocal studies indicated that in larger EBs ($r > 75$ μm), CTR was only able to penetrate 2-3 cell layers (20-30 μm from the EB exterior). Interestingly, the percentage of cells within 30 μm of the exterior for $r = 75$, 100, and 125 μm (the average radii of EBs after 2, 4 and 7 days) are 95, 81, and 70%, respectively. When compared to the observed percentage of CTR labeled cells in dissociated EBs (95, 79 and 60% for days 2, 4 and 7), these figures start out similar but begin to deviate after 7 days. The 95% labeling in day 2 EBs fits the geometric model of 75 μm radius with 30 μm diffusion length very closely, as do day 4 EBs with average radius of 100 μm and 80% CTR labeling. Day 7 EBs, with 125 μm average radii and 60% CTR labeling, extrapolate to a diffusion length of approximately 20 μm. This suggests that processes within the EB that take place between 4 and 7 days restrict the diffusion of extracellular molecules within EBs. The production of ECM and basement membrane, formation of tight cell junctions, and increased cell packing density within EBs over the course of differentiation may all contribute to this behavior.

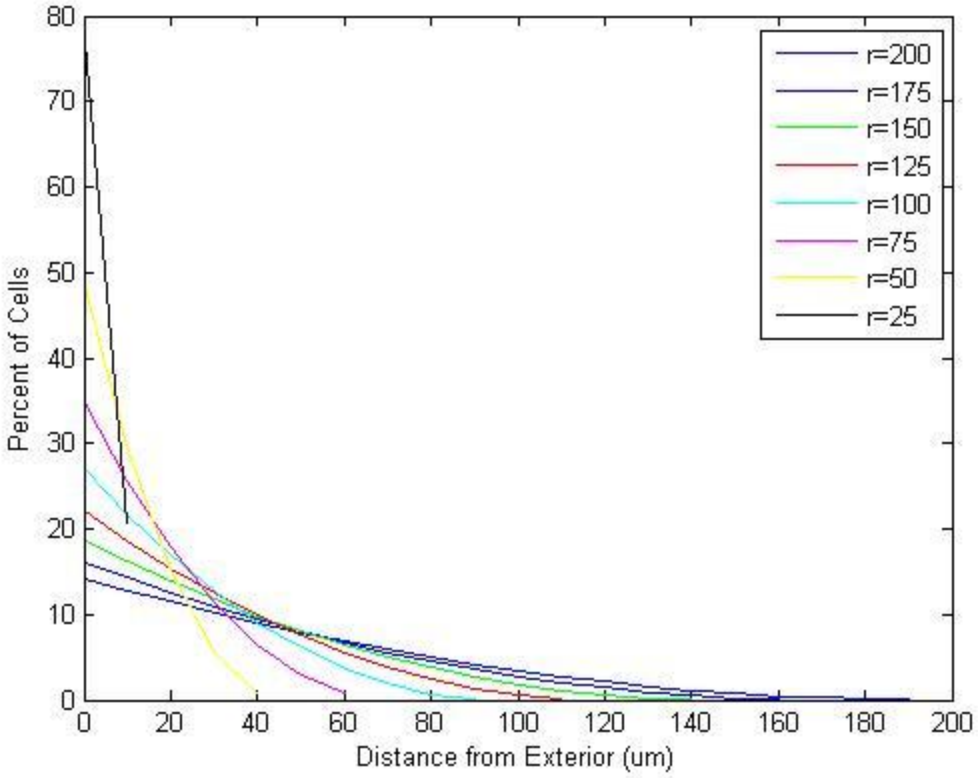

Figure 4.7. Graphical representation of the fraction of cells at a given radial distance. The percentage of cells in each cell layer was plotted for EBs with various dimensions, starting with the outermost layer.

Modeling diffusion in embryoid bodies

A system of equations describing the concentration of a media component both inside and outside a spheroid was derived and is listed in Appendix A. Assuming steady state, radial symmetry, and constant rate of consumption, this system of equations reduces to:

$$C_{\text{int}}(r) = \frac{C_1}{r} + C_2$$

$$C_{ext}(r) = \frac{C_3}{r} + C_4 + \frac{1}{6}Qr^2$$

where $C_{int}(r)$ and $C_{ext}(r)$ are the concentration inside and outside the spheroid, respectively and Q is the consumption rate of the solute divided by the diffusion coefficient in the spheroid (Q=-q/D). The constants in these equations were solved for using initial conditions and boundary conditions, as described in Appendix A. In the simplest scenario, the solute is assumed to diffuse throughout the spheroid, and the concentration is assumed to be continuous across the spheroid border. The equations reduce to:

$$C_{ext}(r) = C_{bulk} - \frac{QR^3}{3r}$$

$$C_{int}(r) = C_{bulk} - \frac{QR^2}{2} + \frac{1}{6}Qr^2$$

where R is the spheroid radius. Numerical examples of this situation are depicted in Figure 4.8 for a range of Q and R values. When Q is very small, consumption is very low and the concentration within the spheroid deviates only slightly from the bulk concentration (Figure 4.8A). As Q increases due to increasing consumption or decreasing diffusion coefficient, the concentration within the spheroid decreases more sharply as the radius approaches zero (Figure 4.8B). This effect is more pronounced as the size of the spheroid increases.

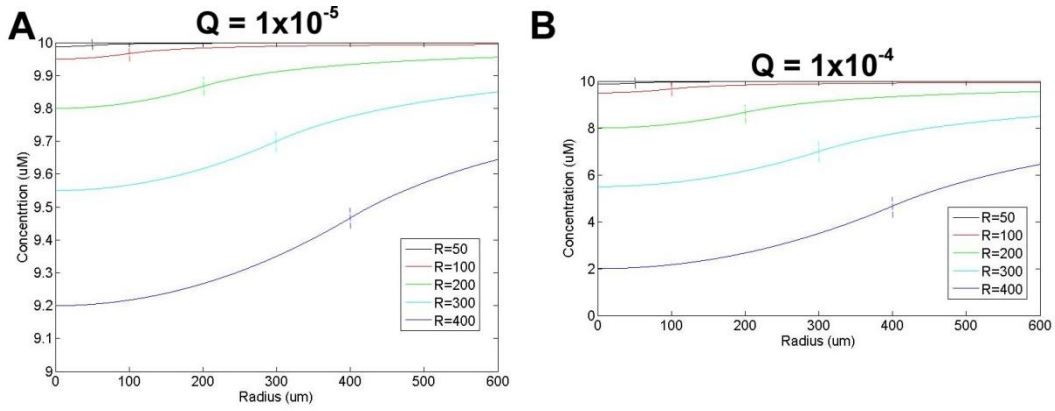

Figure 4.8. Concentration profiles in spheroids without complete depletion. Low Q values result in high concentration throughout the spheroids (A) while higher Q values result in greater depletion (B). Vertical dashed lines represent the spheroid radius for each curve.

As Q continues to increase, the concentration within the spheroid reaches zero, and at a sufficiently high Q value, the above equations are no longer valid as negative concentrations will be obtained. The threshold at which this occurs is defined by the relation:

$$R_0 = \sqrt{\frac{2C_{bulk}}{Q}}$$

where R_0 is the radius at which a zero-concentration zone develops within the spheroid. For a fixed C_{bulk} value, the relationship between Q and R_0 is demonstrated in Figure 4.9.

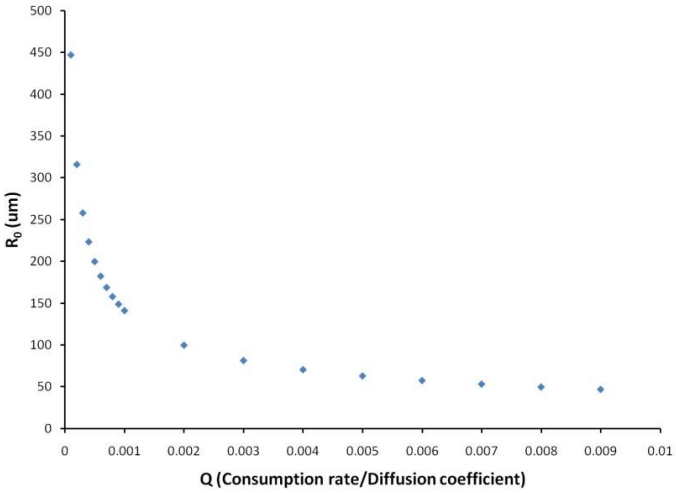

Figure 4.9. Radius at which a zero concentration zone develops as a function of Q. R_0 is proportional to one divided by the square root of Q.

Intuitively, a zero-concentration zone develops in spheroids with very high Q (either high consumption or low diffusion) even if the spheroid dimensions are very small, whereas such as zone will only occur in large spheroids if the radius is large when Q is very low.

For $R>R_0$, new boundary conditions apply (see Appendix A), and recalculation of the constants yields:

$$C_{ext}(r) = C_{bulk} + \frac{Q[(R^2 - {R_0}^2) - R^3]}{3r}$$

$$C_{\text{int}}(r) = C_{bulk} - \frac{Q}{6}(3r^2 - R^2) + \frac{Q(R^2 - {R_0}^2)^{3/2}}{3r}$$

Examples of this case are shown in Figure 4.10. When $Q=1x10^{-3}$, this set of equations only applies to spheroids with R>141 μm. Significant depletion of the solute is observed within the spheroid before the concentration finally drops to zero (Figure 4.10A). At higher Q values, the concentration reaches zero nearly immediately after contact with the spheroid surface (Figure 4.10B).

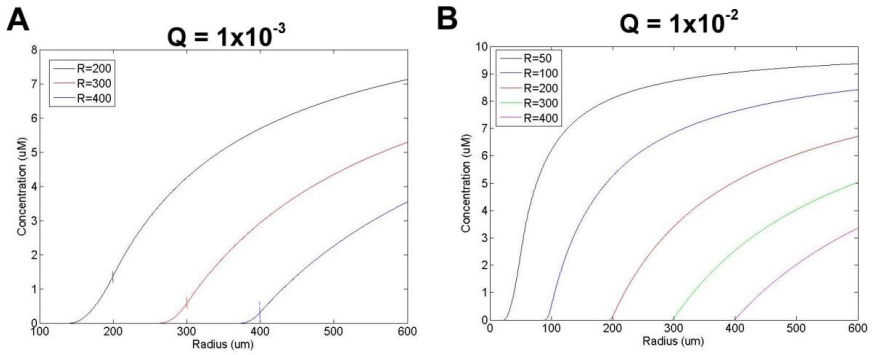

Figure 4.10. Concentration profiles for spheroids in which complete depletion occurs. Depletion occurs more gradually for smaller Q values (A) while larger Q values result in depletion very near the spheroid surface (B).

Finally, the spheroid size was fixed at radii of 75, 100, and 125 μm and the concentration was plotted for a range of Q values (Figure 4.11). For a spheroid of fixed size, there exists a Q value at which a zero-concentration region develops precisely at the spheroid center. For C_{bulk}=10 μM, this Q value is $3.55x10^{-3}$, $2.0x10^{-3}$, and $1.28x10^{-3}$ for R=75, 100 and 125 μm, respectively. This reveals that, for a constant consumption rate, a diffusion coefficient that allows for complete penetration in a spheroid with a 75 μm radius (corresponding to day 2 EBs) would only allow diffusion to 35 and 25 μm into spheroids with 100 and 125 μm radii (corresponding to day 4 and 7 EBs, respectively). Thus, small changes in spheroid parameters, such as radius, diffusion coefficient, and consumption rate, have a pronounced effect on transport properties in this model. Finally, as Q increases in spheroids of all three sizes (Figure 4.11 A, B and C), the concentration curves shift to the right, indicating that consumption begins to dominate over diffusion.

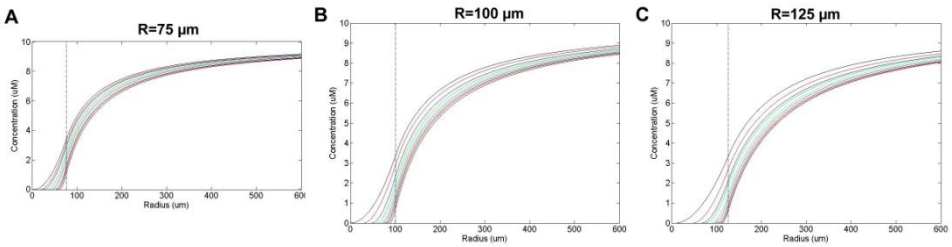

Figure 4.11. Concentration profiles in different size spheroids for a range of Q values. Concentration was plotted for 75, 100, and 125 µm radius spheroids, corresponding to day 2, 4 and 7 EB dimensions.

Discussion

In this study, ultrastructure and fluorescent dye uptake were analyzed in EBs formed via rotary orbital culture. Images acquired using SEM demonstrated the formation of a smooth EB surface and a shell-like outer layer. Multiple methods were used to quantify CTR labeling and diffusion in EBs, including *in situ* multi-photon microscopic imaging, frozen sectioning, and trypsin dissociation of EBs. Confocal imaging revealed incomplete CTR penetration within EBs, producing ring-like staining patterns, particularly in day 4 and 7 EBs, suggesting that diffusion becomes increasingly restricted with time. Fluorescent intensity profiles of confocal images illustrated that the ring-like staining became more prominent at deeper optical sections within EBs. Quantification of the percentage of labeled pixels in confocal images confirmed that the degree of staining decreased as a function of Z-depth. Analysis of cryosections also indicated that staining was most prevalent at the outermost EB regions. The percentage of labeled cells in dissociated EBs was highest at day 2 and decreased at days 4 and 7. A geometric spheroid model suggested a diffusion path length of ~30 µm in day 2 and 4

EBs, but a shorter length (~20 μm) in day 7 EBs. Modeling of diffusion based on Fick's second law confirmed that diffusion is increasingly limited as the spheroid dimensions increase, or as the ratio of consumption to diffusion increases. Collectively, these results demonstrate that free diffusion of solutes does not occur in cell spheroids, and that barriers inherent to EBs restrict transport in a temporal manner.

Previous studies have demonstrated that diffusive transport barriers exist in various multicellular spheroids, including EBs [22,23,207,208]. In general, the diffusion of relatively large molecules, including antibodies (~150,000 Da) [211], FITC-labeled dextrans (typically > 10,000 Da) [23] or even nanoparticles [122], has been reported. While this may be appropriate for cancer therapeutic applications, many ESC differentiation protocols require small, hydrophobic molecules such as retinoic acid (RA; 300.44 Da) [88,90,212]. Diffusion of RA, which generally passes through cell membranes and interacts with cellular binding proteins before binding retinoid receptors in the nucleus [213], is likely to have different properties than that of much larger, hydrophilic molecules. Here we show that the diffusion of a small, hydrophobic fluorescent dye (686.25 Da) is restricted within EBs, despite the membrane-permeability of this molecule. It is expected that the diffusion of larger, non-membrane-permeable molecules will be more severely restricted than CellTracker Red.

Directed differentiation protocols for ESCs generally rely on the addition of morphogenic factors in order to alter the gene and protein expression of cells in various states of potency. The ability of morphogens to uniformly access cells and evoke cellular changes may be important for the production of a pure population of a desired cell type. In development, morphogens are generally secreted from a source such that a gradient of

the signal is formed. This gradient is used to specify cell fate and ensure that proper patterning occurs in developing tissue [214,215]. The formation of morphogen gradients in ESC differentiation protocols *in vitro* may not be desirable, as a heterogeneous population specified by morphogen concentration will likely result. However, EB culture is advantageous over monolayer culture for a number of reasons, including the ability to scale production in bioreactors and the rich microenvironment provided by spheroid culture. For these reasons, methods to overcome diffusional barriers within EBs and present morphogens to differentiating cells uniformly and with temporal control are of great interest.

CHAPTER 5
INCORPORATION OF POLYMER MICROSPHERES WITHIN EMBRYOID BODIES USING ROTARY SUSPENSION CULTURE*

Introduction

Embryonic stem cells (ESCs) are pluripotent cells derived from the inner cell mass of developing blastocysts with the inherent ability to differentiate into all somatic cell types [2-5]. The pluripotent nature of ESCs has attracted interest in these cells as a renewable cell source for tissue engineering and other cell based therapies as well as for *in vitro* drug screening and studies in mammalian development [216-218]. Differentiation of ESCs can be induced using a variety of methods, including monolayer culture [14,42,219], co-culture with stromal cells [19,43,47], and aggregation into multicellular spheroids called embryoid bodies (EBs) [1,2,5]. The use of EBs for ESC differentiation is particularly common due to their ability to differentiate to cells from all three germ lineages and similarities to embryonic development; however, the microenvironment within EBs is complex and dynamic, resulting in spontaneous and heterogeneous differentiation events [21]. Efforts to control and direct differentiation of ESCs comprising EBs have traditionally focused on the addition of soluble morphogens to the culture media [88,220]. While soluble treatment can improve the efficiency of

---

*Modified from:
RL Carpenedo†, SA Seaman† and TC McDevitt. *Microsphere size effects on embryoid body incorporation and embryonic stem cell differentiation.* J Biomed Mater Res A (in press).
†These authors contributed equally, and
RL Carpenedo, AM Bratt-Leal, RA Marklein, SA Seaman, NJ Bowen, JF McDonald, TC McDevitt. *Homogeneous and organized differentiation within embryoid bodies induced by microsphere-mediated delivery of small molecules.* Biomaterials, 2009, 30(13): 2507-2515

directed differentiation to specific cell types, a high degree of heterogeneity is still common. Studies investigating the diffusion of molecules into tumor spheroids [123,211,221,222] and EBs [22,23,207] have shown that diffusion into cell spheroids is hindered by spheroid size, extracellular matrix (ECM) content, and tight cell junctions. The inability of morphogens to effectively penetrate cell spheroids limits the efficacy of soluble morphogen delivery strategies for EB-based differentiation.

Recently, two approaches have been examined to overcome the diffusional limitations posed by EBs. One approach has been to disrupt ECM in EBs using proteinases in order to enhance morphogen penetration into EBs [22]. However, ECM is an important component of the 3-D microenvironment of EBs, and its disruption may negatively impact cell organization, viability and differentiation. Additionally, the kinetics of ECM degradation and remodeling in EBs have not been characterized, indicating that the timescale during which enhanced diffusion into EBs is permitted is unknown. Alternatively, the diffusional barriers posed by the EB exterior can be circumvented by incorporating biodegradable polymer microspheres containing morphogenic molecules directly within the interior of EBs [223,224]. Such an approach facilitates the presentation of morphogens to ESCs directly within the EB microenvironment rather than relying on passive diffusion to transport morphogens into the EB interior. Additionally, microsphere-mediated delivery more closely replicates embryogenic processes in which morphogens are secreted locally to differentiating cells and tissues in a spatially and temporally controlled manner.

The objectives of this work were to incorporate polymer microspheres within EBs formed via rotary suspension culture, and evaluate the ability to control the level of

incorporation using both microsphere and mixing parameters (Figure 5.1). Distinct size populations of PLGA microsphere were fabricated and analyzed using scanning electron microscopy. Microspheres were mixed with ESCs in various ratios and at three rotary speeds (25, 40, and 55 RPM). Additionally, different adhesive proteins and polypeptides were used to coat microsphere surfaces prior to mixing. Incorporation of fluorescently-labeled microspheres was quantified as a function of initial mixing conditions using fluorescent spectroscopy. The morphology of EBs was assessed using hematoxylin and eosin (H&E) staining, and gene expression was analyzed using polymerase chain reaction (PCR). Cell viability within EBs containing microspheres was examined using Live/Dead and alamarBlue® assays. The results of the studies demonstrate that polymer microspheres can be incorporated into EBs under rotary suspension mixing conditions and that initial mixing parameters can be varied to control the degree of incorporation.

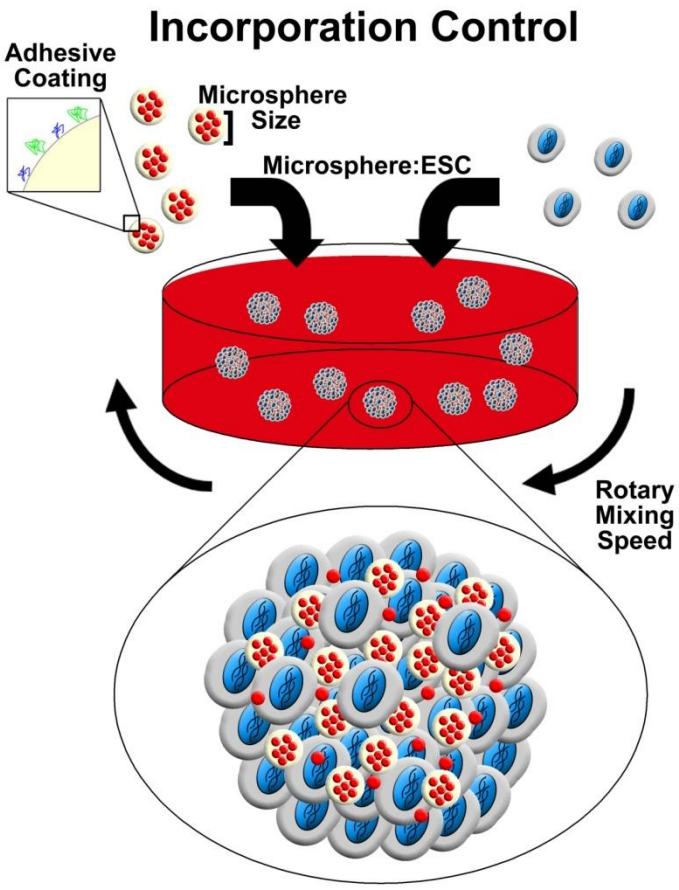

Figure 5.1. Schematic representation of parameters used to control microsphere incorporation. Microsphere coating, microsphere size, ratio of microspheres to cells and rotary mixing speed are all varied in order to achieve control over microsphere levels in the embryoid body microenvironment.

Methods

Microsphere fabrication

Poly(lactic-co-glycolic acid) (PLGA, 50:50, 0.55-0.75 dL/g, ester terminated, Absorbable Polymers International) microspheres encapsulating CellTracker™ Red (Molecular Probes, Eugene, OR) were fabricated using a single emulsion solvent evaporation technique as described previously [223]. Briefly, PLGA dissolved in dichloromethane (DCM) (20 mg/mL) was added to a 0.3% poly(vinyl alcohol) solution

and different sized microspheres were formulated by homogenization at 1000, 3000, 5000, or 12,000 RPM (Polytron PT 3100, Kinematica Inc, Bohemia, NY). The residual organic solvent was evaporated under light stirring for four hours before the microspheres were lyophilized for 24-36 hours (Freezone 4.5, Labconco, Kansas City, MO) and stored at -20°C until use.

Scanning electron microscopy

Microspheres suspended in dH_2O were attached to SEM stubs with carbon double-sided adhesive discs (SPI Supplies, West Chester, PA), frozen at -80ºC and lyophilized for ~6 hours until stubs were completely dehydrated. After lyophilization, stubs were gold sputter coated using a Polaron range sputter coater (Quorum Technologies, East Sussex, United Kingdom) and imaged using Hitachi S-800 SEM microscope. Microsphere size was quantified using ImageJ software to measure the diameter of a minimum of 100 microspheres for each group. The resulting distribution of microsphere sizes was plotted as a histogram with an equal number of bins between the largest and smallest values for each experimental group.

Embryonic stem cell culture

Embryonic stem cells (D3[1]) were grown on 0.1% gelatin coated tissue culture dishes in Dulbecco's modified Eagle's medium (DMEM) (Mediatech Inc., Manassas, VA). The media was supplemented with 15% fetal bovine serum (Atlanta Biologicals, Lawrenceville, GA), 0.1 mM 2-mercaptoethanol (MP Biomedicals, LLC, Solon, OH), 100 U/mL penicillin (MP Biomedicals, LLC, Solon, OH), 100 μg/mL streptomyocin (MP

Biomedicals, LLC, Solon, OH), 0.25 μg/mL amphotericin (MP Biomedicals, LLC, Solon, OH), 1x MEM nonessential amino acid solution (Lonza, Walkersville, MD), 2 mM L-glutamine (Mediatech, Inc., Manassas, VA), and 10^3 U/mL leukemia inhibitory factor (Millipore, Temecula, CA). Cells were passaged routinely every 2-3 days before reaching 70% confluence.

Embryoid body formation

To initiate formation of EBs containing PLGA microspheres, microspheres were first coated with an adhesive substrate and then mixed with ESCs under rotary mixing conditions. For studies on microsphere coating, microspheres were suspended in either PBS (uncoated), poly(L-lysine) (PLL, 1 mg/mL), gelatin (0.1%) or laminin (0.71 mg/mL, Invitrogen) and placed on a rotisserie rotator at 37°C for 3 hours. Studies on microsphere size were performed by suspending equal masses of the different size microspheres in a 0.1% gelatin solution. Coated microspheres were collected by centrifugation at 3000 RPM for five minutes and resuspended in differentiation media (ESC media without LIF). Embryonic stem cell colonies were dissociated into single cells with a 0.05% trypsin-EDTA solution and resuspended in 10 mL of differentiation media (2×10^5 cells/mL final concentration) with coated microspheres in 100 mm bacteriological-grade Petri dishes. The ratio of microspheres to cells was controlled by varying the volume of resuspended microspheres added to the Petri dishes. Embryoid body formation was initiated by placing dishes on an orbital rotary shaker set at 25, 40 or 55 rotations per minute (RPM) [68]. Phase images of EBs were acquired after two days using a Nikon TE 2000 inverted microscope equipped with a SpotFLEX (Diagnostic Instruments)

camera. Image J software was used to quantify the cross-sectional area of EBs formed with and without microspheres.

Microsphere incorporation quantification

After two days of rotary suspension culture, EBs were collected by gravity-induced sedimentation in conical tubes, spent media containing unincorporated microspheres was aspirated, and EBs were resuspended in 10 mL of fresh media. Phase and fluorescent images were obtained as described above. A fraction of the EBs (1/10) were counted using a Nikon TE 2000 inverted microscope after being suspended in a 60:40 PBS:glycerol solution. The remaining EBs were suspended in 5% SDS 0.1M NaOH solution and rotated overnight at 37°C in order to lyse the EBs and hydrolyze the microspheres to release encapsulated fluorescent dye (CellTracker^{TM} Red). The number of microspheres incorporated within EBs was determined using a standard curve relating fluorescence intensity to a known number of microspheres hydrolyzed in NaOH/SDS overnight at 37°C. Fluorescence readings were acquired with a microplate reader (SpectraMax M2^{e}, 586 nm excitation, 613 nm emission) and average fluorescence readings were plotted against initial microsphere concentration to determine the average number of incorporated microspheres per EB.

Confocal microscopy analysis

EBs formed at 40 RPM in a 2:1 (gelatin-coated, CellTracker^{TM} Red-loaded microsphere:ESC) ratio were collected after 2 days. EBs were counterstained for 30 minutes at 37°C in 5 μM CellTracker^{TM} Green (Molecular Probes) in serum-free media.

The CellTracker™ staining solution was removed and EBs were cultured for an additional 30 minutes in full differentiation media prior to imaging. Images were acquired in Z-stacks with 5 µm optical sections using a Zeiss LSM 510 confocal microscope. Additionally, EBs containing different size microspheres were harvested after 2 and 7 days of differentiation, fixed in 10% formalin for 30 minutes at room temperature on a rotisserie rotator, rinsed three times in PBS and permeabilized in a 1% Triton/PBS solution for 10 minutes with rotation. The fixed EB samples were stained with a 1:50 Phalloidin (FITC) (Alexis Biochemicals, San Diego, CA) and Hoechst (10 µg/mL) solution in PBS for 30 minutes. Samples were stored in PBS at 4ºC until imaging was performed on a Zeiss LSM 510 confocal microscope.

Histological analysis

Embryoid bodies with incorporated microspheres were harvested at days 7 and 10 of differentiation and fixed in 10% formalin for 30 minutes on a rotisserie rotator at room temperature. Following fixation, the samples were washed three times with PBS and re-suspended in HistoGel (Richard-Allan Scientific, Kalamazoo, MI). Fixed samples were dehydrated in a series of graduated alcohol solutions (70-100%) and xylene prior to being embedded in paraffin. Sections (5 µm) were stained with hematoxylin and eosin (H&E) and imaged using a Nikon 80i microscope with a SpotFLEX camera.

Polymerase Chain Reaction

RNA was extracted from undifferentiated ES cells on day 0 and from EBs on days 4, 7, and 10 using the RNeasy Mini kit (Qiagen Incorporated, Valencia, CA,

http://www.qiagen.com). Reverse transcription for complementary DNA synthesis was performed with 1 µg of RNA per sample using the iScript cDNA synthesis kit (Bio-Rad, Hercules, CA, http://www.bio-rad.com), and real-time PCR was performed with SYBR green technology on the MyiQ cycler (Bio-Rad). Forward and reverse primers for *Oct4*, *Brachyury-T* (B-T), *α-fetoprotein* (AFP), and *glyceraldhyde-3-phosphate-dehydrogenase* (GAPDH) were designed with Beacon Designer software, purchased from Invitrogen and validated with appropriate controls. *Oct4* relative gene expression was quantified as compared to undifferentiated ES cell expression levels using the Pfaffl method of quantification [174]. *Brachyury-T* and *AFP* concentrations were calculated using standard curves and normalized to GAPDH expression levels.

Live/Dead assay

EBs were formed as described above, and after 2, 4, 7, and 10 days of differentiation, cell viability was assessed using LIVE/DEAD® staining (Molecular Probes Inc., Eugene, OR, http://probes.invitrogen.com). Samples were incubated in serum-free, phenol red-free media containing 2µM calcein AM and 4µM ethidium homodimer I at room temperature for 45 minutes. EBs were then washed three times with PBS, resuspended in fresh PBS, transferred to 6-well plates and immediately imaged using fluorescent microscopy.

AlamarBlue® assay

Equal quantities of untreated EBs and EBs formed from 1:2, 1:1, and 2:1 mixing ratios of microspheres to ESCs were collected after 2, 4, 7 and 10 days of differentiation.

The EBs were incubated in 10% alamarBlue® solution (Biosource) for 6 hours in a 37°C, 5% CO_2 incubator. Supernatant (100 µL) was collected from each sample and analyzed with a fluorescent plate reader (excitation: 545 nm, emission: 590 nm). After subtracting the blank reading (naïve alamarBlue® solution), emission values were normalized to the average of untreated EB readings at each time point to calculate relative viability.

Statistical analysis

Values are reported as mean ± standard deviation (n=3). Statistical significance was determined using one or two way ANOVA coupled with Tukey's post hoc analysis using Systat (v12, Systat Software Inc.).

Results

Microsphere analysis

The morphology and size distribution of different sized microspheres were assessed in order to determine the relative sizes of the microspheres fabricated at different homogenization speeds. AS expected, microspheres were round with smooth surfaces and the average size of the microsphere populations decreased with increasing homogenization speed (Figure 5.2 A-C, Figure 5.3A). The lowest homogenization setting (1000 RPM) yielded microspheres with an average diameter of 10.9 ± 3.2 µm (Figure 5.2D), whereas 5000 RPM produced 3.01 ±0.71 µm (Figure 5.2E), and 12,000 RPM yielded microspheres with an average diameter of 1.09 ± 0.27 µm (Figure 5.2F). Additionally, homogenization at 3000 RPM produced microspheres with an average

diameter of 7.8 ± 1.8μm (Figure 5.3B). These results demonstrated that microsphere size could be controlled through simple modulation of homogenization speed.

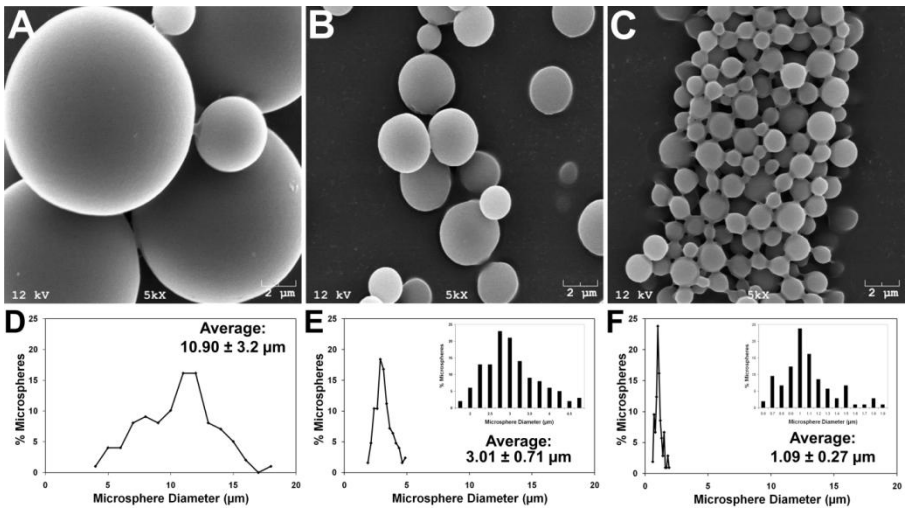

Figure 5.2. Scanning electron microscopy (SEM) and size distribution analysis of PLGA microspheres. The average diameter of the microspheres was controlled by varying the homogenization speed during fabrication of the microspheres. Microspheres were homogenized at 1000 RPM (A), 5000 RPM (B), and 12000 RPM (C). Increased homogenization speeds yielded smaller average size microspheres (D-F).

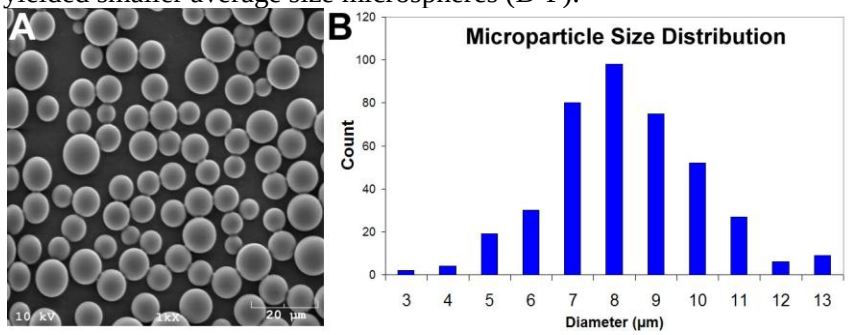

Figure 5.3. Characterization of microsphere formed at 3000 RPM. Microspheres displayed smooth spherical morphology in SEM micrographs (A). Image analysis determined the microsphere diameter to be 7.8 ± 1.8 μm (mean ± standard deviation) (B).

Incorporation of microspheres within EBs

Microsphere coating

Initially, microspheres fabricated at 3000 RPM (8 μm mean diameter) were mixed with ESCs at 40 RPM rotary speed in a 2:1 (microspheres to ESCs) ratio. Prior to

mixing, microspheres were coated with PBS (i.e. uncoated microspheres), poly(L-lysine) (PLL), gelatin or laminin. EB formation and microsphere incorporation were assessed after 2 days of rotary mixing of microspheres with ESCs and compared to ESCs alone. Similar to previous results, rotary orbital culture produced relatively uniform populations of EBs (Figure 5.4). Quantitative analysis of microsphere incorporation indicated that uncoated and PLL coated microspheres were incorporated with poor efficiency, with 17 ± 11 and 14 ± 4 microspheres per EBs, respectively (Figure 5.4). Gelatin and laminin coating each enhanced the uptake of microspheres into EBs relative to uncoated and PLL coated microspheres and resulted in 112 ± 50 and 160 ± 5 microspheres per EBs ($p<0.01$ for gelatin and laminin compared to both uncoated and PLL). However, incorporation of gelatin and laminin coated microspheres was not statistically different ($p=0.180$); for all subsequent incorporation studies, gelatin coating was used.

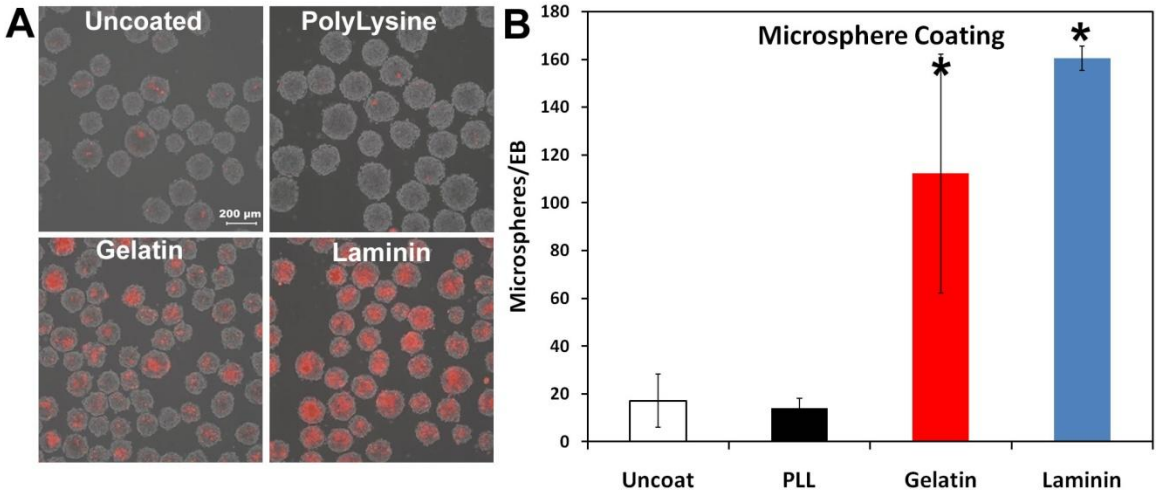

Figure 5.4 Microsphere incorporation as a function of adhesive coating. Fluorescent images of CellTracker™ Red-loaded microspheres with different adhesive coatings incorporated within EBs (A). Quantification of microsphere incorporation confirmed that gelatin and laminin coating enhanced microsphere incorporation relative to uncoated or PLL coated microspheres (B). Scale bar = 200µm. * denotes $p<0.01$ compared to uncoated and PLL.

Microsphere size

In order to quantify the relative incorporation of the different size microspheres within EBs, ESCs were mixed with the 1, 3, and 11 μm (average diameter) microspheres using rotary orbital shaking. The addition of equivalent masses of the different size microsphere populations did not affect the average yield of EBs (Figure 5.5A), and the average size of the resulting EBs did not change significantly with or without microspheres, regardless of the size of the microspheres (Figure 5.5B). Interestingly, microscopic images revealed more intense and widespread fluorescent signal emanating from EBs as microsphere size decreased (Figure 5.6). Quantitative spectroscopic analysis of lysed EB populations indicated that the number of incorporated particles was significantly different for each of the different size microsphere populations examined ($p < 0.001$). The microspheres with an average diameter of 11 μm yielded 72 ± 7 microspheres per EB, whereas microspheres with average diameters of 3 μm and 1 μm yielded 295 ± 11 and 411 ± 21 microspheres per EB, respectively (Figure 5.6B). Altogether, the analysis of microsphere incorporation within EBs indicated that decreasing the average size of microspheres from 11 μm to 1 μm significantly increased the incorporation within EBs.

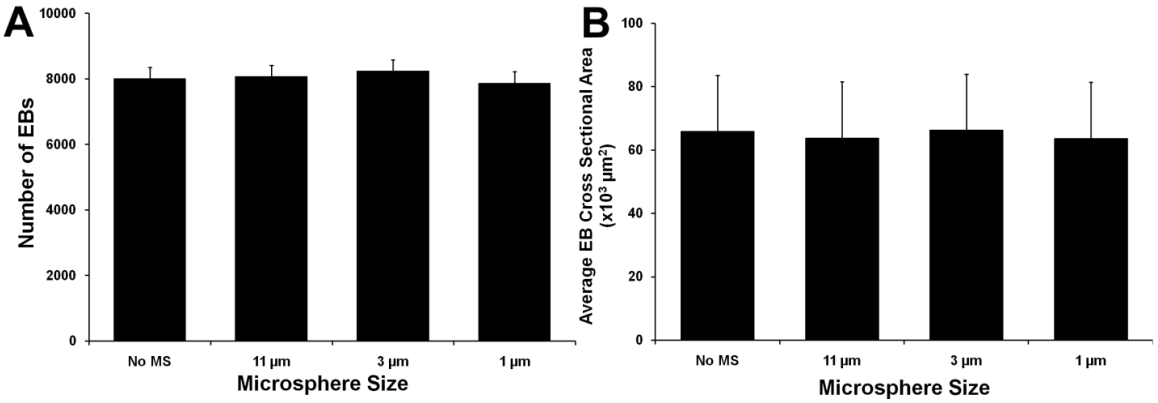

Figure 5.5. EB size and Yield. Average number of EBs formed and average cross sectional area of EBs for different treatment groups. Statistical significance was not observed between the treatment groups for number of EBs (A) or average cross-sectional area (B).

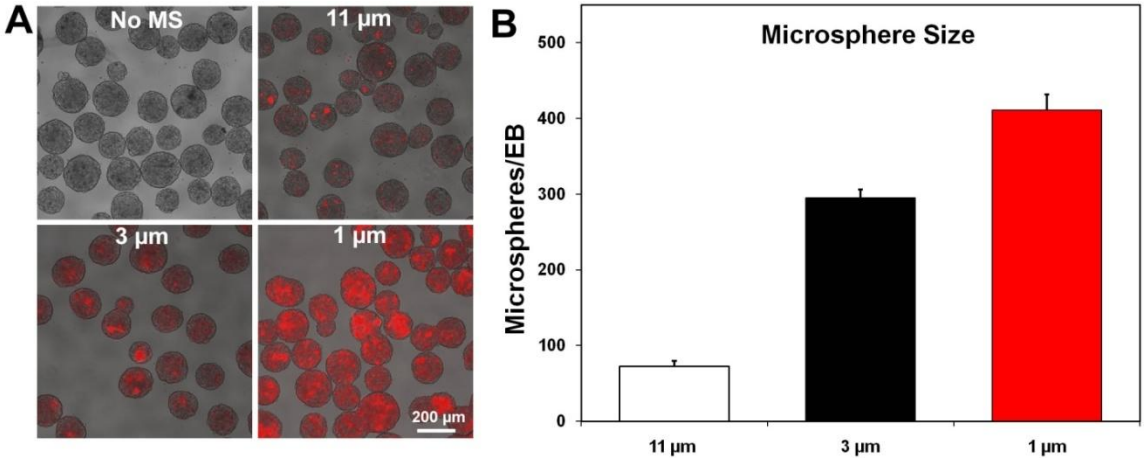

Figure 5.6. Incorporation of microspheres within EBs as a function of size. Embryoid bodies were formed with no microspheres or 11, 3 or, 1 µm microspheres and imaged with fluorescent microscopy (merged with phase images) (A). Incorporation of microspheres within EBs decreased as the average diameter of the microspheres increased (B). All groups are statistically different ($p<0.001$). Scale bar = 200 µm.

Ratio and speed

To further evaluate the ability to control microsphere integration within EBs, the extent of microsphere incorporation was examined as a function of microsphere to cell ratio and orbital mixing speed. Gelatin-coated CellTracker™ Red microspheres were

mixed with ESCs at a range of microsphere to cell ratios (1:2, 2:1, 5:1) and three rotary mixing speeds (25, 40, 55 RPM). Differences in microsphere incorporation for the speeds and mixing ratios were observed using fluorescent microscopy and quantified using fluorescent spectroscopy of lysed EBs (Figure 5.7A). Higher microsphere to cell ratios and slower rotary speeds were found to facilitate greater microsphere incorporation within EBs. However, normalizing microsphere incorporation to average EB volume demonstrated that EBs formed at 25 RPM (slowest speed and largest EBs; see Figure 3.1B) had the lowest level of incorporation, while EBs formed at 40 RPM had the highest incorporation (data not shown), indicating that the greatest microsphere density within EBs was achieved at 40 RPM. Incorporation of microspheres mixed with ESCs at 40 RPM was more rigorously studied using five ratios of microspheres to cells (1:4, 1:2, 1:1, 2:1, and 4:1). No differences were observed between 1:4 and 1:2 mixing ratios, nor were differences seen between 2:1 and 4:1 ($p=1$ for both comparisons). Statistical differences were observed between 1:2 (25 ± 5 microspheres per EB) and 2:1 (92 ± 17) ($p<0.05$). The 1:1 mixing ratio fell between these two values (55 ± 7), yet incorporation was not statistically different than either the 1:2 or 2:1 group. These studies suggest that while mixing ratio of microspheres to cells can be used to control incorporation, saturation occurs above a 2:1 ratio, and a linear relationship only exists between 1:2 and 2:1 ratios.

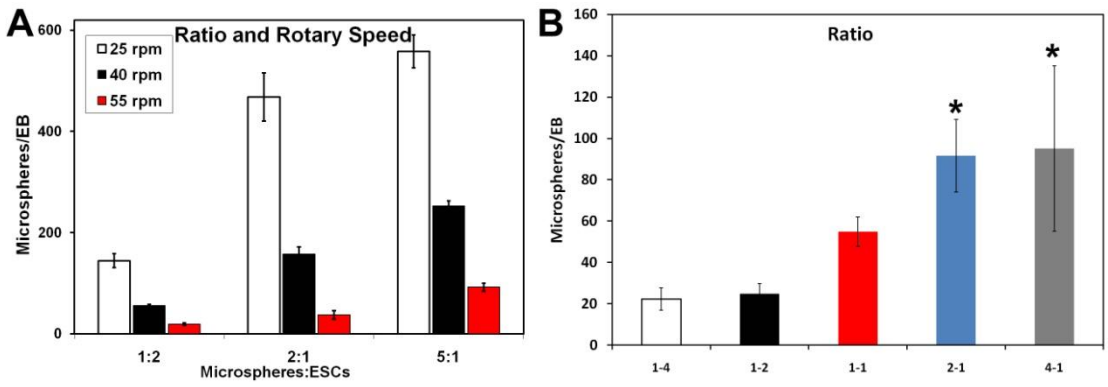

Figure 5.7. Influence of mixing speed and microsphere to cell ratio on incorporation. Decreasing rotary speed and increasing microsphere to cell ratio resulted in increased incorporation within EBs (A). Examination of a broader range of ratios at 40 RPM mixing revealed a linear relationship between ratio and incorporation between 1:2 and 2:1 (B). * denotes $p<0.05$ compared to 1:4 and 1:2.

Spatial distribution of microspheres within embryoid bodies

While spectroscopic analysis of lysed EB populations gave quantitative data on microsphere incorporation, microsphere localization within EBs could not be assessed by this technique. In order to examine the spatial distribution of microspheres incorporated within EBs, fluorescently-labeled EBs and microspheres were imaged using confocal microscopy. After 2 days, EBs containing CellTracker™ Red-labeled gelatin-coated microspheres (8 µm) mixed in a 2:1 (microsphere:cell) ratio at 40 RPM were counterstained with CellTracker™ Green prior to imaging. Counterstaining was limited to the outermost 1-2 cell layers (Figure 5.8) of most EBs, which indicated that the shell-like EB exterior impeded diffusion of molecules into the interior. In contrast, red microspheres appeared at all focal planes within the EBs, demonstrating that microspheres were distributed throughout the entire depth of the EBs, as opposed to preferentially residing at the EB surface or core.

Next, to investigate the distribution of the different sized microspheres throughout EBs, confocal imaging of fixed, permeabilized EBs was performed. After 2 days of rotary culture, microspheres containing CellTracker^{TM} Red were visible in optical sections distributed throughout EBs formed with the different size microspheres (Figure 5.9B-D). Estimates of microspheres per EB, based on the number of visible microspheres within optical sections, scaled with the results obtained via quantitative analysis for the three sizes of microspheres above (Figure 5.5B). Additionally, microspheres appeared to reside within the interstitial space rather than becoming internalized by ESCs. Interestingly, although ESCs were initially mixed with microspheres with distinct size distributions (Figure 5.2D-F), the observed size of microspheres incorporated within EBs was similar in confocal sections for each of the three treatment groups (Figure 5.9B-D). Image analysis revealed that EBs formed by mixing ESCs with 11 μm average diameter microspheres contained particles with an average diameter of 4.3 μm (4.3 ± 1.2), and similarly, the average diameter of incorporated microspheres from the 3 μm population was 4.0 μm (4.0 ± 1.1). In addition, the average diameter of the incorporated microspheres from the 1 μm population was actually 2.7 μm (2.7 ± 1.0). After 7 days of differentiation, the spatial distributions of microspheres within EBs were similar to those observed after 2 days (Figure 5.9E-H) and similar densities of fluorescent microspheres were observed in the interstitial spaces between cells, indicating that many of the particles remained largely intact for the first week of culture. Altogether these data suggest that although the microsphere populations examined were of three distinct size distributions, microspheres in the range of 2-5 μm appeared to be preferentially incorporated within EBs using rotary orbital mixing.

However, fluorescent image analysis of microsphere diameters from confocal sections of EBs after 2 and 7 days may not provide an accurate assessment of the size of microspheres that were initially incorporated into EBs, as CellTracker™ Red is released and PLGA degrades over time, both of which may affect the observed microsphere size in confocal images.

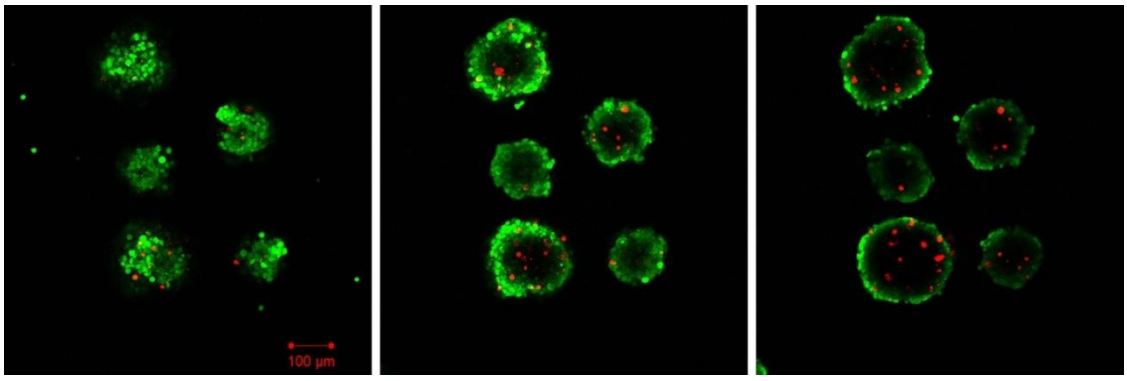

Figure 5.8. Confocal microscopy of EBs. EBs were formed at 40 RPM with a 2:1 ratio of 8 µm microspheres to cells. Microspheres labeled with CellTracker™ Red were observed in multiple focal planes (30 µm between images), while soluble treatment of CellTracker™ Green labeled the outermost 1-2 cell layers. Scale bar = 100 µm.

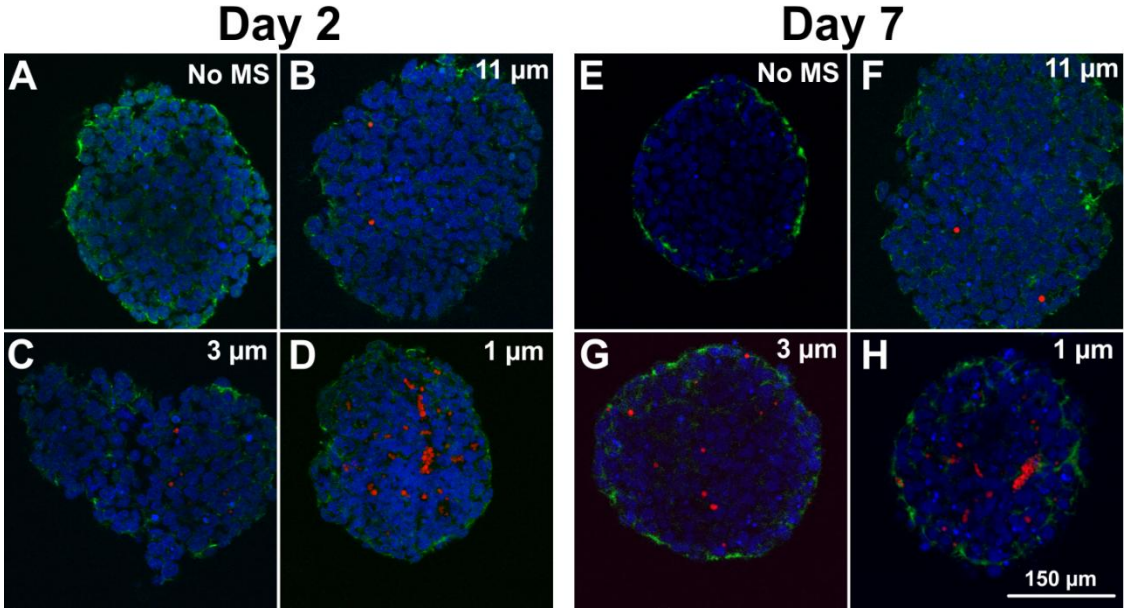

Figure 5.9. Spatial distribution of different size microspheres within EBs. Confocal analysis was performed on EBs with CellTracker™ Red microspheres of different sizes after 2 (A-D) or 7 (E-H) days of differentiation with counterstaining for F-actin (FITC-Phalloidin) and nuclei (Hoechst). Embryoid bodies were formed with no microspheres (A, E), 11 µm microspheres (B, F), 3 µm microspheres (C, G), and 1 µm microspheres (D, H). Scale bar = 150 µm.

Morphology

In order to assess cell organization and gross EB morphology in response to incorporation of PLGA microspheres, H&E staining was performed on fixed EB sections. EBs containing 8 μm microspheres formed from three different mixing ratios (1:2, 1:1, and 2:1; Figure 5.10) were examined, as were EBs containing different size microspheres (11, 3, and 1 μm; Figure 5.11). After 7 days of differentiation, untreated EBs and EBs containing 8 μm microspheres in the three ratios appeared similar with no notable gross morphological differences observed (Figure 5.10). Additionally, EBs collected after 10 days also appeared similar in all the groups studied, and comparison of day 7 and day 10 EBs revealed no EB growth or striking cell reorganization (indicative of differentiation). Interestingly, subtle differences were noted in EB size, with the 1:2 EBs appearing slightly larger than the other groups. Quantitative analysis of phase images acquired at day 10 revealed that untreated EBs were significantly smaller than all other EBs, yet no other statistical differences were observed. Examination of EBs containing different size microspheres revealed that the EBs were able to form regular spheroids (i.e. similar appearance to EBs with no microspheres) regardless of the microsphere size (Figure 5.11). EBs containing the largest microspheres (11 μm) did not display large void spaces, as might have been expected; however, EBs containing the smallest microspheres (1 μm) appeared to be more densely packed than other groups, including untreated EBs. Day 10 EBs appeared larger and less densely packed than the corresponding day 7 EBs, but no notable differences were observed among the treatment groups.

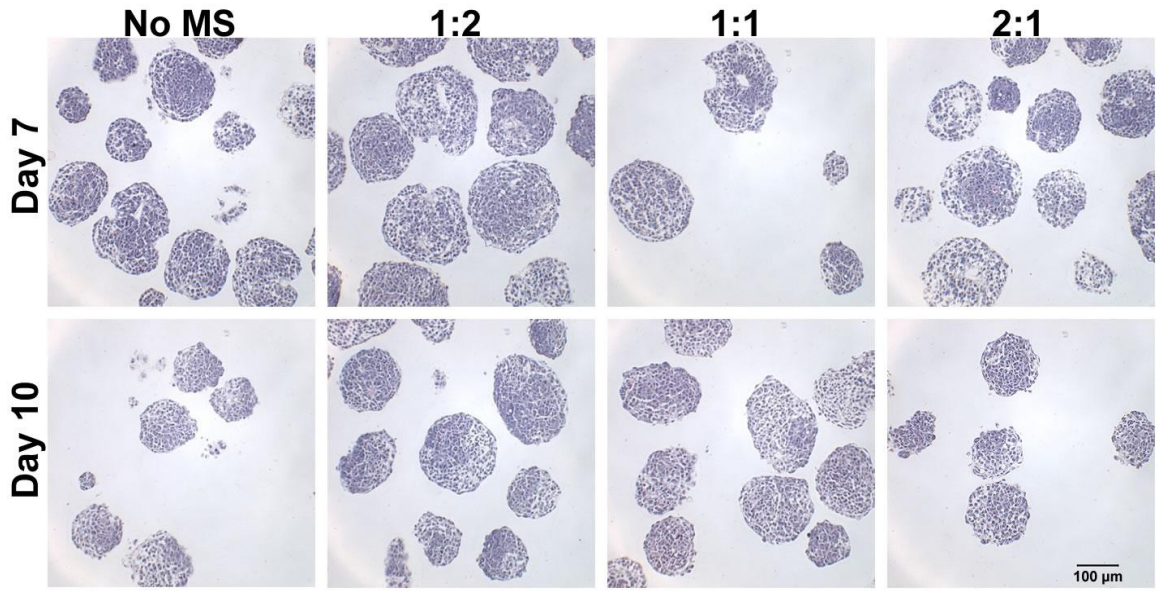

Figure 5.10. Hematoxylin and eosin staining of EBs formed from different mixing ratios. Incorporation of microspheres did not appear to significantly affect cell organization or overall EB morphology.

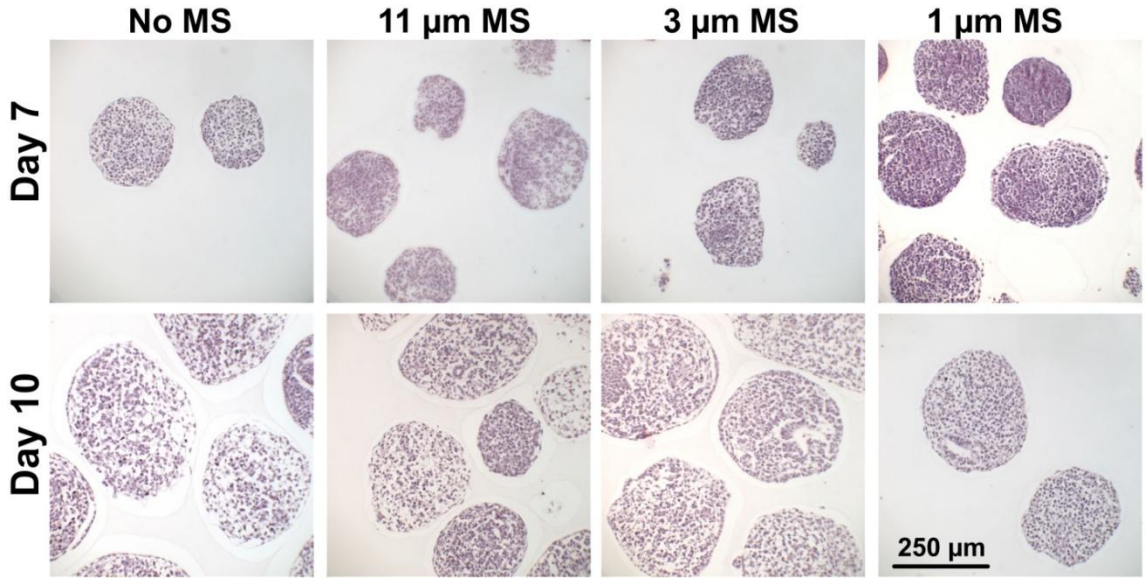

Figure 5.11. Morphology of EBs containing different size microspheres. EBs containing no microspheres or 11, 3, or 1 µm microspheres were stained with H&E after 7 and 10 days. Overall morphology appeared similar among different treatments.

Gene expression

While only subtle differences were observed in morphology among EBs formed from different ratios of microspheres to cells, further analysis was undertaken in order to determine whether differentiation trajectory was being modulated through microsphere incorporation (Figure 5.12). Expression of *Oct4*, a transcription factor associated with pluripotency, was assessed in untreated EBs and EBs from the three mixing ratios (1:21:1, and 2:1) after 4, 7 and 10 days. Although no statistically significant differences were observed, levels of *Oct4* expression were consistently higher in EBs containing the most microspheres, particularly after 4 and 7 days, compared to untreated EBs. *Brachyury T*, a transcription factor involved in primitive streak formation and transiently expressed in early EBs, was observed to increase in all EBs after 4 and 7 days, suggesting that differentiation to mesoderm and/or endoderm lineages is taking place. No differences were observed in *Brachyury T* expression among all the treatment groups, indicating that microspheres neither inhibit nor promote mesendoderm differentiation. *Alpha-fetoprotein* (AFP), a protein expressed in primitive as well as definitive endoderm cells, increased in all groups after 10 days of differentiation. Significant differences were observed in the 1:2 treatment group relative to untreated EBs and the 2:1 group ($p=0.025$ and 0.036, respectively). Expression of *AFP* appeared to decrease as the level of microsphere incorporation decreased, suggesting that a low level of PLGA microspheres may promote endoderm differentiation in EBs.

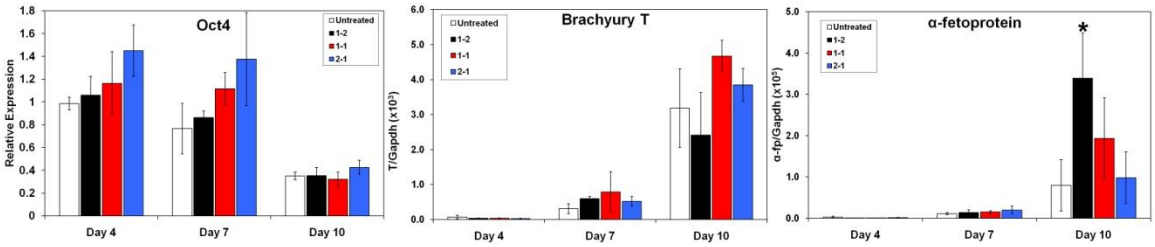

Figure 5.12. Gene expression analysis of EBs containing microspheres. EBs containing different levels of microspheres were analyzed for pluripotent (*Oct4*), mesendoderm (*Brachyury T*) and endoderm (*AFP*) markers. *denotes $p<0.05$ compared to untreated and 2:1.

Cell viability within embryoid bodies

Finally, to determine whether microsphere incorporation within EBs had an impact on cell metabolism and cell death, alamarBlue® and Live/Dead assays were performed. After 2, 4, 7 and 10 days, EBs formed from 1:2, 1:1, and 2:1 mixing ratios as well as untreated EBs were collected and stained with Live/Dead (Figure 5.13). At all days studied, a majority of the cells in EBs from all experimental groups were viable, as indicated by intense Calcein staining (green fluorescence, indicating live cells). Dead cells (red fluorescence) were also observed in all groups; however, the presence of microspheres did not appear to create a preponderance of dead cells. In order to quantitatively assess cell viability among populations of EBs, an alamarBlue® assay was utilized. Data was normalized to untreated EBs for all the experimental groups at each time point. No negative impact on cell viability from microsphere incorporation was observed. In fact, after 7 and 10 days, small though statistically insignificant increases in cell metabolic activity were observed in microsphere-containing EBs. Together, these data suggest that PLGA microspheres neither inhibit cell metabolism nor promote cell death in EBs.

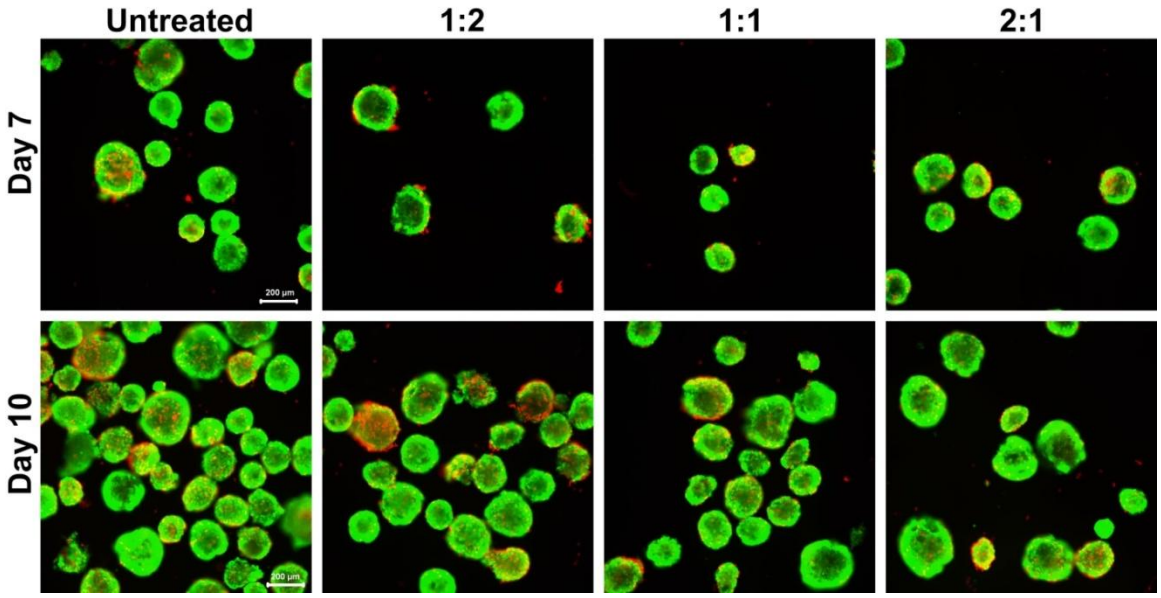

Figure 5.13. Live/Dead staining of embryoid bodies. Majority of cells were viable (green stain) in all groups at both 7 and 10 days, though dead cells (red) were found within all EBs.

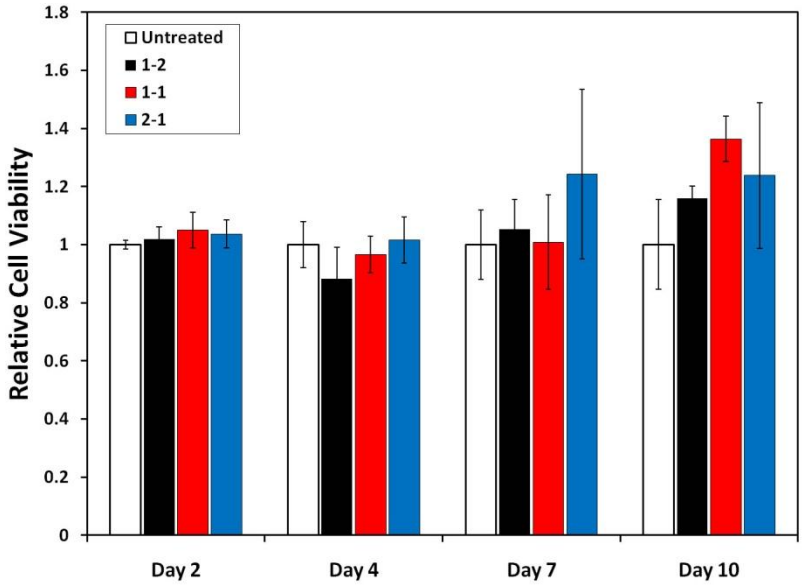

Figure 5.14. Cell viability within embryoid bodies. AlamarBlue® was used to assess metabolic activity in EBs containing different ratios of microspheres to cells. Incorporation of microspheres did not negatively impact metabolic activity.

Discussion

In this study, the ability to modulate microsphere incorporation within EBs as a function of various mixing conditions was examined. Different microsphere coatings, microsphere sizes, ratios of microspheres to ESCs, and rotary mixing speeds were all evaluated for their capacity in controlling microsphere incorporation within EBs. Quantitative analysis of incorporation demonstrated that gelatin and laminin were effective in enhancing microsphere incorporation, while uncoated and poly(lysine) coated microspheres were incorporated with low efficiency. The size of PLGA microspheres had a significant effect on incorporation, as smaller microspheres were incorporated to a greater extent than larger microspheres. The ratio of microspheres to cells used to initiate EB formation was found to modulate incorporation, with higher ratios inducing greater incorporation. Rotary mixing speed also impacted microspheres per EB, as the intermediate speed (40 RPM) promoted the greatest density while the slowest speed (25 RPM) induced the lowest microsphere density. Confocal analysis revealed that incorporated microspheres were distributed throughout EBs. Examination of EB morphology, differentiation, and viability revealed few differences among EBs containing different levels of incorporated microspheres, demonstrating that the presence of microspheres did not in and of itself significantly alter the course of EB formation and differentiation. These results suggest that PLGA microspheres can be safely incorporated within EBs without adverse effects, making this approach appealing for manipulation of differentiating stem cell microenvironments.

Multiple approaches for controlling microsphere incorporation were investigated in this study. While each approach (coating, size, ratio, and mixing speed) displayed

some degree of success in controlling incorporation, some were more effective than others. The inability of PLL coating to enhance incorporation was an unexpected result, as the polycation was expected to interact with the net negatively charged cell membranes. Protein coatings (gelatin and laminin) were significantly more effective in promoting incorporation. In additional studies, gelatin, laminin and fibronectin coatings were observed to induce similar levels of incorporation, suggesting that microspheres are incorporated within EBs via an integrin-mediated mechanism. Coating of microspheres with specific integrin-binding domains may provide a novel route for directing ESC differentiation trajectory. Modulation of the rotary speed at which ESCs and microspheres were mixed dramatically affected the size of the EBs formed (see Figure 3.1B); 25 RPM produced very large EBs, while 40 and 55 RPM produced progressively smaller EBs. While the absolute number of microspheres incorporated was significantly higher in 25 RPM EBs than either 40 or 55, when normalized to EB volume, incorporation density was highest in 40 RPM EBs. This suggests that slower speeds promote aggregation of large cells clusters, but the more rigorous mixing at faster speeds enhances the integration of microspheres within the cell clusters. The seeding ratio of microspheres to cells was also observed to affect incorporation within EBs. Interestingly, incorporation was controlled within a relatively narrow range; incorporation reached a minimum at 1:2 and a maximum at 2:1. Ratios outside of this range did not significantly affect incorporation. Overall, these results demonstrate the diverse toolset that can be used to engineer microsphere-mediated regulation of EB microenvironments.

Control over stem cell microenvironments is an important concept for both studying basic mechanisms involved in differentiation and self-renewal and applying

stem cells for various therapeutic technologies. A multitude of techniques have been utilized in order to control stem cell environments in two dimensions, including micropatterning and microfluidics. Micropatterning provides a power means for controlling cell-cell and cell-matrix interactions [225-228], two key concepts in dictating cell fate [21,37]. The relative size and positions of mouse embryonic fibroblasts (MEFs) and ESCs in self renewal cultures can be controlled through the use of micropatterning [229,230], which in turn allows for control over the degree of homotypic and heterotypic cell-cell interactions, a concept known to be important for cell phenotype [231,232]. The same approach can be applied for controlling ESC interactions with stromal cells for directed differentiation [233]. Micropatterning has also been applied to control the size of ESC colonies in feeder-free conditions in order to modulate the cell differentiation trajectory [73,234,235]. Interactions of ESCs with an array of biomaterials synthesized on the nanoliter scale in high throughput fashion have also been studied using micropatterning techniques[236], as have interactions of various stem cells with ECM [138,237,238]. Microfluidics is another powerful technique for controlling stem cell environments [239-241], as precise control over shear forces and nutrient, growth factor, and cytokine delivery can be achieved [242-245]. However, both micropatterning and microfluidics are generally applied to cell monolayers. Three-dimensional systems more accurately replicate the *in vivo* niche and therefore are a more relevant approach for studying stem cell biology and applying stem cell technologies.

Microencapsulation is a common technique for culture and delivery of multiple cell types, particularly those that are commonly grown as spheroids. Microencapsulation can be used to isolate spheroids from one another, allowing for spheroid size control,

inhibition of agglomeration, which alleviates issues with reduced cell viability, and large-scale culture (i.e. bioreactors) [70,246]. The materials used for encapsulation can be tailored for specific applications. For example, semi-interpenetrating polymer networks (SIPNs) with functionalized peptide sequences have been successfully utilized for propagation of ESCs in the absence of MEF feeder layers [142]. Alginate hydrogels were shown to influence differentiation in EBs in a dose dependant manner, as low concentrations produced cystic EBs with spontaneously beating foci while higher concentrations evoked neither of these responses [247]. Microbeads made from alginate-PLL were shown to facilitate hepatocyte differentiation of encapsulated ESCs, as indicated by urea secretion and intracellular albumin levels [248]. Additionally, RGD-modified PEG hydrogels were shown to facilitate chondrogenic differentiation of ESC-derived MSC-like cells [76].

Biodegradable polymer microspheres have previously been incorporated within cell spheroids in order to modulate cell survival and differentiation. PLGA microspheres containing nerve growth factor (NGF) were incorporated within spheroids of fetal rat brain cells, which were subsequently transplanted into adult rats [156]. Cell survival was enhanced by the presence of microspheres, but the differentiation of cells was not assessed. Interestingly, PLGA microspheres coated with poly(L-lysine) were readily incorporated within spheroids in a dose-dependent fashion; however, incorporation is reported in relative rather than absolute values, so the data cannot be directly compared to the current study. PLGA microspheres were also incorporated into human EBs [224]. Different size microspheres were used (25, 6 and 0.24 μm) and while incorporation was not assessed quantitatively, fluorescent imaging suggested that small microspheres were

incorporated more effectively. The smallest particles, however, were shown to be internalized by ESCs comprising the EBs. In the current study, internalization was not observed, even with the smallest microsphere diameter (1 μm). This likely reflects the size-dependence of particle uptake, which has also been observed in other cell types [249,250]. Additionally, in contrast to the rotary method used in the current study, a forced aggregation technique was used to make EBs, making the coating of microspheres unnecessary.

An important result from this study was that the presence of microspheres within EBs did not significantly affect differentiation or viability. The degradation of PLGA by ester bond hydrolysis results in acidic products that in some applications has shown to have negative effects on cell viability [251]. However, H&E sections of EBs containing microspheres did not indicate development of necrotic regions. Assessment of cell viability through both Live/Dead and alamarBlue® assays indicated that cell death was not enhanced by incorporation of microspheres. Analysis of gene expression indicated that differentiation was also similar to that in untreated EBs. However, a few subtle differences were observed between the groups. *Oct4* levels showed dose-dependent (though statistically insignificant) expression after 4 and 7 days, with higher levels of microspheres displaying the highest expression, indicating that microspheres may slightly delay down-regulation of this gene. *Afp* levels, however, were highest in the 1:2 EBs after 10 days and progressively decreased as the ratio increased. Together, these results suggest that any inhibition of differentiation that may occur during the first 4-7 days of differentiation is overcome by day 10, and that the presence of microspheres may even enhance endoderm differentiation. However, the relative contributions of PLGA

degradation byproducts, disruption of cell-cell interactions, and addition of cell-matrix interactions is not known. In general, the relatively low response elicited by microspheres incorporated in EBs is advantageous in that studies intended to examine the effect of morphogen delivery via microspheres will not be significantly confounded by the effects of microspheres alone. Future work may include functionalization of microsphere surfaces in order to direct cell differentiation within EBs.

CHAPTER 6

HOMOGENEOUS AND ORGANIZED DIFFERENTIATION WITHIN EMBRYOID BODIES INDUCED BY MICROSPHERE-MEDIATED DELIVERY OF SMALL MOLECULES*

Introduction

Pluripotent embryonic stem cells (ESCs) are a renewable cell source for studies of embryonic development, regenerative medicine and *in vitro* diagnostics. ESCs, derived from the inner cell mass of the blastocyst stage embryo [2-4], can be induced to differentiate via aggregation into multi-cellular spheroids referred to as embryoid bodies (EBs) [1]. Cells within EBs differentiate in response to a variety of environmental stimuli, including cell-cell adhesions, cell-matrix interactions [252], cytokines [13], growth factors [220], and small molecules [253]. Because the EB microenvironment is comprised of a complex mixture of these extracellular stimuli, differentiation within EBs is typically heterogeneous and spatially disorganized. Efforts to manipulate the EB environment and subsequent ESC differentiation have focused primarily on controlling media composition [220] and assembly of EBs using different culture methods [20];

---

*Modified from:
RL Carpenedo†, SA Seaman† and TC McDevitt. *Microsphere size effects on embryoid body incorporation and embryonic stem cell differentiation.* J Biomed Mater Res A (in press).
†These authors contributed equally, and
RL Carpenedo, AM Bratt-Leal, RA Marklein, SA Seaman, NJ Bowen, JF McDonald, TC McDevitt. *Homogeneous and organized differentiation within embryoid bodies induced by microsphere-mediated delivery of small molecules.* Biomaterials, 2009, 30(13): 2507-2515

however, precise control over the molecular milieu within the interior of EBs has not been achieved by such approaches [254].

During development, morphogens are secreted locally and presented to embryonic cells in a spatially and temporally controlled manner to direct appropriate differentiation and tissue formation [255-258]. *In vitro* strategies to deliver morphogenic factors to EBs, namely diffusion of supplemental media components, do not accurately replicate this process, with exogenous morphogens originating in the external fluid rather than within the cell spheroid. In addition, the diffusion of soluble factors into EBs may be restricted by the formation of an exterior shell composed of collagenous matrix and tight E-cadherin mediated cell-cell adhesions at the EB surface [22]. These fundamental challenges in morphogen presentation to ESCs limits the ability of EBs to accurately serve as controlled models of embryogenesis *in vitro* and perhaps limits the homogeneity of differentiated phenotypes that can be attained using EB differentiation methods. Engineering of biomaterials-based approaches has been used successfully to control the spatiotemporal presentation of morphogens to 3D assemblies of cells [156,259]. Thus, the use of biodegradable microspheres to deliver morphogens directly within EBs may enable production of more homogeneous populations of differentiated cells.

In this study, we describe the differentiation effects of spatially and temporally controlled presentation of morphogenic factors to ESCs comprising EBs from degradable biomaterials. Microsphere incorporation within EBs was assessed as a function of initial mixing conditions, and the release and cellular uptake of a fluorescent dye from incorporated microspheres was evaluated. The morphology, gene and protein expression, and ultrastructure of EBs containing retinoic acid (RA)-loaded poly(lactic-co-glycolic

acid) (PLGA) microspheres are reported. These studies demonstrate that biomaterials can be used to engineer the microenvironment within EBs to efficiently direct ESC differentiation, which may be applied in regenerative cell therapies, *in vitro* pharmaceutical screening and models of developmental biology.

Methods

Microsphere fabrication

Poly(lactic-co-glycolic acid) (PLGA, 50:50, 0.55-0.75 dL/g, ester terminated, Absorbable Polymers International) microspheres were fabricated using a water-in-oil single emulsion, as described [150]. Briefly, 200 mg PLGA was dissolved in dichloromethane (DCM) containing 50 µg CellTracker Red (Molecular Probes, Invitrogen Corp, Carlsbad, CA) or 600 µg RA (all trans, Acros Organics, Geel, Belgium), added to 0.3% PVA, and homogenized at 3000 rpm (Polytron PT 3100, Kinematica Inc, Bohemia, NY). Microspheres of different sizes were also fabricated through modulation of homogenization speed (12,000, 5,000, and 1,000 RPM). DCM was evaporated for 4 hours and microspheres were collected by centrifugation, washed with dH_2O, and lyophilized for 1-2 days (Freezone 4.5, Labconco, Kansas City, MO).

Microsphere characterization

Initial CellTracker Red (CTR) loading in PLGA microspheres was determined by hydrolyzing microspheres in 0.1 M NaOH containing 5% SDS solution overnight,

analyzing the solution with a fluorescent plate reader (SpectraMax M2^e, Molecular Devices, Sunnyvale, CA), and comparing relative fluorescence to a standard curve of CTR constructed under equivalent conditions; unloaded microspheres served as a blank. A CTR release profile was constructed over the course of 14 days by incubating CTR microspheres in PBS under light mixing, centrifuging the microspheres at various time points, and collecting and analyzing the supernatant in a fluorescent plate reader. Values were reported as the percent of initially loaded CTR released. RA release was characterized under the same conditions by hydrolyzing centrifuged microspheres in 0.1 M NaOH/5% SDS and analyzing this solution spectrophotometrically at 355 nm. In order to image microspheres via scanning electron microscopy, microspheres suspended in dH_2O were attached to SEM stubs with carbon double-sided adhesive discs (SPI Supplies, West Chester, PA), frozen at -80ºC and lyophilized for ~6 hours until stubs were completely dehydrated. After lyophilization, stubs were gold sputter coated using a Polaron range sputter coater (Quorum Technologies, East Sussex, United Kingdom) and imaged using an Hitachi S-800 SEM microscope. Microsphere size was quantified using ImageJ software to measure the diameter of a minimum of 100 microspheres for each group. The resulting distribution of microsphere sizes was plotted as a histogram with an equal number of bins between the largest and smallest values for each experimental group.

Embryonic stem cell culture

Murine embryonic stem cells (D3) [1] (passages 23-32) were maintained in an undifferentiated state on tissue culture dishes coated with 0.1% gelatin in Dulbecco's

modified Eagle's medium (DMEM) (Mediatech Inc., Herndon, VA), supplemented with 15% fetal bovine serum (FBS) (Hyclone, Logan, UT), 2mM L-glutamine (Mediatech), 100 U/mL penicillin, 100 μg/mL streptomyocin, and 0.25 μg/mL amphotericin (Mediatech), 1x MEM nonessential amino acid solution (Mediatech), 0.1 mM 2-mercaptoethanol (Fisher Chemical, Fairlawn, NJ), and 10^3 U/mL leukemia inhibitory factor (LIF, Chemicon International, Temecula, CA). Cells were routinely passaged every 2-3 days prior to reaching 70% confluence.

Embryoid body formation

To initiate formation of EBs containing PLGA microspheres, microspheres were first coated with gelatin (0.1%, Chemicon) and placed on a rotisserie rotator at 37°C for 3 hours. Studies examining different size microspheres were performed by suspending equal masses of the different size microspheres in a 0.1% gelatin solution. Coated microspheres were collected by centrifugation at 3000 RPM for five minutes and resuspended in differentiation media (ESC media without LIF). Embryonic stem cell colonies were dissociated into single cells with a 0.05% trypsin-EDTA solution and resuspended in 10 mL of differentiation media (2×10^5 cells/mL final concentration) with coated microspheres in 100 mm bacteriological-grade Petri dishes. Embryoid body formation was initiated by placing dishes on an orbital rotary shaker set at 25 or 40 rotations per minute (RPM) [68]. EB media was exchanged every 1-2 days as needed. EBs were treated with 0.1 μM RA in DMSO between days 2 and 6 as a soluble RA treatment control. Phase images of EBs were acquired using a Nikon TE 2000 inverted microscope equipped with a SpotFLEX (Diagnostic Instruments) camera.

Histology

Between days 6 and 10 of differentiation, EBs were collected, fixed in 10% formalin, embedded in Histogel (Richard-Allan Scientific), processed and paraffin embedded, as described [68]. Paraffinized samples were cut into 5 µm-thick sections, placed on glass slides and deparaffinized before staining with hematoxylin and eosin (H&E) or immunofluorescence. Prior to immunostaining, slides were subjected to 15 minutes pressure-cooker treatment in 10 mM citrate buffer. Samples were then permeabilized and blocked in 0.05% Triton X-100/2% BSA for 30 minutes, incubated with FoxA2 primary antibody (Santa Cruz Biotech., 1:400) in 2% BSA solution overnight at 4ºC, rinsed with PBS (3x 5 min) and incubated with Alexa Fluor 488-conjugated secondary antibody (donkey-anti-goat, 1:200 dilution, Molecular Probes) for 1 hour. Slides were counterstained with Hoechst, mounted, cover-slipped and imaged using a Nikon 80i microscope (Nikon Inc, Melville, NY). For whole-mount EB immunofluorescence, EBs were washed in PBS, fixed for 1 hour in 4% parafomaldehyde at 4ºC, and washed again 3 times in wash buffer (150mM NaCl, 1 mg/mL bovine serum albumin, 0.1% Tween-20, 50 mM Tris). EBs were permeabilized for 30 minutes in 2% TritonX-100, re-fixed in 4% paraformaldehyde for 15 minutes, and then blocked in wash buffer for 1-3 hours. Samples were incubated in Oct4 primary antibody (1:100, Santa Cruz Biotech.) overnight at 4ºC, washed again (3 times, 15 minutes), and then incubated in a FITC-conjugated goat anti-rabbit secondary antibody (1:200, Southern Biotech.) for 4 hours at 4ºC. EBs were then stained with Alexa Fluor 546 phalloidin (1:40, Molecular

Probes) and Hoechst (1:100). Finally, samples were re-suspended in a low volume of PBS and imaged with a Zeiss LSM 510 Confocal Microscope (Carl Zeiss Inc.).

Quantitative PCR

After 2, 4, 7 and 10 days, RNA was extracted from EBs with an RNeasy Mini kit (Qiagen Inc, Valencia, CA). Reverse transcription for complementary DNA synthesis was performed with 1 µg of RNA per sample using the iScript cDNA synthesis kit (Bio-Rad, Hercules, CA, http://www.bio-rad.com), and real-time PCR was performed with SYBR green technology on the MyiQ cycler (Bio-Rad). Forward and reverse primers for *Oct4*, *Brachyury-T* (*B-T*), *fibroblast growth factor 5* (*Fgf5*), and *glyceraldhyde-3-phosphate-dehydrogenase* (*GAPDH*) were designed with Beacon Designer software, purchased from Invitrogen and validated with appropriate controls. *Oct4* relative gene expression was quantified as compared to undifferentiated ESC expression levels using the Pfaffl method of quantification [174]. *Brachyury-T* and *Fgf5* concentrations were calculated using standard curves and normalized to *GAPDH* expression levels.

Affymetrix microarray

Total RNA was extracted from day 10 EBs containing unloaded microspheres and RA-loaded microspheres using an RNeasy Mini kit (Qiagen). Labeled cRNA from three micrograms of total RNA was generated using the One-Cycle Target Labeling and Control Reagents Kit (Affymetrix Inc, Santa Clara, CA) and hybridized to the Mouse Genome 430 2.0 Array according to manufacturer's protocols (Affymetrix). CEL files generated by the Affymetrix Gene Chip Operating System (GCOS) were converted to

expression level values using the affy and GCRMA packages of the Bioconductor project (www.bioconductor.org) for the R statistical programming environment (www.rproject.org). After GCRMA preprocessing, SAM [260] (Significance Analysis of Microarrays v.3.02) analysis was performed on the probe sets with log2 intensity values ≥ 5.0 in at least one of the experimental replicates using the following relevant parameters: Delta=1.35, minimum fold change = 3, number of permutations = 500, and False Discovery Rate = 0%. SAM yielded 1270 significantly differentially expressed probe sets (DEPs) between the RA treated and untreated EBs. These probe sets were filtered to exclude non-existent and redundant Gene Titles by Affymetrix Annotation (file Mouse430_2 Annotations, CSV format (13 MB, 3/19/08)), to produce 1057 differentially expressed genes (DEGs). The log2 expression values for the 1057 DEGs were normalized by Z-score calculation and used to generate the heat map for presentation using Spotfire DecisionSite 9.1.1 (http://spotfire.tibco.com). Microarray data were deposited at the Gene Expression Omnibus website (http://www.ncbi.nlm.nih.gov/geo/) under accession GSE12333.

Scanning electron microscopy

Samples were fixed in 2.5% gluteraldehyde (Electron Microscopy Sciences) diluted in sodium cacodylate buffer (Electron Microscopy Sciences) for 1 hour. After rinsing, samples were further treated in 1% osmium tetroxide (Electron Microscopy Sciences) for 1 hour. Samples were dehydrated in graded acetone dilutions and critically point dried using a Polaron E3000 critical point dryer (Quorum Technologies Inc, Guelph, ON, Canada). Samples were sputter coated for 120 seconds at 2.2 kV using a

Polaron SC7640 sputter coater and imaged using an Hitachi S-800 scanning electron microscope (Hitachi High Technologies, Pleasanton, CA).

Statistical analysis

Values are reported as mean ± standard deviation (n=3). Statistical significance was determined using one or two way ANOVA coupled with Tukey's post hoc analysis using Systat (v12, Systat Software Inc.).

Results

Microsphere analysis

As described previously, microspheres fabricated at 3000 RPM homogenization speed were spherical with smooth surfaces and displayed a relatively uniform size distribution (Figure 6.1A, B; mean diameter = 7.8 μm). CellTracker Red was incorporated within the microspheres, resulting in intensely fluorescent particles (Figure 6.1C). Microspheres released retinoic acid with an initial burst phase during the first 6-12 hours, followed by sustained release for up to 10 days (Figure 6.1D).

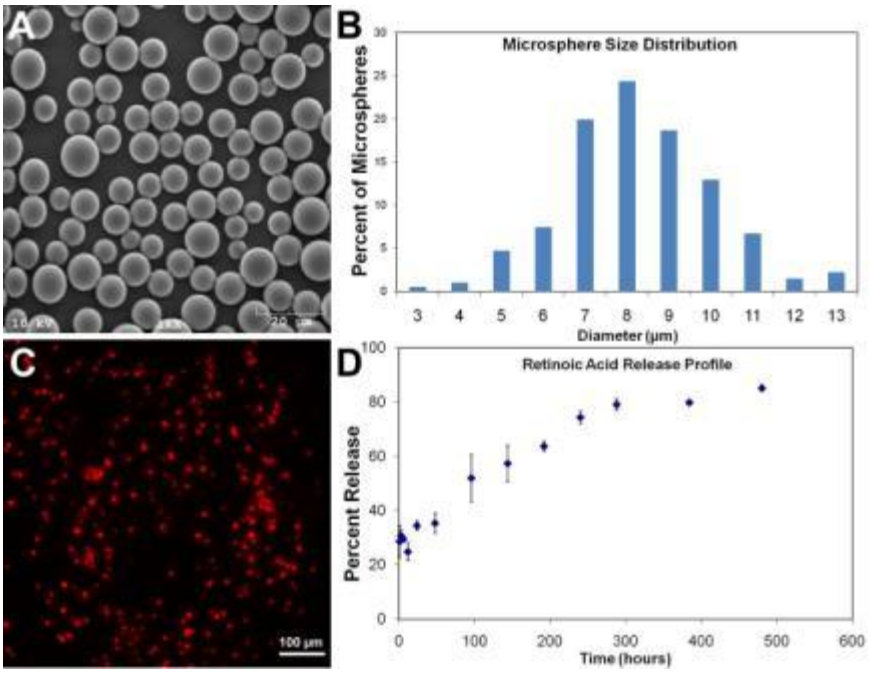

Figure 6.1. Micropshere analysis. Microspheres were fabricated using an oil-in-water emulsion and displayed smooth, spherical morphology in SEM micrographs (A). The size distribution was determined using image analysis of SEM micrographs, and the diameter was found to be 7.8 ± 1.8 µm (mean ± standard deviation (B). CellTracker Red™ was incorporated within microspheres allowing visualization with fluorescent microscopy (C). Release of RA from microspheres took place over the course of 14 days, and displayed a burst phase followed by sustained release (D).

Molecule release within EBs

Small molecule release from microspheres within the EB interior and uptake by cells were investigated using CellTracker™ Red (CTR) loaded PLGA microspheres. Labeled microspheres were incorporated in EBs, and after three days of differentiation, the microspheres appeared largely as individual, punctate fluorescent spheres, with some diffuse fluorescence in the vicinity of the microspheres (Figure 6.2A-C). In contrast, after 10 days of culture, individual microspheres exhibited reduced fluorescent intensity, and many of the EBs displayed uniform fluorescence throughout the cell aggregate (Figure 6.2D-F). The fluorescent intensity profile across a day 3 EB contained multiple peaks (dashed line, Figure 2C), corresponding to the presence of individual microspheres,

whereas day 10 EBs exhibited uniform fluorescence throughout an entire cell aggregate (Figure 6.2G), suggesting CTR was released from microspheres and taken up by cells. CTR release from microspheres incubated in PBS was triphasic (Figure 6.2H), consisting of a burst phase (up to 24 hours), sustained release (1-7 days) and a plateau region (7-14 days), where the rate of release decreased as CTR availability diminished. After 3 days, (black arrow) <60% of CTR was released from microspheres, whereas >90% release was observed after 10 days (red arrow), indicating that CTR release was nearly complete before uniform fluorescence was exhibited in day 10 EBs. Collectively these results indicate that delivery vehicles incorporated within EBs present small molecules locally to cells throughout the entire aggregate. Additionally, these results suggested that microsphere-mediated delivery within EBs distributed molecules more uniformly to cells in EBs than traditional soluble treatment methods, which are limited by diffusional barriers created at the exterior surface of EBs.

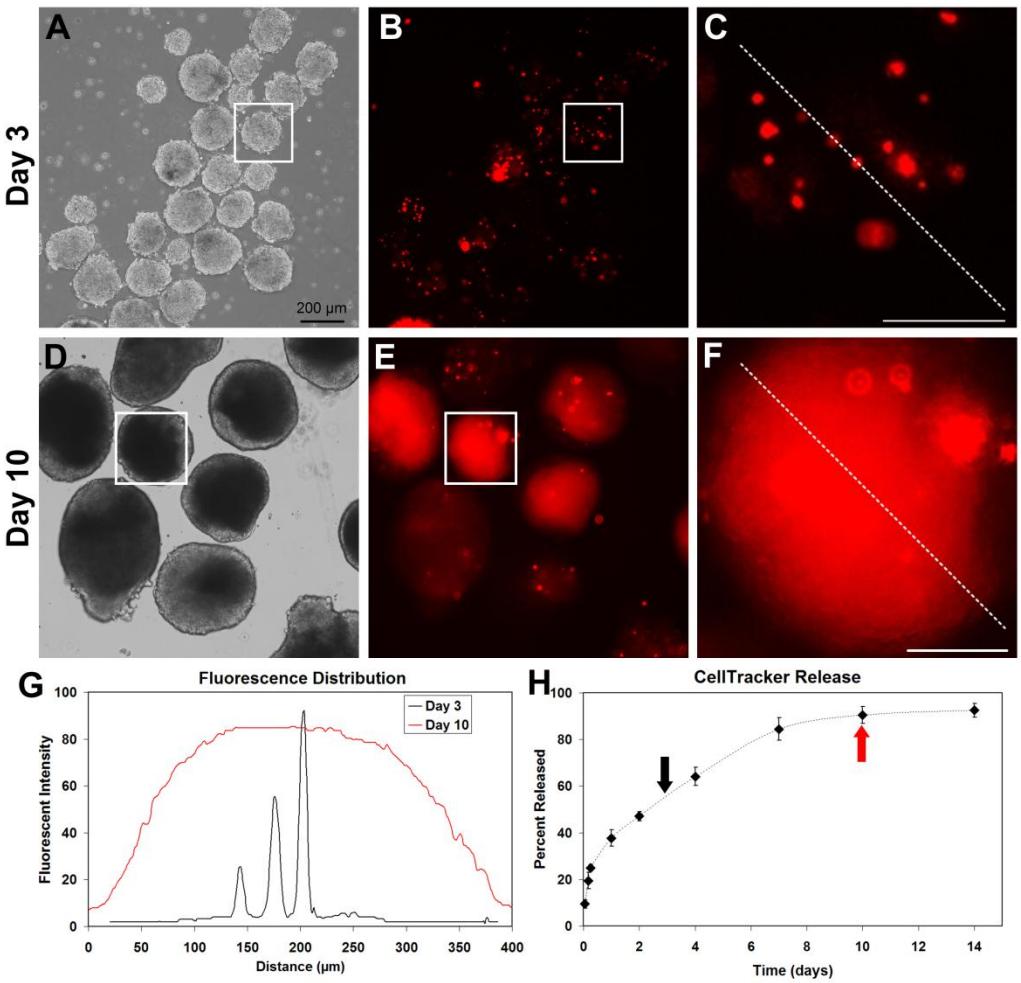

Figure 6.2. Small molecule release within EBs. EBs formed at 40 rpm with a 2:1 microsphere to cell ratio were imaged after 3 (A-C) and 10 days (D-F). (A-C) After 3 days, microspheres were visible within EBs as individual, punctuate spheres. (D-F) EBs imaged after 10 days contained diffuse fluorescence throughout and fewer individual spheres were apparent. (G) Fluorescent intensity plots across day 3 and day 10 EBs (dashed lines in C and F, respectively) revealed the presence of individual microspheres in day 3 EBs and uniform fluorescence throughout day 10 EBs. (H) CellTracker was released from microspheres over the course of 14 days, and a burst phase (up to one day), sustained release phase (1-7 days), and plateau phase (7-14 days) were observed (n=3, mean ± standard deviation). (A,B,D,E bar = 200 µm; C,F bar = 100 µm).

The time course of microsphere retention and dye release was assessed for the EB populations with different size microspheres incorporated as well. Regardless of size, microspheres remained embedded within the EBs for at least ten days (Figure 6.3). In agreement with confocal images (see Figure 5.9), 1 µm microspheres appeared to be

incorporated within EBs as clusters, whereas 3 and 11 μm microspheres displayed fewer agglomerates within EBs. The microsphere agglomerates were apparent after 4, 7 and 10 days, suggesting that the cells within EBs do not significantly alter the distributions of microparticles after initial incorporation. Low levels of fluorescent signal were detectable in regions of EBs lacking microspheres and provided a visual outline of EB boundaries that overlapped with phase images (phase images not shown). The fluorescent outline was more pronounced in EBs containing smaller microspheres suggesting that the CTR dye release from the microspheres was taken up by cells in EBs to varying extents depending on microsphere size. These results motivated additional studies examining the response of EBs to a morphogen delivered via different size microspheres.

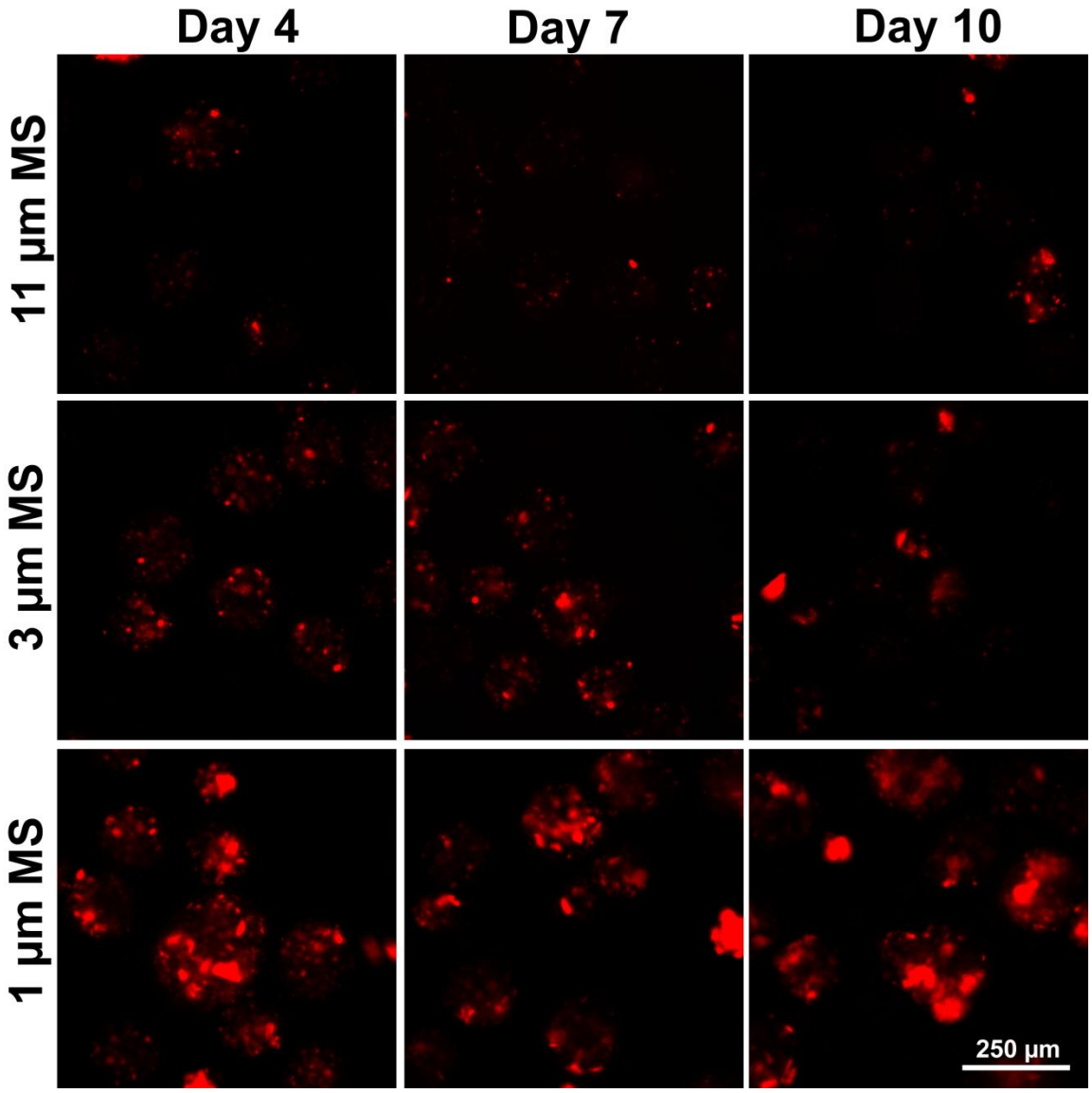

Figure 6.3. Temporal analysis of EBs containing CellTracker Red microspheres. EBs containing 11, 3 and 1 µm microspheres were imaged after 4, 7 and 10 days of differentiation. Microspheres were stably incorporated with fluorescent dye remaining visible during the time course examined. Scale bar = 250 µm.

Retinoic acid delivery

Differentiation of ESCs in response to microsphere-mediated delivery of a small molecule morphogen was examined. Retinoic acid (RA), a derivative of vitamin A important in regulating embryonic development [261], was encapsulated in microspheres (3μg RA/mg PLGA, with release profile in Figure 6.1D) and mixed with ESCs to form EBs. EBs treated with soluble RA (0.1 μM, days 2-6) or unloaded microspheres as well as untreated EBs served as controls. At early time points, EBs containing RA microspheres (RA MS EBs) appeared smaller than the other treatment groups, though after 6 days, RA MS EBs appeared noticeably larger than other EBs. After 10 days of differentiation, the RA microsphere-containing EBs exhibited a dramatically different morphology than controls. While untreated (Figure 6.4A) and soluble RA (Figure 6.4C) treated EBs were solid spheroids, EBs containing unloaded microspheres displayed small void spaces (Figure 6.4B) and EBs with RA microspheres formed large cystic structures that comprised the majority of the EB (Figure 6.4D). Small cystic regions were observed in 90.0±4.0% of RA MS EBs, compared to 29.1±11.5%, 9.7±2.3% and 5.6±7.9% for unloaded MS, soluble RA and untreated EBs, respectively (Figure 6.4I). Completely cystic EBs, which consisted entirely of the two epithelial layers, were found in 30.6±12.7% of RA MS EBs, compared to <1% for all other treatment groups. Additionally, the degree of cavitation was quantified for RA MS EBs compared to unloaded MS EBs (Figure 6.4H). The area of cystic regions was quantified using ImageJ and was normalized to the area of the entire EB. A histogram plot of this data demonstrates that majority of unloaded MS EBs contain cavitation fractions less than 0.1, while RA MS EBs had a greater extent of cavitation, with fractions as high as 0.7

observed. Upon inspection at higher magnification, the bilayer morphology of cystic EBs consisted of a flattened endoderm-like cell population (red arrows, Figure 6.4G,H) enveloping a pseudo-stratified columnar epithelial cell layer (black arrows, Figure 6.4G,H). Higher concentrations of soluble RA ($\geq$10 μM) did not induce formation of cystic EBs and instead resulted in formation of fewer, smaller EBs, while lower RA concentrations ($\leq$10 nM) resulted in EBs similar in appearance to untreated spheroids, indicating that morphological differences between RA MS and soluble RA EBs were not solely attributed to differences in RA concentration (Figure 6.5 A-C). The temporal effect of RA delivery was also examined. Soluble RA was added to EBs (0.1 μM) starting at EB formation and added daily throughout differentiation (Figure 6.6). While some cystic regions were observed, the extent of cavitation demonstrated by RA MS EBs was not approached. This suggests that while temporal aspects of delivery play a role in cystic spheroid formation, it is the unique spatial delivery using microspheres that induces widespread cavitation. Similar to soluble treatment, microspheres containing higher levels of RA (30μg RA/mg PLGA) reduced EB size and microspheres with less RA (0.3μg RA/mg PLGA) exhibited slightly fewer cystic EBs, indicating a dose dependent response to microsphere-mediated RA delivery (Figure 6.7). The formation of cysts in RA MS EBs took place over the course of ~4 days, with multiple small cystic regions appearing within EBs after 6 days of differentiation (Figure 6.8). By 8 days, individual cysts were noticeably larger within EBs containing RA-releasing microspheres, and complete cavitation occurred by 10 days of differentiation, indicating that the continuous columnar layer of cells arose from the progressive merger of the smaller cystic structures.

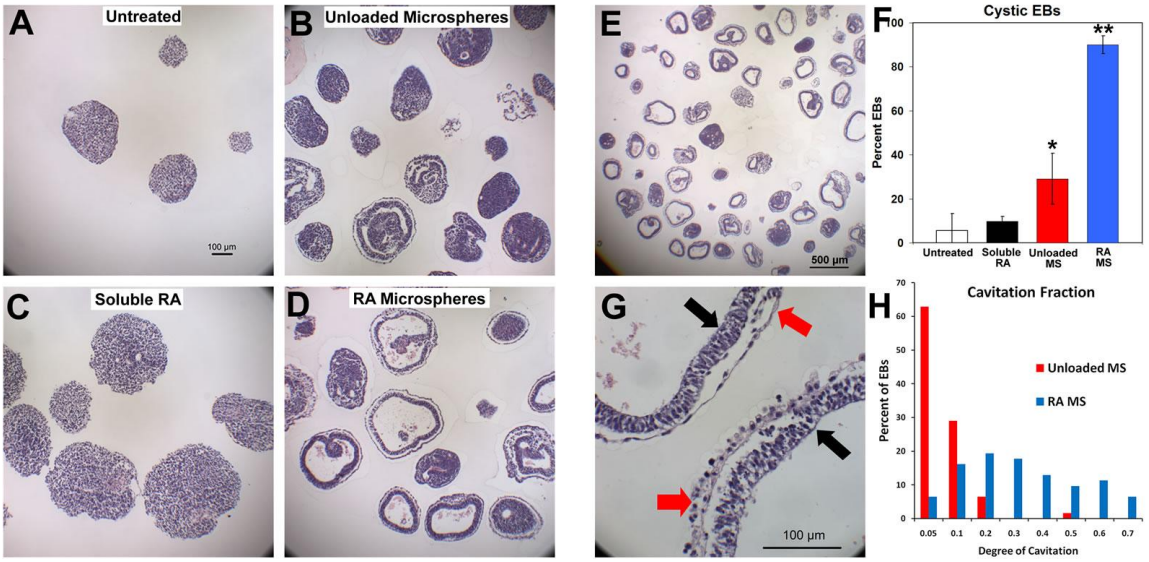

Figure 6.4. Delivery of retinoic acid to EBs. Untreated EBs as well as EBs treated with soluble RA, unloaded microspheres, or RA-loaded microspheres were formalin-fixed, sectioned and stained with H&E after 10 days of differentiation. (A) Untreated EBs and (C) soluble RA treated EBs formed solid spheroids while (B) EBs containing unloaded microspheres contained small void spaces. (D,E) EBs containing RA microspheres frequently were completely cystic. (F) Cystic EB formation was significantly enhanced in RA MS EBs compared to all other treatments (n=3, mean ± standard deviation). (G) Cystic RA MS EBs contained bi-epithelial morphology, with a columnar, pseudo-stratified inner cell layer (black arrows) and an adjacent, flattened outermost cell layer (red arrows). (H) A histogram of the degree of cavitation (Cystic Area/EB area) confirmed that RA MS EBs cavitate to a greater extent than unloaded MS EBs. * denotes $p<0.05$ vs. untreated, soluble RA; ** denotes $p=6x10^{-6}$ vs. all treatments.

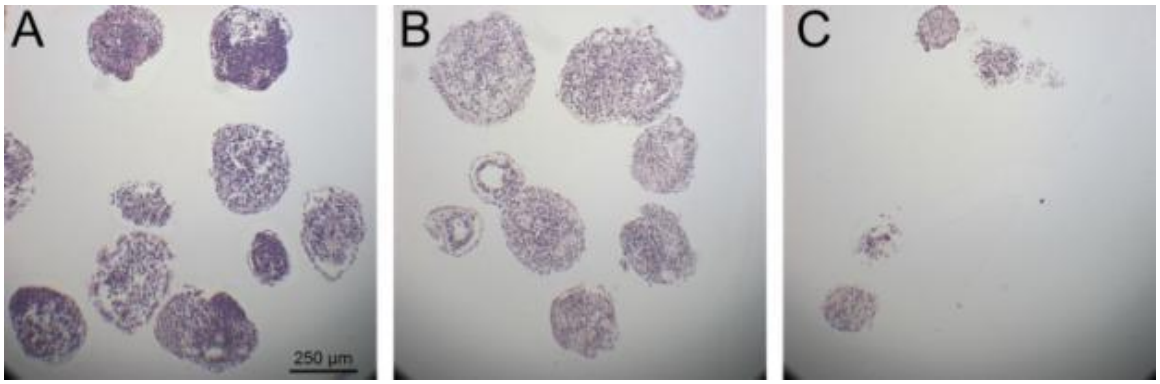

Figure 6.5. Dose dependent response of EBs to soluble RA. Treatment of EBs with soluble RA with low (A, 0.01 µM) and medium (B, 0.1 µM) RA concentration results in solid spheroids after 10 days, while high RA (C, 10 µM) results in survival of few EBs and decreased EB size. Scale bar = 250 µm.

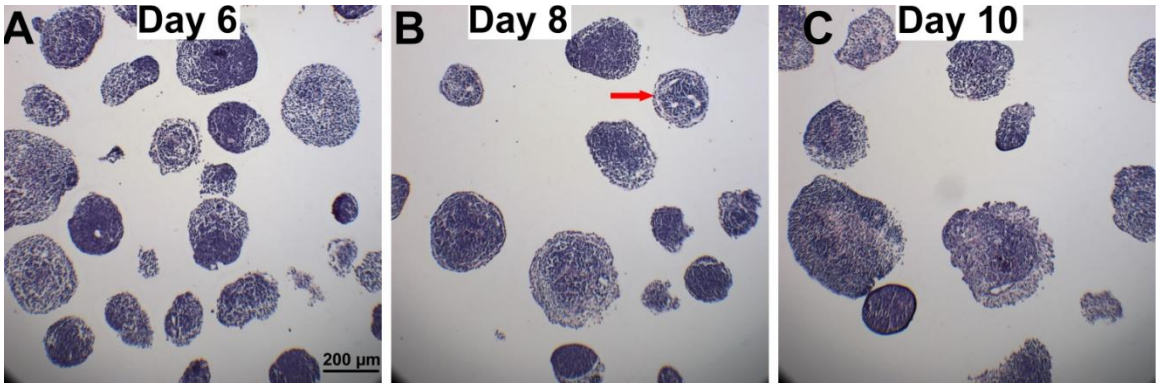

Figure 6.6. Temporal response of EBs to soluble RA. RA was delivered solubly to EBs starting at the onset of EB formation continuing throughout differentiation with daily supplement. EBs were largely solid after 6 (A) and 8 (B) days, though some cavitation was observed after 8 days (red arrow). EBs were larger but mostly solid after 10 days (C).

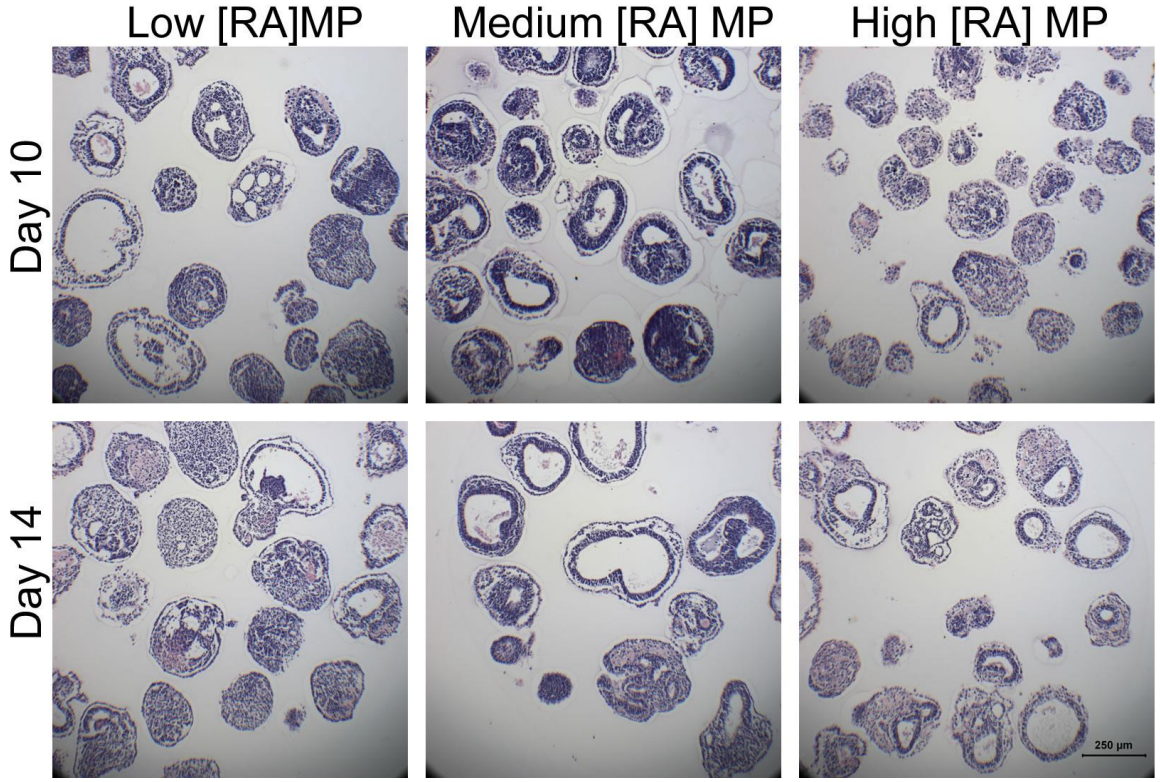

Figure 6.7. Dose dependent response of EBs to microsphere-mediated delivery. EBs containing microspheres with low RA concentration (0.3 µg RA/mg PLGA) induced formation of fewer cystic EBs and incomplete cystic regions compared to medium RA concentration (3 µg RA/mg PLGA). EBs containing microspheres with high RA (30 µg RA/mg PLGA) induced formation of small EBs with few cystic regions. Scale bar = 250 µm.

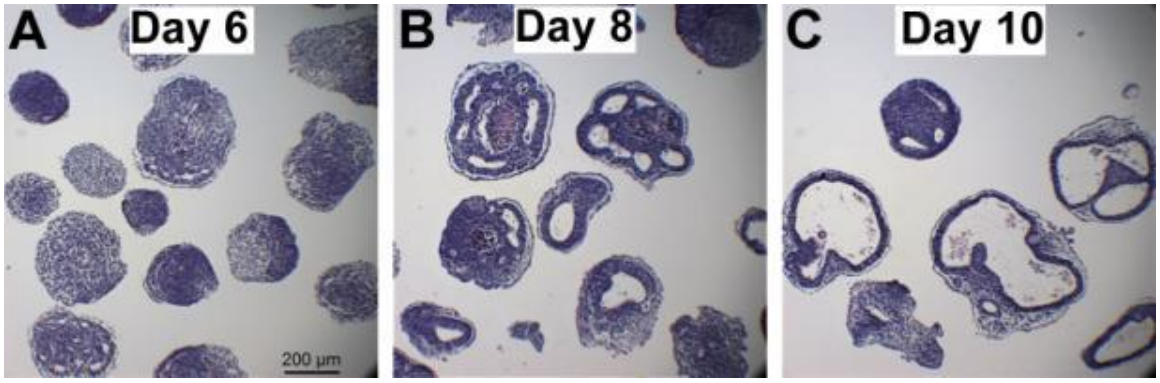

Figure 6.8. Time course of cystic EB formation. (A) Small cystic regions were visible in RA MS EBs after 6 days. (B) After 8 days, cysts appeared larger, and columnar cell layers become apparent. (C) By 10 days of differentiation, smaller cystic regions expanded and merged to form completely cystic EBs. Bar = 200 µm.

Previous studies have shown that microsphere incorporation and distribution within EBs can be modulated through microsphere size (see Figures 4.6 and 4.9). In order to investigate the microsphere size dependence of RA-induced cavitation, ESCs were mixed with RA-loaded microspheres with the three size distributions (1, 3, and 11 µm; Figure 6.9). After 7 days, EBs containing 11 µm RA microspheres did not appear morphologically different than untreated EBs. However, EBs containing 1 and 3 µm microspheres began to display small cystic regions and reorganization of cells within EBs. After 10 days, 11 µm RA MS EBs contained multiple void regions, but formation of columnar cell morphologies was not observed. EBs with 3 µm RA MS contained cystic regions surrounded by pseudo-stratified columnar cells EBs as well as an outer, endoderm-like cell layer. This bi-layered cystic morphology was most pronounced and uniform in EBs containing 1 µm RA microspheres. These results illustrate that the response of ESCs in EBs to microsphere mediated morphogen delivery can be modulated via microsphere size, with smaller microspheres inducing accelerated and more uniform differentiation within EBs.

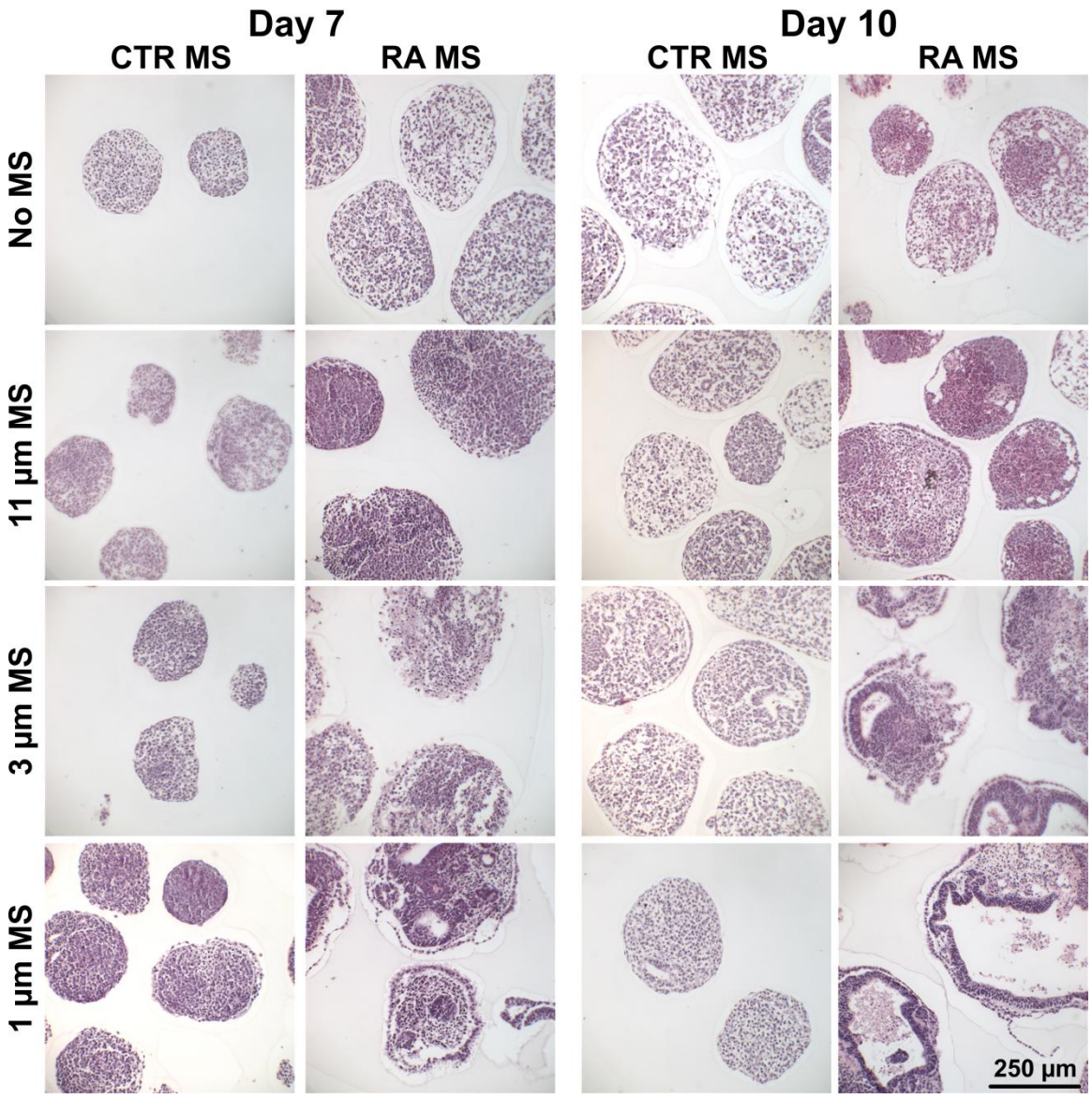

Figure 6.9. Morphology of EBs containing different size RA microspheres. Microspheres encapsulating CellTracker Red (CTR MS) induce little to no change in morphology and shape after 7 and 10 days. Microspheres containing retinoic acid (RA MS) induce cavitation, with smaller diameter retinoic acid microspheres inducing earlier and more complete cavitation than larger retinoic acid microspheres. Scale bar = 250 µm.

Finally, the rotary speed at which RA MS EBs were formed was altered in order to assess the effect of this parameter on EB morphology. Slower rotary speeds (25 RPM) were shown to produce larger EBs than 40 RPM and incorporate more microspheres per EB (see Figures 3.1B and 4.7A). However, microsphere density within EBs formed at 25

RPM was found to be less than that of EBs formed at 40 RPM. The incorporation of RA MS within EBs formed at 25 RPM (RA MS 25) led to endoderm-like cell formation in some EBs after 6 days (Figure 6.10). By 8 days, cystic regions lined by pseudo-stratified cells formed, and by 10 days, some of these regions became larger. In general, cavitation was less pronounced in RA MS 25 EBs than RA MS 40 EBs. This may be attributed to the lower microsphere density in the 25 RPM EBs, though differences in the hydrodynamic environment may contribute to the observed morphological discrepancies.

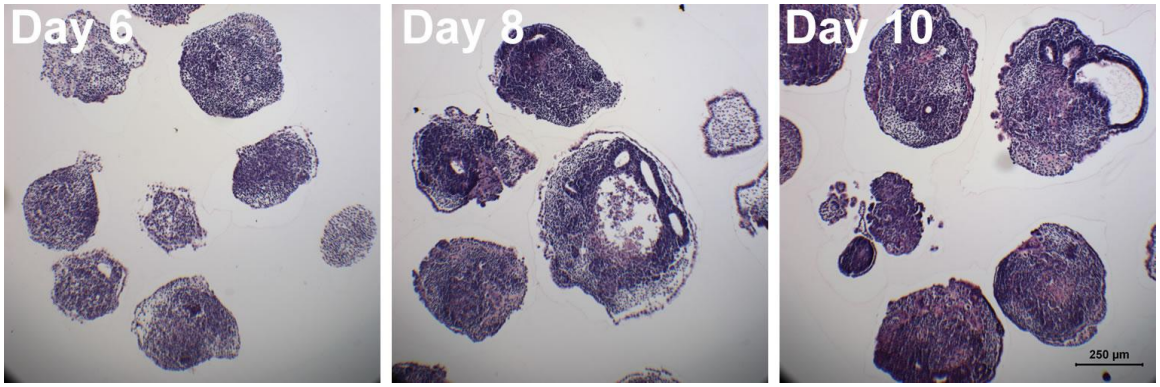

Figure 6.10. Time course of EB cavitation for RA MS EBs formed at 25 RPM. Cystic regions formed at day 8 and expanded by day 10, yet cavitation did not reach the same frequency and expansiveness observed with 40 RPM EBs. Scale bar = 250 µm.

Gene expression analysis

Based on the significant differences in EB morphology elicited by RA MS treatment, transcriptional profiling using Affymetrix GeneChip mouse genome arrays was performed in order to characterize the phenotype of the differentiating cells. RNA expression was compared between day 10 RA MS treated EBs (40 RPM, 8µm microspheres), and EBs containing unloaded microspheres and significant gene expression changes were identified using significance analysis of microarrays (SAM) [260]. SAM analysis identified 1,057 genes with a minimum three fold expression

change (and $p<0.005$), 410 of which were up-regulated in RA MS EBs, and 647 were down-regulated relative to unloaded MS EBs (Figure 6.11). Many of the genes that were up-regulated in RA MS EBs are phenotypic markers of structures specific to the early post-implantation embryo [262], including visceral endoderm, epiblast, and early primitive streak. The visceral endoderm surrounds the epiblast and provides a substrate for epiblast attachment, promotes nutrient and gas exchange, and secretes signals to direct epiblast patterning and differentiation [263,264]. The cells comprising the epiblast are pluripotent and differentiate into the entire embryo proper [265]. Primitive streak formation occurs at E6.75 in mouse embryos and is characterized by ingression of epiblast cells, which go on to form mesendodermal progenitor cells [266,267]. Visceral endoderm genes identified in the array as being significantly up-regulated in RA MS EBs included: *Dkk1* (31 fold change), *Cer1* (22), *Sox17* (20), *Hex* (18), *amnionless* (17), and *Dab2* (6.2). Epiblast-related genes up-regulated in RA MS EBs included: *Fgf5* (271), *Foxd4* (13), *Pou5f1* (aka *Oct4*, 11), *Tdgf1* (aka C*ripto1*, 6) and *Sox2* (5). Up-regulated primitive streak genes included: *Brachyury T* (195), *Eomes* (177), *Follistatin* (38), and *Mix1* (8). Genes expressed in multiple structures included: *Lhx1* (endoderm and primitive streak, 86), *Foxh1* (endoderm and epiblast, 73), *Otx2* (endoderm and epiblast, 55), and *Foxa2* (endoderm and primitive streak, 12). Other notable genes significantly up-regulated in RA MS EBs included: *Pim2* (anti-apoptosis, 785 fold change), *DNA methyltransferase 3B* (DNA methylation, 321), *cytochrome p450 family 26* (retinoic acid degradation, 74) and *laminin α1* (basement membrane, 16). Many of the genes down-regulated in RA MS EBs relative to unloaded MS EBs were related to mesoderm and definitive endoderm differentiation, including plasma proteins (albumin, transferrin,

apoplipoproteins, hemopexin), contractile proteins (myosin, actin and troponin), hemoglobin chains, growth factors (PDGF, VEGF, HDGF), and matrix molecules (collagen, fibronectin, vitronectin, osteopontin, versican). In summary, EBs containing unloaded microspheres exhibited reduced expression of epiblast and visceral endoderm markers and increased expression of more mature mesoderm and definitive endoderm genes, whereas treatment of EBs with RA microspheres for 10 days resulted in cystic EBs with transcriptional profiles similar to early post-implantation mouse embryos, consisting of visceral endoderm, epiblast, and early primitive streak cell phenotypes.

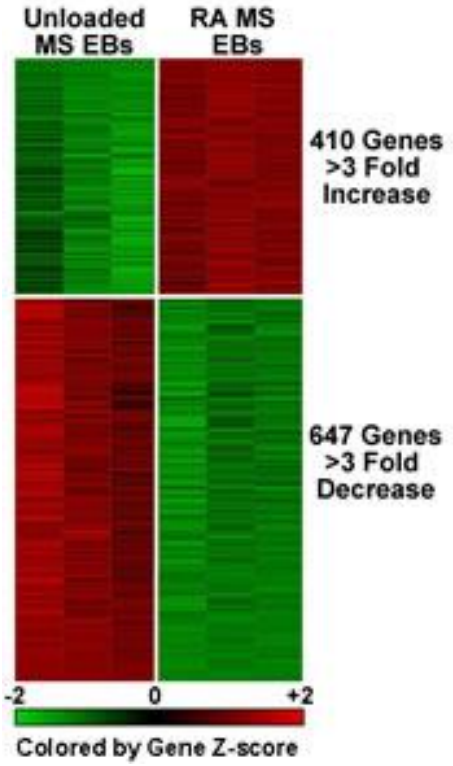

Location	Gene	Fold
Endoderm	Lhx1	86
	Otx2	55
	Dkk	31
	Cer1	22
	Sox17	20
	Hex	18
	Foxa2	12
	Dab2	6
Epiblast	Fgf5	271
	Foxh1	73
	Foxd4	13
	Oct4	11
	Tdgf1	6
	Sox2	5
Primitive Streak	T	196
	Eomes	178
	Fst	38
	Mixl1	8

Figure 6.11. Microarray analysis of gene expression. 410 genes were identified as up-regulated greater than 3-fold in RA microsphere EBs compared to unloaded microsphere EBs after 10 days of differentiation, while 647 genes were observed to decrease in RA MS EBs. Many genes with large fold changes in RA MS EBs were associated with early embryonic structures, including visceral endoderm, epiblast and primitive streak.

Temporal transcriptional analysis by quantitative PCR was performed to assess the expression of several genes found to change significantly in microarray analysis. The pluripotent transcription factor *Oct4*, expressed by cells in the inner cell mass as well as the epiblast [268], was significantly enhanced after 7 days in RA MS EBs relative to both untreated and unloaded MS EBs (Figure 6.12, left). The epiblast marker *Fgf5* was also analyzed, and in agreement with previous reports of mouse EB differentiation [53,86], untreated and unloaded MS EBs exhibited a transient increase in *Fgf5* after 2 and 4 days which subsided by day 7 (Figure 6.12, center). In contrast, relatively high levels of *Fgf5* expression by RA MS EBs were present at 7 and 10 days of differentiation. Importantly, the pattern of *Fgf5* expression in RA MS EBs correlated with the appearance of columnar, epiblast-like cells at day 7 and completely cystic spheroids at day 10. *Brachyury T*, a transcription factor expressed in the primitive streak by mesendodermal progenitor cells [269], was also observed to transiently increase in untreated and unloaded MS EBs between days 2 and 7 of differentiation (Figure 6.12, right). Levels of *Brachyury T* mRNA in RA MS EBs remained almost undetectable until day 10, at which point a small increase in the transcript was observed, suggesting that a subset of cells in day 10 RA MS EBs were entering the primitive streak stage. This data, together with microarray analysis, demonstrates that while EBs containing unloaded microspheres expressed markers of epiblast, primitive streak and more mature phenotypes over the course of 7 days of differentiation, RA microspheres directed EBs to form spheroids with gene expression patterns closely resembling the early post-implantation E6.75 mouse embryo.

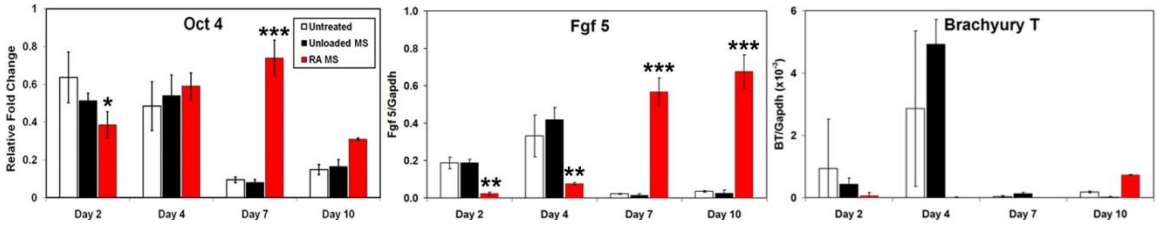

Figure 6.12. Temporal analysis of gene expression by qPCR. The epiblast markers *Oct4* and *Fgf5* were significantly enhanced in RA MS EBs after 7 days, and *Fgf5* was enhanced after 10 days as well. Expression of *Brachyury T*, a marker for primitive streak, in RA MS EBs was delayed until day 10, when a small increase was observed (n=3, mean ± standard deviation). * denotes p=0.02 vs. untreated; ** denotes p<0.05 vs. all treatments; *** denotes $p=5.2x10^{-6}$ vs. all treatments.

Embryoid body immunostaining

The spatial organization of the epiblast and visceral endoderm cell populations was analyzed by immunofluorescence staining for OCT4 and FOXA2, respectively. OCT4+ cells in day 10 RA MS EBs were localized to the inner layer of columnar, pseudo-stratified cells, while the adjacent endoderm-like cells were OCT4- (Figure 6.13C). The patterns of OCT4 expression were consistent for both confocal imaging of whole, permeabilized EBs and histological sections of formalin-fixed, paraffin embedded samples. In contrast, day 10 untreated and unloaded MS EBs contained regions of OCT4+ cells randomly distributed throughout the spheroid (Figure 6.13A, B). Similarly, FOXA2, a marker for visceral endoderm [264], was expressed in clusters of cells dispersed throughout untreated and unloaded MS day 10 EBs (Figure 6.13D, E). However in RA MS EBs, FOXA2 expression was restricted to cells in the exterior, endoderm-like layer, while cells in the epiblast-like, OCT4+ cell layer were FOXA2- (Figure 6.13F). These data demonstrate that cystic RA MS EBs consist of spatially distinct populations of FOXA2+ endoderm and OCT4+ epiblast organized similar to an early streak mouse embryo.

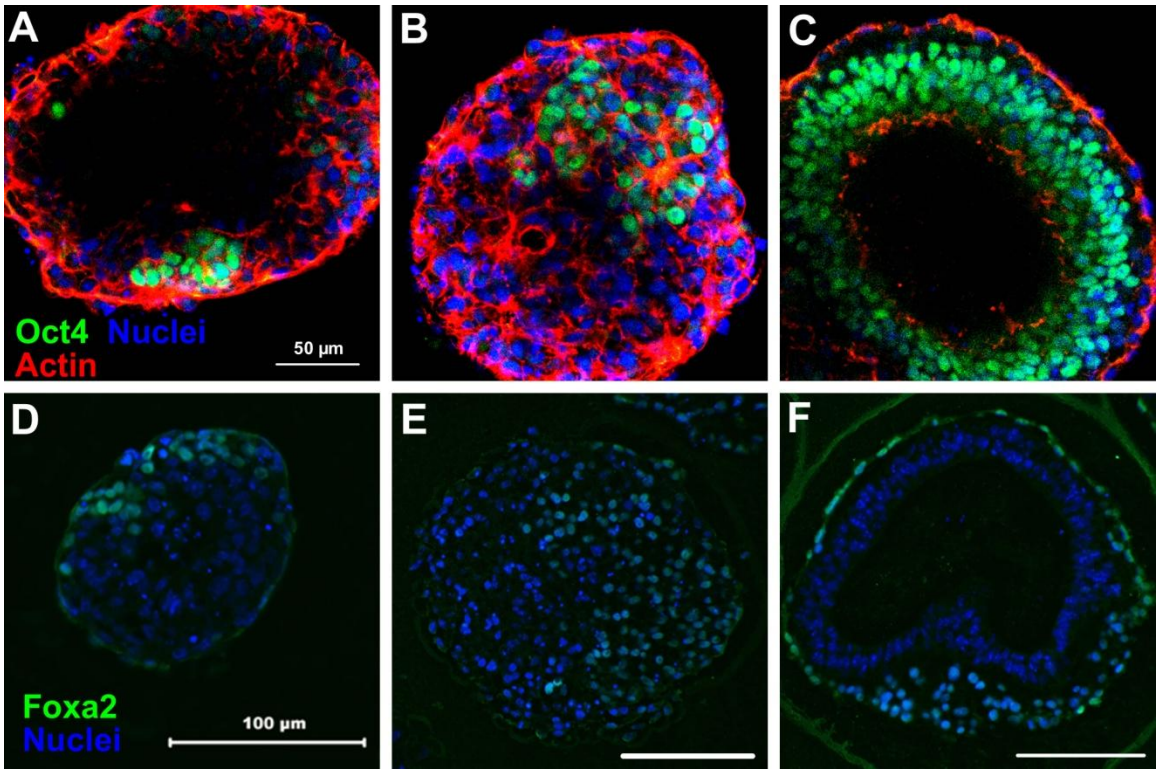

Figure 6.13. Immunostaining of EBs. (A-C) OCT4 staining was performed on day 10 untreated (A), unloaded MS (B) and RA MS EBs (C). Untreated and unloaded MS EBs contained clusters of OCT4+ cells, while OCT4+ cells in RA MS EBs were localized to the columnar cell layer. (D-E) FOXA2, a marker of visceral endoderm, was also expressed in clusters of untreated (D) and unloaded MS EBs (E), but was localized to the outermost layer of cell in RA MS EBs (F). A-C, bar = 50 µm; D-F, bar = 100 µm.

Embryoid bodu ultrastructure

Embryoid bodies containing RA microspheres were examined ultrastructurally after 10 days using SEM, with micrographs displaying the two distinct epithelial layers (Figure 6.14A-E). The columnar, pseudo-stratified organization of the inner layer of epiblast-like cells was readily apparent (Figure 6.14B,C), as was the simple, squamous morphology of the overlaying endoderm layer. Interestingly, the RA MS EBs did not contain the matrix-rich outer layer observed in untreated EBs (Figure 5.2 B,C), but displayed a dense coat of microvilli roughly 100 nm in diameter on the exterior surface of

the endodermal cell layer (Figure 6.14F). These microvilli structures are similar to those that are present on the surface of visceral endoderm in day 5-7 mouse embryos [270]. Altogether, these observations demonstrate the high level of organization attained in day 10 RA MS EBs closely resembles the structural organization and phenotype of E6.75 mouse embryos.

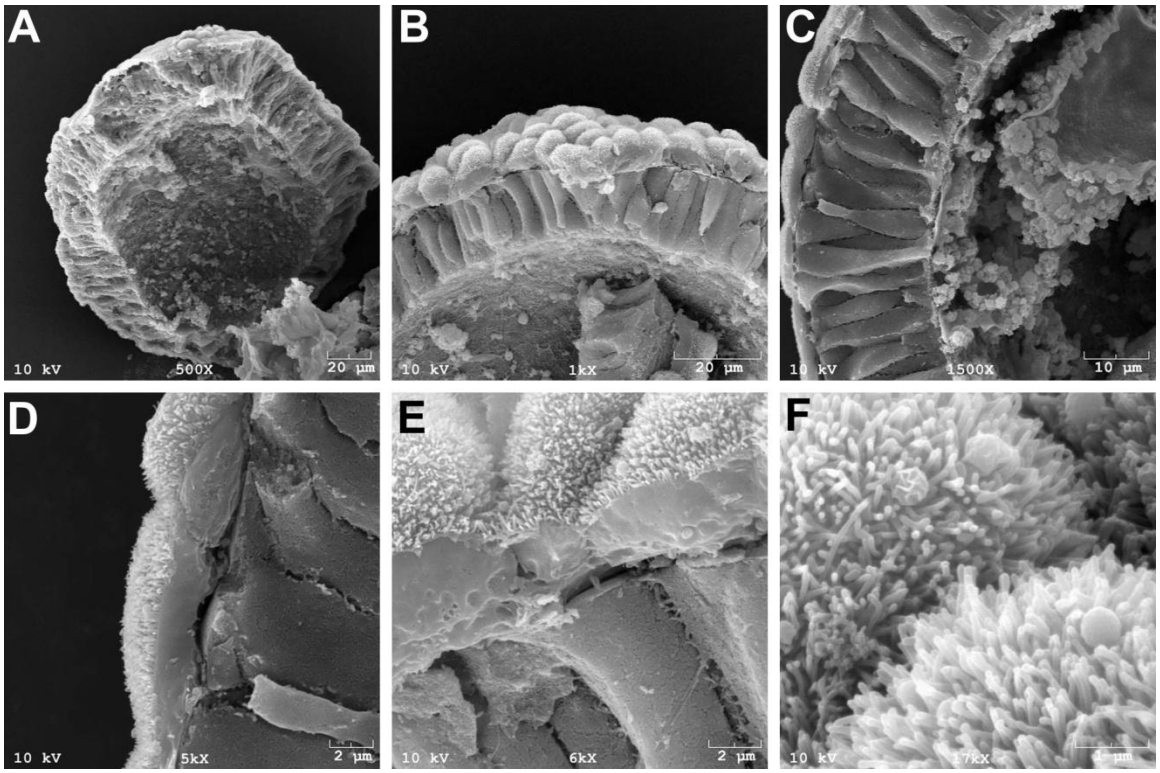

Figure 6.14. Embryoid body ultrastructure. (A-C) SEM micrographs of day 10 RA MS EBs reveal the structure of the distinct squamous endoderm and pseudo-stratified epiblast layers. (D-F) A dense coat of microvilli was observed on the surface of the endoderm cells, similar to that observed on early streak stage mouse embryos.

Discussion

The efficient formation of highly organized, cystic EBs is significant for a number of reasons, including improved *in vitro* models of embryogenesis and biomanufacturing of differentiated cell types for regenerative medicine and *in vitro* diagnostic applications.

Currently, directed differentiation strategies using EBs are limited in their ability to produce a homogeneous differentiated cell population, due largely to the fact that EBs consist of a population of cells exposed to a diverse set of instructive cues within the microenvironment [5,271,272]. The variability in the interactions of different cells within an EB with soluble morphogens, extracellular matrix, and neighboring cells leads to significant heterogeneity in cell differentiation microscopically within an individual EB and macroscopically among a population of EBs [37]. However, by specifying EB differentiation to two cell phenotypes initially – visceral endoderm and epiblast – it may be possible to subsequently direct cells more efficiently to specific lineages by reducing endogenous signaling, thereby allowing defined media components to more potently dictate cell fate decisions. Moreover, while untreated EBs contain a matrix-dense outer layer that appears to hinder diffusion of soluble media components, RA MS EBs contain an outer cell layer densely coated with microvilli. The appearance of microvilli strongly suggests that the outer cells may be proficient in the absorption of nutrients and soluble signaling molecules from the media, allowing such molecules to reach the interior epiblast cells more efficiently and thereby enhance subsequent directed differentiation.

The striking similarity of RA MS EBs to E6.75 embryos has significant implications for *in vitro* studies of embryogenesis. EBs have been utilized to study the roles of specific genes in development, particularly for genes in which knockout models *in vivo* are unavailable due to embryonic lethality [56,273]. However, EBs formed using conventional methods may not provide an accurate representation of the roles of such genes in later stages of embryogenesis, since EBs commonly differentiate in a heterogeneous, disorganized manner within a fairly short period of time (<7 days). The

use of RA MS EBs may provide greater insight into developmental processes due to their close phenotypic resemblance to early streak (E6.75) embryos [262]. Additionally, the roles of specific secreted molecules during development can be studied in the well-controlled, *in vitro* environment created using RA MS EBs, which may lead to a better understanding of early differentiation events, such as axis formation, specification of epiblast cells, and germ layer formation.

RA treatment of ESCs most commonly promotes neurogenesis [88-90,106,107,212]; however, enhanced cardiogenesis [111] and pancreatic beta-like cell formation [113] in response to RA have also been reported, indicating this retinol-derived morphogen is a potent inducer of differentiation to various cell lineages. Similar to the effects of RA *in vivo* [274], the concentration of RA and the timing of its delivery appear to be critical in dictating cell differentiation *in vitro* [89,108]. We report here that delivery of RA directly within the EB interior via microspheres maintains the pluripotency of ESCs through the formation of a highly organized OCT4+ epiblast, suggesting that the mode of presentation of RA (media supplement vs. microsphere-mediated) is a key determinant of cellular response, as soluble RA treatment at a wide range of concentrations [10 nM – 10 μM] was unable to efficiently produce comparable cystic EBs. These discrepancies may be attributed to the fact that soluble factor delivery only affects cells at the exterior surface of EBs and prevents the remaining interior cells from being directly exposed to exogenous biochemical stimuli, such as RA. Interestingly, ESCs that constitutively express *Nodal*, a member of the TGF-β superfamily, form cystic spheroids with similar characteristics as RA MS EBs, whereas addition of recombinant Nodal to the culture media did not elicit a similar effect [275].

This suggests that 1) diffusion of Nodal into EBs is restricted and results in distinct responses between soluble delivery and constitutive local expression, and 2) the RA and TGF-β signaling pathways may share common elements [276,277], resulting in similar outcomes for local RA delivery and Nodal over-expression. Differentiation of EBs in media conditioned by HepG2 cells, a hepatocarcinoma-derived endodermal cell line, induces formation of uniform cystic EBs that lack an outer endoderm cell layer [53,54]. This suggests that in the absences of an epithelial exterior, morphogens contained within the conditioned media may more efficiently diffuse into EBs and direct differentiation. Thus, the diffusional limitations posed by EBs may be an underappreciated facet of ESC biology that may lead to an incomplete understanding of the roles of specific molecules in ESC differentiation [22].

Previous studies have reported the incorporation of PLGA microspheres containing growth factors into spheroids of fetal brain cells [156] as well as human EBs [224] in order to manipulate the biochemistry of 3D spheroid microenvironments. PLGA microspheres containing nerve growth factor (NGF) were assembled with fetal rat brain cells to form programmable neo-tissues and transplanted into adult rats. The controlled-release microspheres were able to support transplanted cell survival, but specific effects on cell differentiation were not described or compared directly to soluble delivery methods. Recently, microspheres containing angiogenic growth factors (vascular endothelial, placenta and basic fibroblast growth factors) were incorporated into EBs using forced aggregation, and expression of vascular cell markers was assessed after 10 days of differentiation. However, compared to soluble growth factor treatment, this approach did not improve vascular differentiation of human ESCs, likely due to the lack

of release of growth factors after 24 hours and the low overall growth factor availability. In contrast, small hydrophobic molecules (such as RA) are readily incorporated into PLGA microspheres using a single emulsion and release is sustained over the course of days-weeks, allowing sufficient morphogen availability within EBs to elicit significant differences in ESC differentiation compared to soluble delivery methods.

These results demonstrate that the locally controlled presentation of morphogens from microspheres to cells comprising an EB more closely mimics characteristics of early embryogenesis than simple soluble delivery of signaling molecules to cell spheroids. In addition to developmental studies, microsphere-mediated presentation of morphogenic cues to stem cell spheroids represents a powerful enabling technology readily capable of being integrated into biomanufacturing strategies to obtain stem cell derivatives for regenerative medicine therapies and *in vitro* diagnostic cell technologies. Thus, the application of biomaterials and drug delivery principles to stem cell biology significantly enhances the efficiency of directed differentiation strategies and more clearly reveals the effects of specific molecules on morphogenic events.

CHAPTER 7

DIFFERENTIATION OF MICROSPHERE-MEDIATED RETINOIC ACID TREATED EMBRYOID BODIES IN DEFINED MEDIA CONDITIONS

Introduction

Embryonic stem cells (ESCs) are a commonly studied cell type for applications in developmental biology, regenerative medicine, and pharmaceutical development [7,25,216]. These pluripotent cells, derived from the inner cell mass of the developing blastocyst [2-4], are often differentiated in suspension as three dimensional spheroids known as embryoid bodies (EBs) [5,20,24]. The microenvironment within EBs is complex and dynamic, with cell-cell and cell-extracellular matrix (ECM) interactions, paracrine factor secretion, and media components all contributing to cell fate decisions [21]. The complex milieu of EBs results in spontaneous and heterogeneous cell differentiation, an undesirable result in applications requiring a pure cell population [24]. Efforts to direct differentiation of ESCs comprising EBs have traditionally focused exclusively on treatment with exogenous growth factors and defined media components. Morphogens, including various growth factors [220], bone morphogenetic proteins (BMPs) [278,279], Wnts [87,280], and retinoic acid (RA) [90,212], vitamins [281], small molecule inhibitors [22,282-284], and other organic compounds [285] have been examined in attempts to control the differentiation trajectory within EBs. However, significant barriers limit the ability of such molecules to diffuse throughout EBs in order to interact with cells and regulate gene expression. Basement membrane and tight cell

junctions are commonplace within EBs, and EB diameters often exceed 400 μm and consist of greater than 10,000 cells. Reports confirming transport limitations within EBs underscore the need for alternative methods to direct differentiation within EBs [22].

Polymer microspheres have been incorporated within EBs in order to present morphogens directly within the EB interior, thereby circumventing diffusional barriers at the EB exterior [22,223]. Previous work has utilized PLGA microspheres to deliver RA within EBs in efforts to uniformly direct ESC differentiation [223]. Interestingly, unlike soluble RA treatment, which typically results in neural differentiation [89,90,108,212], microsphere-mediated RA delivery promoted the formation of cystic spheroids with gene and protein expression patterns equivalent to the early primitive streak stage of mouse development. The organization and synchronicity was enhanced in these EBs relative to untreated EBs, which characteristically expressed transcripts indicative of all three germ layers and various stages of development. Cells on the exterior of EBs treated with RA microspheres were microvillous, suggestive of an absorptive phenotype. Transcripts for genes associated with absorption, including cubilin, were significantly increased compared to EBs containing unloaded microspheres. The ultrastructure and gene expression of these EBs indicate that the ability of cells to traffic media components, including nutrients and morphogens, toward the EB interior may be enhanced relative to normal EBs. Additionally, because the cystic RA microsphere-treated EBs predominantly consist of two cell layers (endoderm and epiblast), the diffusional path length required for solutes to reach cells is greatly diminished. Collectively, these data suggest that RA microsphere-treated EBs may uniformly differentiate in a controlled manner in the presence of defined media components.

In this study, EBs containing RA loaded microspheres (RA MS EBs) were cultured in defined media after 10 days in regular media, and the differentiation trajectory of the cells was assessed. Media containing low serum (2.5%), low serum supplemented with BMP4, DMEM/F12 supplemented with insulin, transferrin, and selenium (henceforth referred to as ITS), and ITS with BMP4 were all compared to high serum (15%) differentiation media. The overall morphology of the EBs was assessed via phase microscopy. Gene expression of the various EB treatment groups was analyzed using quantitative PCR. Additionally, immunostaining of whole EBs was used to examine protein expression of OCT4 and Brachyury T. Gene expression data indicated that continued culture of RA MS EBs in full serum promoted endoderm formation, while ITS media supported ectoderm induction. Mesoderm differentiation was most prominent in untreated control EBs cultured in full serum. Culture of RA MS EBs in low serum generally resulted in gene transcript levels between those of EBs grown full serum and ITS. Collectively, these data suggest that EBs differentiated via incorporation of RA microspheres to the point of cavitation are receptive to their extracellular environments, and that differentiation trajectory can be influenced via media choice.

Methods

Microsphere fabrication

Poly(lactic-co-glycolic acid) (PLGA, 50:50, 0.55-0.75 dL/g, ester terminated, Absorbable Polymers International) microspheres were fabricated using a water-in-oil single emulsion, as described [150]. Briefly, 200 mg PLGA was dissolved in

dichloromethane containing 600 µg RA (all trans, Acros Organics, Geel, Belgium), added to 0.3% PVA, and homogenized at 3000 rpm (Polytron PT 3100, Kinematica Inc, Bohemia, NY). Dichloromethane was evaporated for 4 hours and microspheres were collected by centrifugation, washed with dH_2O, and lyophilized for 1-2 days (Freezone 4.5, Labconco, Kansas City, MO).

Embryonic stem cell culture

Murine embryonic stem cells (D3) [1] were maintained in an undifferentiated state on tissue culture dishes coated with 0.1% gelatin in Dulbecco's modified Eagle's medium (DMEM) (Mediatech Inc., Herndon, VA), supplemented with 15 % fetal bovine serum (FBS) (Atlanta Biologicals), 2mM L-glutamine (Mediatech), 100 U/mL penicillin, 100 µg/mL streptomyocin, and 0.25 µg/mL amphotericin (Mediatech), 1x MEM nonessential amino acid solution (Mediatech), 0.1 mM 2-mercaptoethanol (Fisher Chemical, Fairlawn, NJ), and 10^3 U/mL leukemia inhibitory factor (LIF, Chemicon International, Temecula, CA). Cells were routinely passaged with 0.05% Trypsin-EDTA every 2-3 days prior to reaching 70% confluence.

Embryoid Body Formation

To initiate formation of EBs containing PLGA microspheres, microspheres (unloaded and RA) were first coated with 0.1% gelatin and placed on a rotisserie rotator at 37°C for 3 hours. Embryonic stem cell colonies were dissociated into single cells with 0.05% trypsin-EDTA solution and resuspended in 10 mL of differentiation media (2 x 10^5 cells/mL final concentration) with coated microspheres in 100 mm bacteriological-

grade Petri dishes. Embryoid body formation was initiated by placing dishes on an orbital rotary shaker set at 40 rotations per minute (RPM) [68]. EB media was exchanged every 1-2 days as needed. Phase images of EBs were acquired using a Nikon TE 2000 inverted microscope equipped with a SpotFLEX (Diagnostic Instruments) camera.

Defined Media Studies

After 10 days of rotary suspension culture, RA microsphere (RA MS) EBs were switched to low serum, ITS, or remained in full serum. Low serum media consisted of regular differentiation media (ESC media described above, without LIF) containing 2.5% serum (full serum media contained 15%). Media denoted ITS consisted of 1:1 DMEM/F12 (Gibco) supplemented with insulin (5 µg/mL), transferrin (50 µg/mL), and selenium chloride (30 nM). Additionally, RA MS EBs were added to low serum or ITS media supplemented with BMP4 (10 ng/mL, R&D Systems). Phase images of EBs were acquired with a Nikon TE2000 microscope equipped with a SpotFlex camera (Diagnostic Instruments).

Quantitative PCR

After 4, 7, 10, 12, 14, and 17 days, RNA was extracted from EBs with an RNeasy Mini kit (Qiagen Inc, Valencia, CA). Reverse transcription for complementary DNA synthesis was performed with 1 µg of RNA per sample using the iScript cDNA synthesis kit (Bio-Rad, Hercules, CA), and real-time PCR was performed with SYBR green technology on the MyiQ cycler (Bio-Rad). Forward and reverse primers for *Oct4*, *Brachyury-T* (B-T), *fibroblast growth factor 5* (*Fgf5*), *α-fetoprotein* (*Afp*), *fetal liver*

kinase 1 (*Flk1*), myosin light chain 2v (*Mlc2v*), N*estin*, *GATA binding protein 4* (*Gata4*), *paired box gene 6* (*Pax6*), *runt related transcription factor 2* (*Runx2*), *forkhead box a2* (*Foxa2*), *myocyte enhancer factor 2c* (*Mef2c*), and *glyceraldhyde-3-phosphate-dehydrogenase* (GAPDH) were designed with Beacon Designer software, purchased from Invitrogen and validated with appropriate controls. For *Oct4* and F*oxa2*, relative gene expression was quantified as compared to undifferentiated ESC expression levels using the Pfaffl method of quantification [174]. For all other genes, concentrations were calculated using standard curves and normalized to GAPDH expression levels.

Histology

In order to perform whole-mount EB immunofluorescent staining, EBs were washed in PBS, fixed for 1 hour in 4% parafomaldehyde at 4ºC, and washed again 3 times in wash buffer (150mM NaCl, 1 mg/mL bovine serum albumin, 0.1% Tween-20, 50 mM Tris). EBs were permeabilized for 30 minutes in 2% TritonX-100, re-fixed in 4% paraformaldehyde for 15 minutes, and then blocked in wash buffer for 1 hour. Samples were incubated in Oct4 or Brachyury T (Santa Cruz Biotech.) primary antibody overnight at 4ºC, washed again (3 times, 15 minutes), and then incubated in an Alexa488 conjugated secondary antibody (Molecular Probes) for 4 hours at 4ºC. Nuclei were then stained in Hoechst solution (1:100). Finally, samples were re-suspended in a low volume of PBS and imaged with a Zeiss LSM/NLO 510 Multi-photon Microscope (Carl Zeiss Inc.).

Statistical analysis

Values are reported as mean ± standard deviation (n=3). Statistical significance was determined using one or two way ANOVA coupled with Tukey's post hoc analysis using Systat (v12, Systat Software Inc.).

Results

Embryoid body morphology

Embryoid bodies were formed under rotary suspension conditions with either no microspheres (untreated EBs), unloaded microspheres (unloaded MS EBs) or with retinoic acid loaded microspheres incorporated (RA MS EBs). After 10 days of culture in regular differentiation media, RA MS EBs were either maintained in full serum media or transferred to low serum (with and without BMP4) or ITS (with and without BMP4) media. Phase images were acquired 2, 4 and 7 days after the media transfer (Figure 7.1). Untreated and unloaded MS EBs each appeared to be solid spheroids at all time points and were largely uniform in size and shape, though some irregular EBs were observed. In both untreated and unloaded MS EBs, EB size decreased with time, particularly after 17 days. RA MS EBs all appeared to be cystic, as the outline of the epiblast cell layer was clearly discernable in phase images. The regular serum and low serum RA MS EBs were larger and darker in phase images acquired on day 17, suggesting that the epiblast and/or endoderm cells may expand to fill the cystic region. ITS EBs also showed enlargement and darkening after 17 days, though to a lesser extent than regular and low

serum EBs. Regular serum RA MS EBs were larger than other treatments after 12 and 14 days, yet smaller after 17 days. The other RA MS groups displayed growth between 14 and 17 days, whereas regular serum RA MS EBs did not appear to increase in size. The subtle morphological differences in EBs grown in different media formulations prompted further investigation into the differentiation states of the EBs.

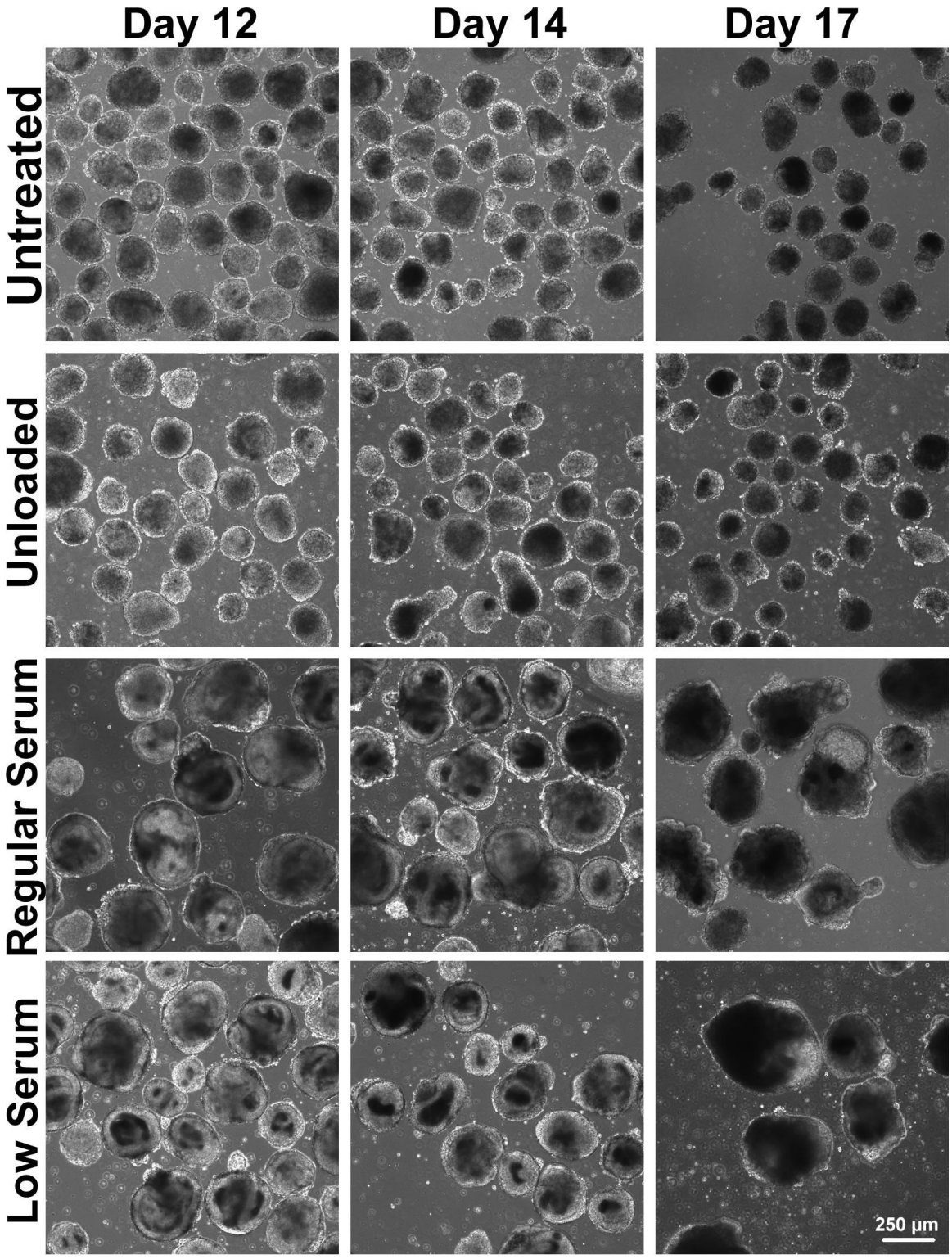

Figure 7.1 Time course of EB morphology. Phase images of EBs were acquired after 12, 14 and 17 days of differentiation for the various treatment groups. Untreated and unloaded MS EBs formed solid spheroids, while RA MS EBs were cystic. Subtle differences in size, growth, and degree of cavitation were noted among the RA MS treatments.

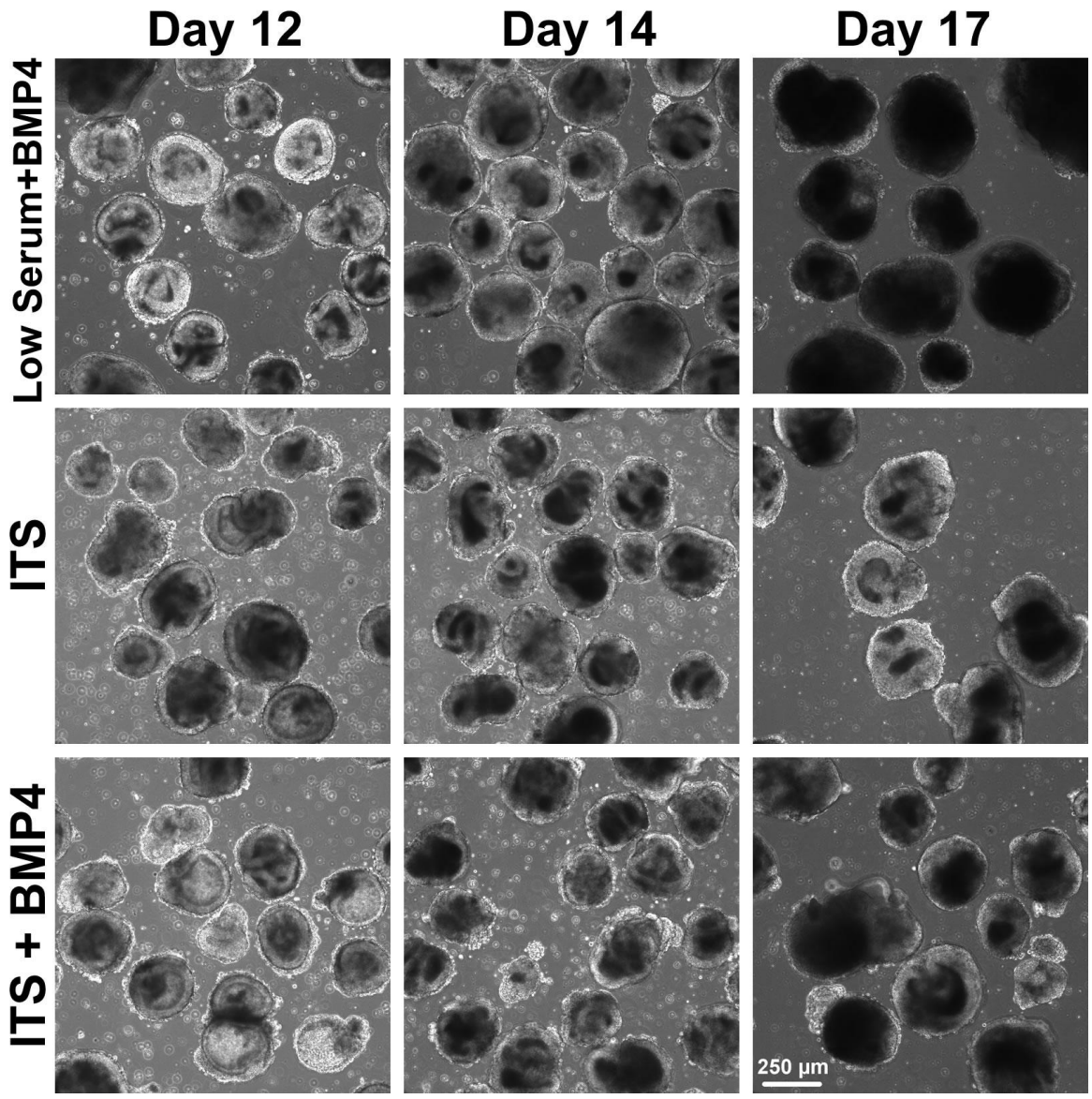

Figure 7.1 continued.

Gene expression analysis

In order to investigate the differentiation state of cells in EBs cultured in the various media formulations, quantitative PCR was performed. Expression of *Oct4*, a transcription factor associated with pluripotency, was significantly lower in RA MS EBs than in untreated or unloaded MS EBs after 4 days, yet higher than both groups after 10 days, which was similar to previous reports (Figure 7.2A). *Oct4* remained higher in full serum RA MS EBs and low serum EBs compared to untreated or ITS EBs after 12 and 14 days. *Fgf5*, a marker for primitive ectoderm (or epiblast) was significantly reduced in EBs cultured in ITS media after 14 and 17 days (Figure 7.2B).

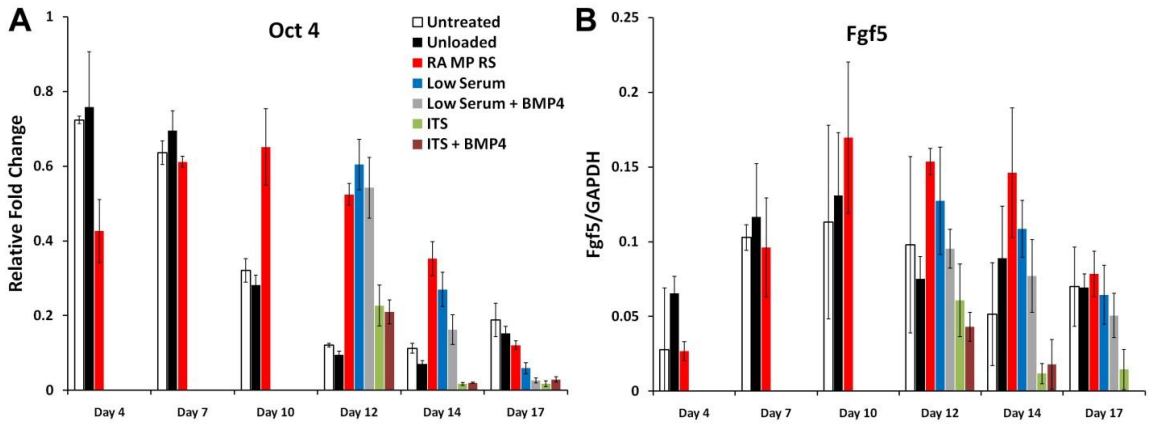

Figure 7.2. Gene expression of pluripotent markers. qPCR was used to analyze expression of the pluripotent gene *Oct4* (A) and the primitive ectoderm gene *Fgf5* (B). *Oct4* was enhanced in regular serum RA MS EBs (red bars) after 10 days, and in regular serum and low serum RA MS EBs (+/-BMP4) after 12 days (red, blue and gray bars). *Fgf5* was significantly reduced in ITS (+/-BMP4) RA MS EBs (green and maroon bars) after 14 and 17 days.

Next, the expression of *Afp*, a phenotypic marker for primitive endoderm, was assessed in the EB treatment groups (Figure 7.3A). RA MS EBs maintained in full serum displayed enhanced *Afp* expression relative to all other groups at all time points (except day 14, at which point comparison to untreated EBs was insignificant). The expression of *Gata4*, a transcription factor expressed by primitive endoderm, mesendoderm and

later cardiac mesoderm [286,287], was also enhanced in full serum RA MS EBs compared to all groups after 7, 10, 12 (except when compared to ITS and unloaded MS), and 17 days (Figure 7.3B).

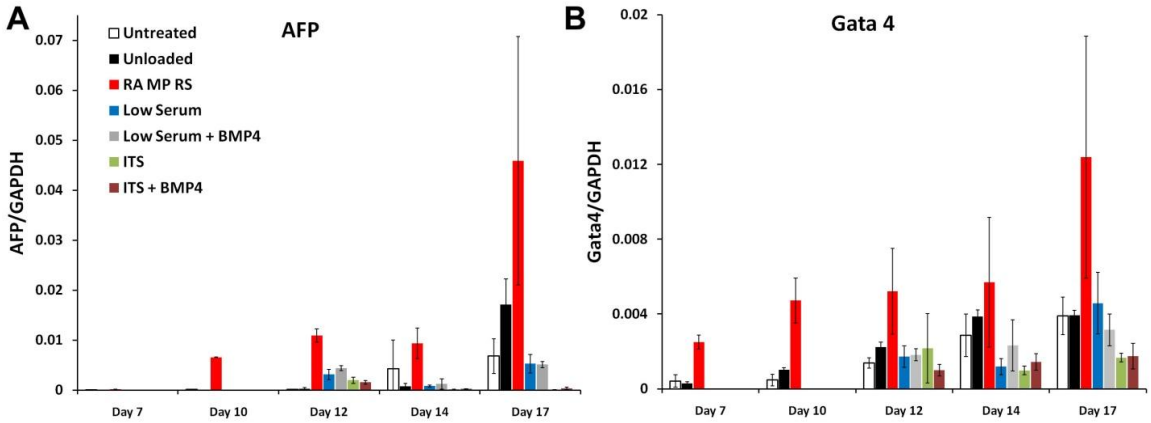

Figure 7.3. Analysis of endoderm and mesendoderm genes. *Afp* (A, primitive endoderm) was enhanced in regular serum RA MS EBs at all time points (except compared to untreated at day 14). *Gata4* (B), an early mesendodermal marker, was likewise enhanced in regular serum RA MS EBs, particularly after 7, 10 and 17 days.

The transcript levels of *Pax6*, a transcription factor expressed during neural development, and *Nestin*, an intermediate filament protein known to be expressed by neural progenitors, were also analyzed (Figure 7.4). In general, expression of these neuroectoderm genes was enhanced in RA MS EBs cultured in ITS media. *Pax6* in particular was strongly enhanced after 12, 14 and 17 days in EBs treated with ITS containing BMP4 (Figure 7.4A). Prior to day 17, *Nestin* expression was most prominent in untreated and unloaded MS EBs, though a spike was observed on day 17 in the ITS EBs (Figure 7.4B). Reports indicate that *Nestin* expression is less specific to neuroectoderm than *Pax6*, suggesting that increased levels of *Nestin* expression by untreated and unloaded MS EBs could be emanating from non-neural cell types [288,289].

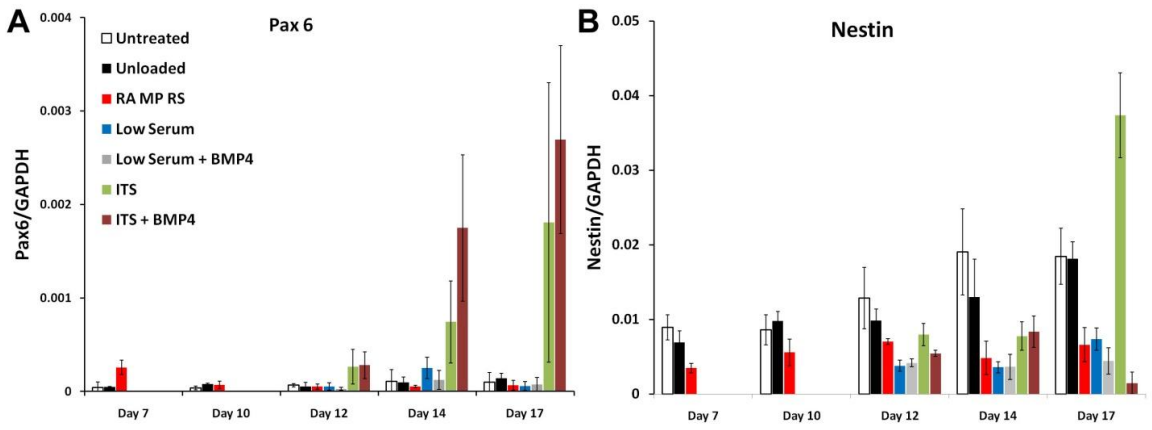

Figure 7.4. Neuroectoderm gene expression. *Pax6* (A) expression was greatest in RA MS EBs in ITS media (green and maroon bars). *Nestin* (B) expression was most consistent in untreated and unloaded MS EBs. Day 17 RA MS ITS EBs displayed a sharp spike in *Nestin* expression.

Next, a panel of mesoderm marker was examined (Figure 7.5). *Flk1*, a gene encoding a VEGF receptor commonly expressed in endothelial cells, *Brachyury T*, a transcription factor expressed in the primitive streak, *Mlc2v*, a cardiac specific motor protein, and *Mef2c*, a transcription factor critical in cardiovascular development, were all analyzed via qPCR. *Brachyury T* (Figure 7.5B) was significantly enhanced in untreated and unloaded MS EBs compared to all other EBs at all time points (except compared to low serum at day 14). *Flk1* (Figure 7.5A) was also generally enhanced in untreated and unloaded MS EBs, particularly after 12 days. Levels of *Mlc2v* (Figure 7.5C) and *Mef2c* (Figure 7.5D) and were very low in all groups except for untreated and unloaded MS EBs. These results demonstrate that mesoderm induction appears to be inhibited in EBs containing RA microspheres. Overall, the gene expression data indicate that culture of RA MS EBs in ITS promotes ectoderm induction, the use of full serum enhances endoderm formation, and that untreated and unloaded MS EBs exhibit the greatest mesoderm formation.

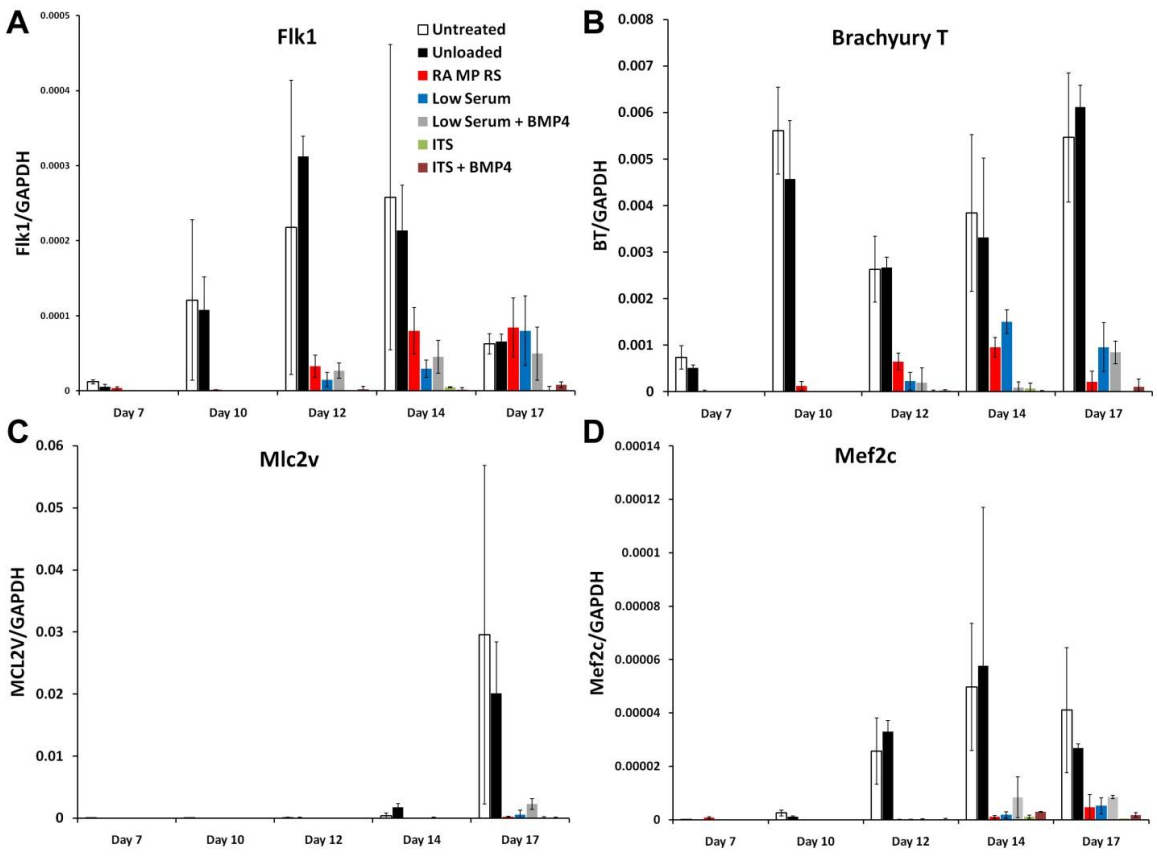

Figure 7.5. Mesoderm gene expression. Transcript levels of *Flk1* (A), *Brachyury T* (B), *Mlc2v* (C), and *Mef2c* (D) were assessed. For all mesoderm related genes, expression was consistently highest in untreated and unloaded MS EBs.

Immunostaining

To further investigate the differentiation of RA MS EBs in various media formulations, immunostaining of whole EBs was performed. Staining for OCT4 in the RA MS EBs in regular serum, low serum (+/- BMP4), and ITS (+/- BMP4) was performed after 12, 14, and 16 days (2, 4 and 6 days, respectively, after switching from full serum media) (Figure 7.6). After 12 days, EBs in regular and low serum displayed an OCT4-negative endoderm-like outer layer enveloping nearly uniformly OCT4-positive cells. EBs cultured in ITS displayed regions of OCT4 staining, but also contained many

OCT4 negative cells. The addition of BMP4 to ITS appeared to enhance the expression of OCT4 in 12 day EBs. After 14 days, OCT4 staining remained prevalent in full serum RA MS EBs. Low serum also supported OCT4 positive cells, though staining was less uniform than in the corresponding day 12 EBs. In contrast, after 14 days, EBs grown in ITS displayed few cells staining positively for OCT4. Finally, after 16 days, full serum and low serum each maintained a high percentage of OCT4-positive cells. Interestingly, the addition of BMP4 to low serum appeared to reduce the percentage of positively stained cells. As with 14 day EBs, ITS EBs after 16 days had low levels of staining, though addition of BMP4 appeared to mildly increase expression. In general, the immunostaining images are in agreement with the gene expression data obtained via qPCR. Full and low serum media supported continued expression of OCT4, whereas ITS did not. Gene expression data suggested that the addition of BMP4 to either low serum or ITS did not significantly affect *Oct4* expression, while analysis of the OCT4 protein suggested that BMP4 may have attenuated expression in low serum while enhancing expression in ITS. However, quantitative analysis of protein expression would be required to validate this observation.

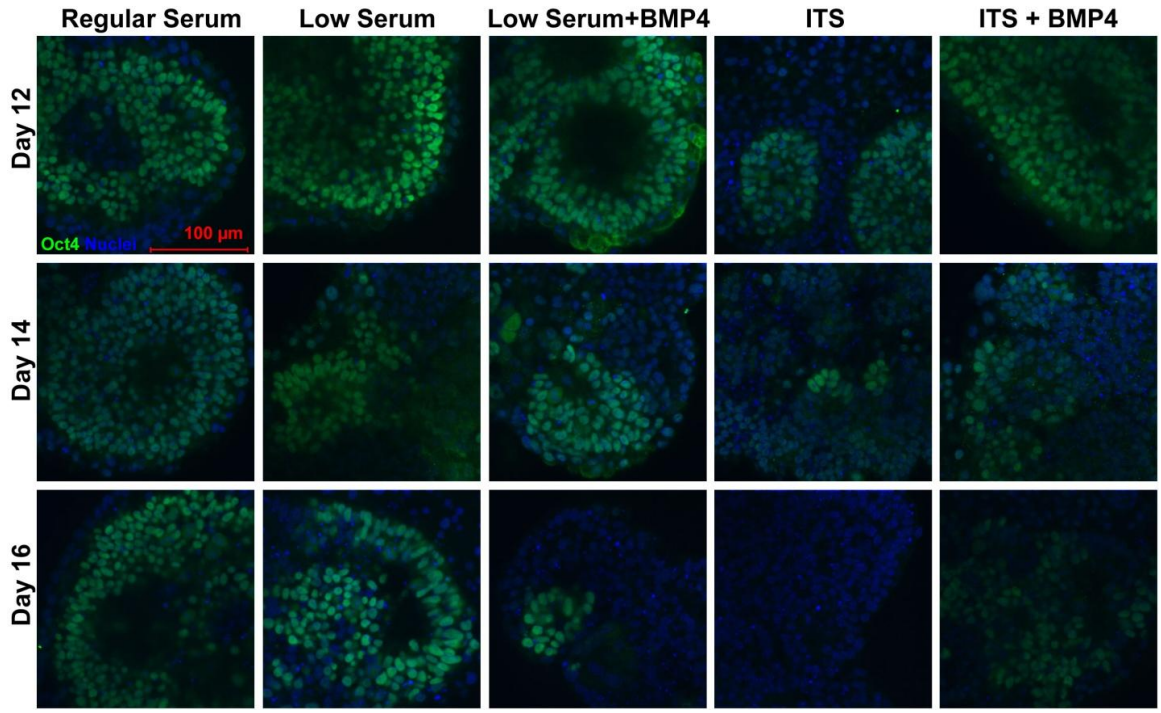

Figure 7.6. OCT4 staining in RA MS EBs cultured in various media conditions. OCT4 expression was most prominent in regular serum and low serum EBs. The addition of BMP4 appeared to foster OCT4 expression in serum-free (ITS) media, yet attenuate expression in low serum.

Expression of the transcription factor Brachyury T was also assessed using whole-mount immunofluorescent staining (Figure 7.7). Brachyury T was expressed less prominently than OCT4 in all EBs. ITS media did not support an appreciable level of Brachyury induction at any of the time points examined, as few labeled cells were observed. Regular serum EBs did not show significant positive staining until 16 days, at which point a region of stained cells was observed. Low serum appeared to support the most consistent induction of Brachyury expression, as positive cells were observed at each time point. The addition of BMP4 did not seem to significantly affect Brachyury T expression in either low serum or ITS media. Protein expression corroborated gene expression data, which showed that low serum evoked the greatest levels of Brachyury

among the RA MS EBs. However, expression in RA MS EBs was generally lower than in untreated or unloaded MS EBs.

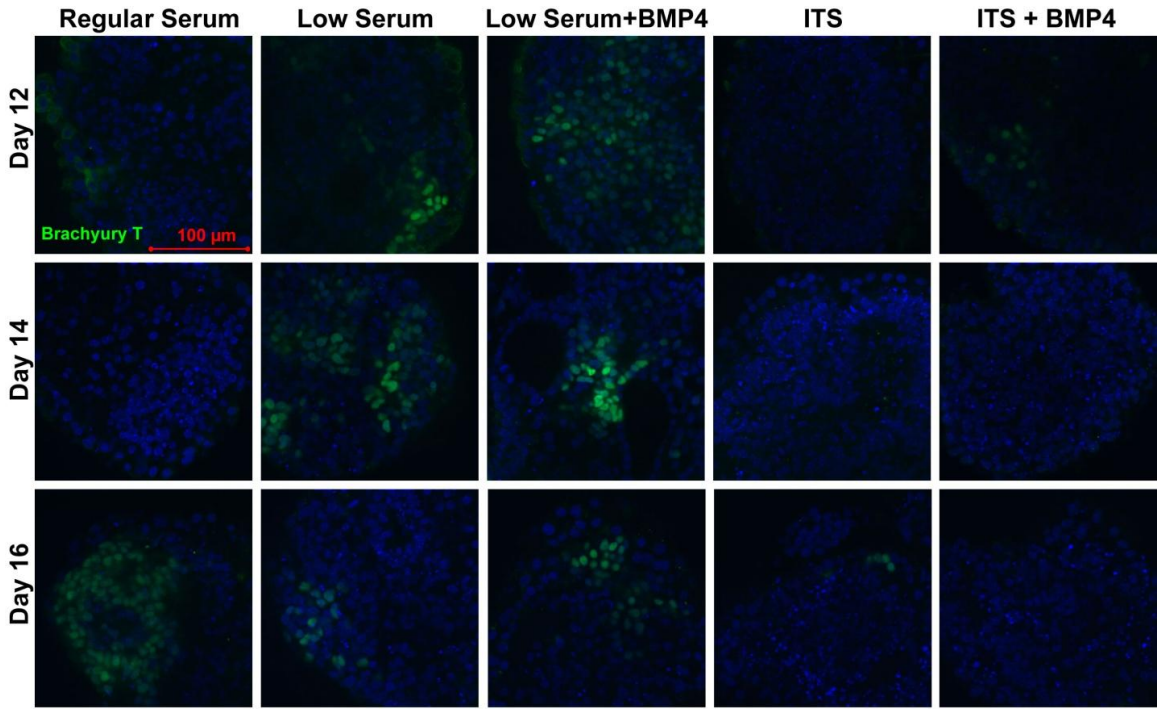

Figure 7.7. Brachyury T expression in RA MS EBs. Staining for Brachyury T was relatively low for all treatment groups. RA MS EBs cultured in low serum media (+/- BMP4) exibited the most positive staining.

Discussion

In these studies, the differentiation of EBs pre-treated with RA MS for 10 days prior to incubation in defined media conditions was examined. The morphology of EBs showed stark differences among untreated and unloaded MS EBs and RA MS EBs. Differences within RA MS EBs cultured in the various media conditions were more subtle, though distinctions in size and cavitation were noted. Gene expression analysis revealed interesting trends within the RA MS EBs; continued culture in full serum appeared to maintain pluripotent cells, but also enhanced expression of primitive endoderm genes. Transfer to ITS media evoked the greatest levels of neuroectoderm gene expression levels among the RA MS EBs. Low serum culture appeared to result in intermediate expression levels between full serum and serum free media EBs. Mesoderm gene expression appeared to be inhibited in all RA MS EBs relative to untreated and unloaded MS EBs, though low serum appeared to be the most meso-inductive among RA MS EBs. Protein expression analysis via whole-mount immunostaining generally confirmed trends noted from qPCR. These results demonstrate that the media environment can be used to direct the differentiation trajectory of RA MS EBs.

The ability to efficiently direct ESC differentiation has implications for fields as diverse as developmental biology, pharmacology, and tissue engineering. While different media formulations have been shown to improve differentiation down specific pathways, it was postulated that the asynchrony of cells within EBs and gradients of instructive media components would contribute to heterogeneity in EB-based differentiation strategies. Many EB protocols call for formation and initial growth of EBs in high serum media, as this best supports cell aggregation and survival. After 2-4 days of growth,

supplemental cues are added to the media, or the high serum media is replaced with defined media. The initial period of EB culture in serum with undefined morphogens and cytokines may result in a heterogeneous cell population that is subsequently exposed to the rigorously defined media of the differentiation protocol. Because instructive cues for ESC differentiation are generally context dependent, with the specific cellular components that the cell possesses dictating the ability of the cell to respond, the lack of synchronicity within EBs may pose a problem for producing a uniform population of differentiated cells. Because RA MS EBs appear to be in a synchronized state after 10 days of culture and consist largely of pluripotent epiblast cells and supportive visceral endoderm cells, we hypothesized that uniform differentiation of the epiblast cells could be induced through selection of media components and supplemental morphogens.

The results of this study indicate that the choice of media could be used to further instruct differentiation of RA MS EBs after 10 days. Broad trends that were noted include maintenance of pluripotency in serum-containing media relative to serum-free (ITS), induction of endoderm in full serum media, enhancement of ectoderm in ITS media, and inhibition of mesoderm in all RA MS EBs relative to RA-free controls. More rigorous assessments of the relative proportions of these cell types will be needed in order to make definitive statements on the effectiveness of the different media formulations on directing differentiation. It was generally noted, however, that the addition of BMP4 to either low serum or ITS media did not have a profound effect on differentiation. This morphogen was chosen as a supplement due to its role in early embryo patterning. The production of BMP4 on the posterior side of the developing embryo and BMP antagonists (Noggin, Chordin, Follistatin) on the anterior side are thought to play a role in

the spatial regulation of primitive streak induction and neuroectoderm formation. By introducing BMP4 to epiblast-like cells, it was expected that primitive streak and mesoderm differentiation would be enhanced. However, significant increases in mesoderm gene expression or Brachyury T protein expression were not observed in EBs treated with BMP4. One possible explanation for this is that the visceral endoderm cells that surround the epiblast secrete a multitude of factors which may provide conflicting signals for differentiating cells. In embryogenesis, factors secreted by the visceral endoderm are spatially regulated such that proper tissue development takes place. However, in the context of the EB, it is not clear what dictates which factors are secreted by visceral endoderm cells. Microarray studies (Chapter 6, Figure 6.10) suggested that genes associated with anterior visceral endoderm (AVE) were expressed in RS MS EBs, including *Follistatin*, *Dkk1*, *Cer1* and *Foxa2*. Factors secreted by the AVE often function to inhibit BMP and Wnt signaling, thereby promoting ectoderm induction. In serum free conditions, these AVE signals may promote the neuroectoderm gene enhancement that was observed in ITS media. The combination of serum proteins and AVE signals may combine to drive endoderm differentiation, as demonstrated by *Afp* and *Gata4* expression. Finally, AVE signaling may be sufficient to block mesoderm induction, even in the presence of full serum.

In summary, these results indicate that media choice is an important consideration for continued differentiation of RA MS treated EBs. The specific signals secreted by the supportive visceral endoderm cells may hinder differentiation to some cell lineages while enhancing differentiation of others. Future directions in this area may include isolation of

epiblast cells from EBs in order to remove visceral endoderm as a competing factor to media constitution.

CHAPTER 8

CONCLUSIONS AND FUTURE DIRECTIONS

In this work, the production of uniform EBs containing polymer microspheres using rotary suspension culture was reported. Rotary culture was utilized to produce EBs homogeneous in size and shape with high efficiency and with high yield. The incorporation of PLGA microspheres into EBs could be modulated through microsphere coating, microsphere size, ratio of microspheres to cells, and rotary mixing speed. The incorporation of microspheres did not negatively impact cell viability, nor did it significantly affect cell differentiation. Diffusion of a fluorescent dye within EBs was examined temporally, and evidence was provided that limitations to diffusive transport within EBs exist. The incorporation of retinoic acid-loaded microspheres within EBs resulted in the formation of cystic spheroids with spatial organization and gene expression similar to the developing embryo at the onset of primitive streak formation. Continued differentiation of the cystic EBs in defined media suggested that differentiation to mesoderm, endoderm or ectoderm could be influenced through the specific media formulation. While these results demonstrate an innovative integration of stem cell engineering, biomaterials, and drug delivery, facets of each of these studies remain to be explored.

Rotary suspension culture is a simple and efficient method for bench-scale production of uniform EBs. The ability to control EB size and therefore downstream differentiation events was alluded to in this work but not rigorously described. Subsequent work in this area has described the use of rotary culture to enhance

cardiomyocyte differentiation in EBs relative to static culture. The ability to control EB size through modulation of rotary speed has also been confirmed. Assessment of differentiation of EBs formed at the different rotary speeds demonstrated that gene expression profiles and the proportions of differentiated cell populations could be modulated through choice of rotary speed. This approach, however, does not separate the variables of hydrodynamic environment and EB size, so the differentiation observed could be in response to EB size alone, shear forces from the fluid environment, or a combination of the two. Ongoing studies are utilizing forced aggregation to form uniform EBs in the absence of rotary culture. By placing the uniform EBs in rotary culture at different speeds, the hydrodynamic effect can be isolated. Conversely, forced aggregation can be used control the size of the aggregates, so EBs of different size can be cultured at the same speed in order to isolate the size effect. These studies will thoroughly exploit the rotary system as a tool for probing EB differentiation mechanisms.

The diffusion of CellTracker Red within EBs was examined in order to mimic the transport of a small, hydrophobic morphogen, such as retinoic acid. However, examination of RA diffusion was not assessed directly. Labeling of RA with a fluorescent probe would significantly increase the molecular weight of RA (MW of RA is 300.44 Da, while typical dyes are 600-1000 Da) and would in turn affect the diffusion properties of the molecule. In order to detect RA diffusion directly in a minimally disruptive manner, radio-labeling of RA could be utilized. Such an approach would allow for more accurate understanding of the diffusion of RA within EBs. Additionally, radio-labeled RA could also prove useful for understanding the kinetics of RA uptake and consumption. While studies of CellTracker Red diffusion indicated that the dye was not

free to diffuse throughout the spheroids, significant EB penetration was observed. Growth factors are typically larger molecules than either RA or CellTracker, and it is expected that diffusion of growth factors within EBs will be more severely restricted. Future studies could strive to characterize the diffusion of larger, hydrophilic molecules within EBs. This may provide a strong rationale for the use of hydrogel-based microspheres to overcome diffusional barriers and deliver growth factors within EBs. In addition, a predictive model was not used to investigate diffusion within spheroids. A model based on Fick's laws could be constructed in order to predict diffusion as a function of spheroid size as well as diffusive parameters of both the solute and EBs. Experimental extraction of parameters such as diffusion coefficients would be required, as would experimental validation of the model.

Polymer microspheres composed of PLGA were incorporated within EBs, and the effects of various parameters on incorporation were studied. Somewhat surprisingly, these studies demonstrated that the presence of microspheres within EBs did not affect viability or differentiation. Because ECM is an integral component of microenvironments both *in vitro* and *in vivo*, it was expected that the choice of ECM microsphere-coating would alter the differentiation of cells within EBs. However, none of the ECM molecules examined, including gelatin, laminin and fibronectin, significantly affected EB gene expression. Future work will explore the use of protein-mimetic peptide sequences in order to target specific integrins on cell surfaces. This should enable greater interaction of the cell-binding motifs with cells than coating microspheres with the full protein. Such experiments may lead to a novel route to directing differentiation of stem cells in 3D culture. Additional molecules may also be used to coat

microspheres in order to control cell-microsphere interactions. Cell-cell adhesions in early EBs are generally mediated by E-Cadherin. Coating of microspheres with E-Cadherin in a controlled orientation may promote controlled assembly of microsphere-cell constructs. Other cell adhesion molecules, such as N-Cadherin, or VE-Cadherin, may also be utilized in these studies. Microspheres coated with these Cadherins could be incorporated within EBs using forced-aggregation techniques. These molecules may be used to mimic cell-cell adhesions in order to determine whether the presence of such molecules can influence stem cell fate. Thus, such an approach may be useful for studying the role of cell-cell interactions in the EB microenvironment in a novel manner and may be useful for directed differentiation.

Retinoic acid was chosen as a morphogen to be delivered via microspheres within EBs due to its ease of encapsulation in hydrophobic polymers and ubiquity in ESC differentiation studies. However, because RA is relatively small and hydrophobic, its diffusion in EBs may be less restricted than larger, more hydrophilic molecules. In spite of this, RA delivered via microspheres produced a profound biological result that could not be reproduced through soluble delivery. The use of microspheres to deliver growth factors within EBs has the potential to induce a more prodigious effect on EB differentiation. Ongoing studies are focused on the development of hydrogel-based microspheres to deliver growth factors within EBs. The presence of the hydrogel materials alone may also have an impact on differentiation and will be assessed. Additionally, some hydrogel materials that have been investigated do not readily incorporate within EBs using the rotary method. The forced aggregation approach has been adopted to incorporate these microspheres within EBs. Preliminary results suggest

that multiple microspheres (e.g. containing different dyes or growth factors) can be incorporated in a spatially controlled manner using forced aggregation. Future studies will be designed to investigate axis formation and cell patterning by purposefully inducing morphogen gradients within the interior of EBs.

The technology developed in this proposal can also be readily adapted to deliver molecules other than traditional morphogens (i.e. growth factors, cytokines and small molecules). For example, small interfering RNA (siRNA) is commonly used to silence gene expression of specific targets without creating knockout genotypes. This approach is advantageous over knockout models in that silencing is inducible rather than constitutive, so temporal assessments are possible, as well as in ease of use. However, as with any other solute, diffusion of siRNA into EBs is likely limited by the matrix and cell-cell junctions in EBs. Microspheres encapsulating siRNAs targeting genes of interest may be used to more effectively silence expression than soluble delivery. Microspheres may also be used to deliver various types of probes within EBs to directly examine properties of the EB microenvironment. For example, live imaging of the redox environment within EBs, which may be useful for understanding the role of reactive oxygen in stem cell differentiation, could be facilitated by microsphere encapsulation. Similarly, pH sensitive probes encapsulated within microspheres may be used to analyze the local pH environment within differentiating EBs. Such an approach would allow for investigation into the buildup of acidic by-products of metabolism within EBs, which may result due to transport limitations within EBs.

PLGA was chosen as the microsphere material in these studies due to its ubiquity in the biomaterials community, ease of microsphere fabrication, and well characterized

degradation and release properties. However, for many applications, a material with a higher degree of sophistication is desirable. Stimulus-responsive materials have been developed to respond to changes in temperature, pH, light, mechanical stimulation, as well as enzyme presence. Such materials are capable of allowing on-demand delivery; that is, no release prior to the stimulus, followed by controlled release after the stimulus. A shift toward stimulus-responsive materials for incorporation into EBs may be advantageous for a number of reasons. It is known that different cell types can respond to the same morphogenic signal in widely different manners. As such, presentation of morphogens to EBs containing cells in various differentiation states is likely to result in further heterogeneous differentiation. If, however, morphogen release from microspheres is delayed until a known differentiation event occurs, differentiation may be more uniform. For example, if differentiation to a specific progenitor were accompanied by an increase in secretion of an enzyme, a biomaterial with a peptide sequence responsive to that enzyme could be designed and used to make microspheres. Encapsulation of a morphogen that induces maturation of the progenitor cell could be used to direct differentiation to terminally differentiated cells. An analogous approach could be used with GFP-linked promoters and other stimulus responsive materials. For example, GFP linked to *Brachyury T* expression could be used to detect primitive streak induction in real-time. Once *Brachyury T* is detected, microspheres could be stimulated (via temperature change, ultrasound, or light exposure) to release their contents in order to direct the differentiation of *Brachyury* positive cells. In this manner, more rigorous control over the EB microenvironment may be achieved.

While it was observed that the incorporation of RA-loaded microspheres into EBs resulted in the formation of cystic structures, a complete understanding of the events driving this morphological change was not acquired. Understanding how and why the cells in these EBs behave the way they do may be useful in further controlling differentiation. Confirmation that the RA signaling pathway is activated in response to microsphere-mediated RA delivery could be demonstrated through analysis of components of this pathway, including cellular retinoic acid binding proteins (CRABP I and II), retinoid acid and retinoid X receptors, as well as retinoic acid response elements (RAREs). Cavitation within EBs could be presumably due to necrosis, programmed cell death (PCD), or simply cell migration. Determining the relative contribution of the processes to cystic EB formation would help provide a mechanistic understanding of the process. Real-time detection of Caspase, or other markers for apoptosis, would allow for rapid identification of PCD in EBs. Migration could be analyzed by first labeling a small fraction of the cells used to form EBs with a long-term fluorescent tracer. A single EB could be isolated, and the fluorescence within the EB assessed periodically with multi-photon fluorescent microscopy in order to track cell movement. It could then be determined whether cavities within EBs form due to cell migration, PCD, or contributions from each process.

Embryoid bodies treated with RA-loaded microspheres were observed to contain spatially distinct endoderm and epiblast cell layers. Future studies will address the spatio-termporal events that lead to the formation of these distinct layers. Fluorescent proteins can be linked to the promoters for epiblast and endoderm specific genes (for example, GFP-Fgf5 and RFP-FoxA2). The expression of these proteins can then be

monitored in a non-destructive manner through confocal microscopy. Fluorescence as a function of radial distance could be quantified in order to obtain spatial information on the two cell types. Additionally, movement over time of endoderm and epiblast cells could be analyzed using these methods. Such an approach would lead to a better understanding of the formation of EBs resembling early primitive streak stage mouse embryos.

It was hypothesized that cystic RA MS EBs could be induced to differentiate to more mature cell types when cultured in defined media conditions. Gene expression data suggested that the three germ lineages preferentially differentiated under different conditions. Ectoderm induction was most prominent in ITS media, endoderm was enhanced in full serum media, while mesoderm induction was greatest in untreated EBs. The starkest differences in gene expression were observed at the last time point studied (17 days), particularly for endoderm and ectoderm genes. It is possible that divergence was beginning at this time and continued culture would have resulted in more pronounced phenotypic differences. Future studies in this area will include time points past 17 days. Additionally, to quantitatively assess differentiation to specific cell types, methods such as flow cytometry will be employed. This will allow for statements on the yield of cells (on a percentage basis) from each of the three germ layers under different conditions to be made.

The addition of BMP4 to either low serum media or ITS media did not seem to strongly alter gene expression. The choice of BMP4 may not have been ideal for the media types chose. It was expected that BMP4 would promote mesoderm formation, as BMP4 contributes to this process *in vivo*. The addition of a morphogenic factor was

expected to be most pronounced in the ITS groups due to its lack of serum proteins which may dilute the effect of the supplemental morphogen. However, ITS alone did not support mesoderm formation and instead enhanced ectoderm induction. The ITS may have been overriding such that the effect of BMP4 was diminished in this environment. A morphogen more complementary to the action of ITS media will be utilized in future studies. However, preliminary studies with Noggin, a BMP inhibitor, did not suggest strong differences compared to ITS alone, though additional characterization is required. Additional morphogens will be examined, including Wnts, Wnt inhibitors, and hedgehog signaling agonists.

The visceral endoderm plays a significant role in embryo patterning and may provide potent instructive cues to epiblast cells in RA MS EBs. Media selection may be insufficient to overcome the signaling prowess of the visceral endoderm, in which case continued screening of media and supplements may be a fruitless effort. The dissociation of RA MS EBs in order to isolate epiblast cells from the endoderm will be attempted. Cell sorting based on OCT4 expression can be utilized, as endoderm cells were observed to be consistently OCT-negative. Successful isolation of epiblast cells may enable more efficient differentiation.

All work described thus far has focused on *in vitro* differentiation of ESCs in EBs. However, the incorporation of microspheres within EBs could also be applicable for transplantation studies on stem cells and *in vivo* differentiation. In traditional cell transplantation studies, the microenvironment of the implanted cells cannot be manipulated, post-procedure. However, the incorporation of microspheres within spheroids allows for control over the factors presented to the cells even after

implantation. As a result, *in vivo* differentiation of ESCs, which typically results in teratoma formation, may be more controlled in the presence of controlled release microspheres. Additionally, microspheres could be labeled in order to track the implanted constructs. For example, a near-infrared dye could be encapsulated in microspheres such that imaging could be performed in live animals. These studies would make the microsphere-mediated delivery approach more relevant in tissue engineering and regenerative medicine applications.

In conclusion, this work has realized a unique approach for stem cell differentiation through modification of the internal microenvironment of ESC spheroids. This novel inside-out method toward engineering EBs demonstrated that the mode of morphogen delivery (soluble or microsphere-mediated) significantly affected the course of differentiation. Future studies will utilize the choice of microsphere material, coating, and morphogen in order to uniquely study mechanisms of ESC differentiation and achieve unparalleled engineering of the EB microenvironment.

REFERENCES

1. Doetschman, TC, Eistetter, H, Katz, M, Schmidt, W and Kemler, R. The in vitro development of blastocyst-derived embryonic stem cell lines: formation of visceral yolk sac, blood islands and myocardium. J Embryol Exp Morphol. 1985;87:27-45.
2. Evans, MJ and Kaufman, MH. Establishment in culture of pluripotential cells from mouse embryos. Nature. 1981;292:154-6.
3. Martin, GR. Isolation of a pluripotent cell line from early mouse embryos cultured in medium conditioned by teratocarcinoma stem cells. Proc Natl Acad Sci U S A. 1981;78:7634-8.
4. Thomson, JA, Itskovitz-Eldor, J, Shapiro, SS, Waknitz, MA, Swiergiel, JJ, Marshall, VS and Jones, JM. Embryonic stem cell lines derived from human blastocysts. Science. 1998;282:1145-7.
5. Itskovitz-Eldor, J, Schuldiner, M, Karsenti, D, Eden, A, Yanuka, O, Amit, M, Soreq, H and Benvenisty, N. Differentiation of human embryonic stem cells into embryoid bodies compromising the three embryonic germ layers. Mol Med. 2000;6:88-95.
6. Desbaillets, I, Ziegler, U, Groscurth, P and Gassmann, M. Embryoid bodies: an in vitro model of mouse embryogenesis. Exp Physiol. 2000;85:645-51.
7. Prelle, K, Zink, N and Wolf, E. Pluripotent stem cells--model of embryonic development, tool for gene targeting, and basis of cell therapy. Anat Histol Embryol. 2002;31:169-86.
8. Lebkowski, JS, Gold, J, Xu, C, Funk, W, Chiu, CP and Carpenter, MK. Human embryonic stem cells: culture, differentiation, and genetic modification for regenerative medicine applications. Cancer J. 2001;7 Suppl 2:S83-93.
9. Cima, LG, Vacanti, JP, Vacanti, C, Ingber, D, Mooney, D and Langer, R. Tissue engineering by cell transplantation using degradable polymer substrates. J Biomech Eng. 1991;113:143-51.
10. Hubbell, JA. Biomaterials in tissue engineering. Biotechnology (N Y). 1995;13:565-76.
11. Nerem, RM and Sambanis, A. Tissue engineering: from biology to biological substitutes. Tissue Eng. 1995;1:3-13.
12. Smith, AG, Heath, JK, Donaldson, DD, Wong, GG, Moreau, J, Stahl, M and Rogers, D. Inhibition of pluripotential embryonic stem cell differentiation by purified polypeptides. Nature. 1988;336:688-90.
13. Williams, RL, Hilton, DJ, Pease, S, Willson, TA, Stewart, CL, Gearing, DP, Wagner, EF, Metcalf, D, Nicola, NA and Gough, NM. Myeloid leukaemia inhibitory factor maintains the developmental potential of embryonic stem cells. Nature. 1988;336:684-7.

14. Tropepe, V, Hitoshi, S, Sirard, C, Mak, TW, Rossant, J and van der Kooy, D. Direct neural fate specification from embryonic stem cells: a primitive mammalian neural stem cell stage acquired through a default mechanism. Neuron. 2001;30:65-78.

15. Cohen, MA, Itsykson, P and Reubinoff, BE. The role of FGF-signaling in early neural specification of human embryonic stem cells. Dev Biol.

16. Mumaw, JL, Machacek, D, Shields, JP, Dodla, MC, Dhara, SK and Stice, SL. Neural differentiation of human embryonic stem cells at the ultrastructural level. Microsc Microanal. 16:80-90.

17. Rajesh, D, Chinnasamy, N, Mitalipov, SM, Wolf, DP, Slukvin, I, Thomson, JA and Shaaban, AF. Differential requirements for hematopoietic commitment between human and rhesus embryonic stem cells. Stem Cells. 2007;25:490-9.

18. Tian, X and Kaufman, DS. Hematopoietic development of human embryonic stem cells in culture. Methods Mol Biol. 2008;430:119-33.

19. Zeng, X, Cai, J, Chen, J, Luo, Y, You, ZB, Fotter, E, Wang, Y, Harvey, B, Miura, T, Backman, C, Chen, GJ, Rao, MS and Freed, WJ. Dopaminergic differentiation of human embryonic stem cells. Stem Cells. 2004;22:925-40.

20. Hopfl, G, Gassmann, M and Desbaillets, I. Differentiating embryonic stem cells into embryoid bodies. Methods Mol Biol. 2004;254:79-98.

21. Bratt-Leal, AM, Carpenedo, RL and McDevitt, TC. Engineering the embryoid body microenvironment to direct embryonic stem cell differentiation. Biotechnol Prog. 2009;25:43-51.

22. Sachlos, E and Auguste, DT. Embryoid body morphology influences diffusive transport of inductive biochemicals: A strategy for stem cell differentiation. Biomaterials. 2008;29:4471-80.

23. Wartenberg, M, Gunther, J, Hescheler, J and Sauer, H. The embryoid body as a novel in vitro assay system for antiangiogenic agents. Lab Invest. 1998;78:1301-14.

24. Keller, GM. In vitro differentiation of embryonic stem cells. Curr Opin Cell Biol. 1995;7:862-9.

25. Eglen, RM, Gilchrist, A and Reisine, T. An overview of drug screening using primary and embryonic stem cells. Comb Chem High Throughput Screen. 2008;11:566-72.

26. Murry, CE and Keller, G. Differentiation of embryonic stem cells to clinically relevant populations: lessons from embryonic development. Cell. 2008;132:661-80.

27. Grabel, L, Becker, S, Lock, L, Maye, P and Zanders, T. Using EC and ES cell culture to study early development: recent observations on Indian hedgehog and Bmps. Int J Dev Biol. 1998;42:917-25.

28. Weitzer, G. Embryonic stem cell-derived embryoid bodies: an in vitro model of eutherian pregastrulation development and early gastrulation. Handb Exp Pharmacol. 2006;21-51.

29. Rossant, J and Tam, PP. Blastocyst lineage formation, early embryonic asymmetries and axis patterning in the mouse. Development. 2009;136:701-13.

30. Takahashi, K and Yamanaka, S. Induction of pluripotent stem cells from mouse embryonic and adult fibroblast cultures by defined factors. Cell. 2006;126:663-76.

31. Lowry, WE, Richter, L, Yachechko, R, Pyle, AD, Tchieu, J, Sridharan, R, Clark, AT and Plath, K. Generation of human induced pluripotent stem cells from dermal fibroblasts. Proc Natl Acad Sci U S A. 2008;105:2883-8.

32. Okita, K, Nakagawa, M, Hyenjong, H, Ichisaka, T and Yamanaka, S. Generation of mouse induced pluripotent stem cells without viral vectors. Science. 2008;322:949-53.

33. Ye, Z, Zhan, H, Mali, P, Dowey, S, Williams, DM, Jang, YY, Dang, CV, Spivak, JL, Moliterno, AR and Cheng, L. Human-induced pluripotent stem cells from blood cells of healthy donors and patients with acquired blood disorders. Blood. 2009;114:5473-80.

34. Ebert, AD, Yu, J, Rose, FF, Jr., Mattis, VB, Lorson, CL, Thomson, JA and Svendsen, CN. Induced pluripotent stem cells from a spinal muscular atrophy patient. Nature. 2009;457:277-80.

35. Colman, A and Dreesen, O. Pluripotent stem cells and disease modeling. Cell Stem Cell. 2009;5:244-7.

36. Carpenedo, RL and McDevitt, TC. Microscale Technologies for Engineering Stem Cell Environments, in Micro and Nanoengineering of the Cell Microenvironment. 2008

37. Metallo, CM, Mohr, JC, Detzel, CJ, de Pablo, JJ, Van Wie, BJ and Palecek, SP. Engineering the stem cell microenvironment. Biotechnol Prog. 2007;23:18-23.

38. Shen, MM and Leder, P. Leukemia inhibitory factor is expressed by the preimplantation uterus and selectively blocks primitive ectoderm formation in vitro. Proc Natl Acad Sci U S A. 1992;89:8240-4.

39. Murray, P and Edgar, D. The regulation of embryonic stem cell differentiation by leukaemia inhibitory factor (LIF). Differentiation. 2001;68:227-34.

40. Reubinoff, BE, Pera, MF, Fong, CY, Trounson, A and Bongso, A. Embryonic stem cell lines from human blastocysts: somatic differentiation in vitro. Nat Biotechnol. 2000;18:399-404.

41. Amit, M, Carpenter, MK, Inokuma, MS, Chiu, CP, Harris, CP, Waknitz, MA, Itskovitz-Eldor, J and Thomson, JA. Clonally derived human embryonic stem cell lines maintain pluripotency and proliferative potential for prolonged periods of culture. Dev Biol. 2000;227:271-8.

42. Ying, QL, Stavridis, M, Griffiths, D, Li, M and Smith, A. Conversion of embryonic stem cells into neuroectodermal precursors in adherent monoculture. Nat Biotechnol. 2003;21:183-6.

43. Kaufman, DS, Hanson, ET, Lewis, RL, Auerbach, R and Thomson, JA. Hematopoietic colony-forming cells derived from human embryonic stem cells. Proceedings of the National Academy of Sciences of the United States of America. 2001;98:10716-21.

44. Jostock, R, Rentrop, M and Maelicke, A. Cell fate specification in an in vitro model of neural development. Eur J Cell Biol. 1998;76:63-76.

45. Munoz-Sanjuan, I and Brivanlou, AH. Neural induction, the default model and embryonic stem cells. Nat Rev Neurosci. 2002;3:271-80.

46. Shi, Y, Hou, L, Tang, F, Jiang, W, Wang, P, Ding, M and Deng, H. Inducing embryonic stem cells to differentiate into pancreatic beta cells by a novel three-step approach with activin A and all-trans retinoic acid. Stem Cells. 2005;23:656-62.

47. Buttery, LD, Bourne, S, Xynos, JD, Wood, H, Hughes, FJ, Hughes, SP, Episkopou, V and Polak, JM. Differentiation of osteoblasts and in vitro bone formation from murine embryonic stem cells. Tissue Engineering. 2001;7:89-99.

48. Park, CH, Minn, YK, Lee, JY, Choi, DH, Chang, MY, Shim, JW, Ko, JY, Koh, HC, Kang, MJ, Kang, JS, Rhie, DJ, Lee, YS, Son, H, Moon, SY, Kim, KS and Lee, SH. In vitro and in vivo analyses of human embryonic stem cell-derived dopamine neurons. J Neurochem. 2005;92:1265-76.

49. Mummery, C, Ward, D, van den Brink, CE, Bird, SD, Doevendans, PA, Opthof, T, Brutel de la Riviere, A, Tertoolen, L, van der Heyden, M and Pera, M. Cardiomyocyte differentiation of mouse and human embryonic stem cells. J Anat. 2002;200:233-42.

50. Grabel, LB and Casanova, JE. The outgrowth of parietal endoderm from mouse teratocarcinoma stem-cell embryoid bodies. Differentiation. 1986;32:67-73.

51. Shukla, S, Nair, R, Rolle, MW, Braun, KR, Chan, CK, Johnson, PY, Wight, TN and McDevitt, TC. Synthesis and Organization of Hyaluronan and Versican by Embryonic Stem Cells Undergoing Embryoid Body Differentiation. J Histochem Cytochem. 2009;

52. Coucouvanis, E and Martin, GR. Signals for death and survival: a two-step mechanism for cavitation in the vertebrate embryo. Cell. 1995;83:279-87.

53. Rathjen, J, Haines, BP, Hudson, KM, Nesci, A, Dunn, S and Rathjen, PD. Directed differentiation of pluripotent cells to neural lineages: homogeneous formation and differentiation of a neurectoderm population. Development. 2002;129:2649-61.

54. Rathjen, J, Lake, JA, Bettess, MD, Washington, JM, Chapman, G and Rathjen, PD. Formation of a primitive ectoderm like cell population, EPL cells, from ES

cells in response to biologically derived factors. J Cell Sci. 1999;112 (Pt 5):601-12.

55. Li, L, Arman, E, Ekblom, P, Edgar, D, Murray, P and Lonai, P. Distinct GATA6- and laminin-dependent mechanisms regulate endodermal and ectodermal embryonic stem cell fates. Development. 2004;131:5277-86.

56. Li, X, Chen, Y, Scheele, S, Arman, E, Haffner-Krausz, R, Ekblom, P and Lonai, P. Fibroblast growth factor signaling and basement membrane assembly are connected during epithelial morphogenesis of the embryoid body. J Cell Biol. 2001;153:811-22.

57. Maye, P, Becker, S, Kasameyer, E, Byrd, N and Grabel, L. Indian hedgehog signaling in extraembryonic endoderm and ectoderm differentiation in ES embryoid bodies. Mech Dev. 2000;94:117-32.

58. Maye, P, Becker, S, Siemen, H, Thorne, J, Byrd, N, Carpentino, J and Grabel, L. Hedgehog signaling is required for the differentiation of ES cells into neurectoderm. Dev Biol. 2004;265:276-90.

59. Coucouvanis, E and Martin, GR. BMP signaling plays a role in visceral endoderm differentiation and cavitation in the early mouse embryo. Development. 1999;126:535-46.

60. Pelton, TA, Sharma, S, Schulz, TC, Rathjen, J and Rathjen, PD. Transient pluripotent cell populations during primitive ectoderm formation: correlation of in vivo and in vitro pluripotent cell development. J Cell Sci. 2002;115:329-39.

61. Maltsev, VA, Wobus, AM, Rohwedel, J, Bader, M and Hescheler, J. Cardiomyocytes differentiated in vitro from embryonic stem cells developmentally express cardiac-specific genes and ionic currents. Circ Res. 1994;75:233-44.

62. Dang, SM, Kyba, M, Perlingeiro, R, Daley, GQ and Zandstra, PW. Efficiency of embryoid body formation and hematopoietic development from embryonic stem cells in different culture systems. Biotechnol Bioeng. 2002;78:442-53.

63. Ling, V and Neben, S. In vitro differentiation of embryonic stem cells: immunophenotypic analysis of cultured embryoid bodies. J Cell Physiol. 1997;171:104-15.

64. Cameron, CM, Hu, WS and Kaufman, DS. Improved development of human embryonic stem cell-derived embryoid bodies by stirred vessel cultivation. Biotechnol Bioeng. 2006;

65. Dang, SM and Zandstra, PW. Scalable production of embryonic stem cell-derived cells. Methods Mol Biol. 2005;290:353-64.

66. Gerecht-Nir, S, Cohen, S and Itskovitz-Eldor, J. Bioreactor cultivation enhances the efficiency of human embryoid body (hEB) formation and differentiation. Biotechnol Bioeng. 2004;86:493-502.

67. Kurosawa, H. Methods for inducing embryoid body formation: in vitro differentiation system of embryonic stem cells. J Biosci Bioeng. 2007;103:389-98.

68. Carpenedo, RL, Sargent, CY and McDevitt, TC. Rotary suspension culture enhances the efficiency, yield, and homogeneity of embryoid body differentiation. Stem Cells. 2007;25:2224-34.

69. Ungrin, MD, Joshi, C, Nica, A, Bauwens, C and Zandstra, PW. Reproducible, ultra high-throughput formation of multicellular organization from single cell suspension-derived human embryonic stem cell aggregates. PLoS One. 2008;3:e1565.

70. Dang, SM, Gerecht-Nir, S, Chen, J, Itskovitz-Eldor, J and Zandstra, PW. Controlled, scalable embryonic stem cell differentiation culture. Stem Cells. 2004;22:275-82.

71. Sargent, CY, Berguig, GY and McDevitt, TC. Cardiomyogenic differentiation of embryoid bodies is promoted by rotary orbital suspension culture. Tissue Eng Part A. 2009;15:331-42.

72. Sargent, CY, Berguig, GY, Kinney, MA, Hiatt, LA, Carpenedo, RL, Berson, RE and McDevitt, TC. Hydrodynamic modulation of embryonic stem cell differentiation by rotary orbital suspension culture. Biotechnol Bioeng. 105:611-26.

73. Mohr, JC, de Pablo, JJ and Palecek, SP. 3-D microwell culture of human embryonic stem cells. Biomaterials. 2006;27:6032-42.

74. Hwang, YS, Chung, BG, Ortmann, D, Hattori, N, Moeller, HC and Khademhosseini, A. Microwell-mediated control of embryoid body size regulates embryonic stem cell fate via differential expression of WNT5a and WNT11. Proc Natl Acad Sci U S A. 2009;106:16978-83.

75. Ng, ES, Davis, RP, Azzola, L, Stanley, EG and Elefanty, AG. Forced aggregation of defined numbers of human embryonic stem cells into embryoid bodies fosters robust, reproducible hematopoietic differentiation. Blood. 2005;106:1601-3.

76. Hwang, NS, Varghese, S, Zhang, Z and Elisseeff, J. Chondrogenic differentiation of human embryonic stem cell-derived cells in arginine-glycine-aspartate-modified hydrogels. Tissue Engineering. 2006;12:2695-706.

77. Liu, H, Collins, SF and Suggs, LJ. Three-dimensional culture for expansion and differentiation of mouse embryonic stem cells. Biomaterials. 2006;27:6004-14.

78. Gerecht, S, Burdick, JA, Ferreira, LS, Townsend, SA, Langer, R and Vunjak-Novakovic, G. Hyaluronic acid hydrogel for controlled self-renewal and differentiation of human embryonic stem cells. Proc Natl Acad Sci U S A. 2007;104:11298-303.

79. Ferreira, LS, Gerecht, S, Fuller, J, Shieh, HF, Vunjak-Novakovic, G and Langer, R. Bioactive hydrogel scaffolds for controllable vascular differentiation of human embryonic stem cells. Biomaterials. 2007;28:2706-17.

80. Dasgupta, A, Hughey, R, Lancin, P, Larue, L and Moghe, PV. E-cadherin synergistically induces hepatospecific phenotype and maturation of embryonic stem cells in conjunction with hepatotrophic factors. Biotechnol Bioeng. 2005;92:257-66.

81. Nourse, MB, Halpin, DE, Scatena, M, Mortisen, DJ, Tulloch, NL, Hauch, KD, Torok-Storb, B, Ratner, BD, Pabon, L and Murry, CE. VEGF induces differentiation of functional endothelium from human embryonic stem cells: implications for tissue engineering. Arterioscler Thromb Vasc Biol. 30:80-9.

82. Ferreira, LS, Gerecht, S, Shieh, HF, Watson, N, Rupnick, MA, Dallabrida, SM, Vunjak-Novakovic, G and Langer, R. Vascular progenitor cells isolated from human embryonic stem cells give rise to endothelial and smooth muscle like cells and form vascular networks in vivo. Circ Res. 2007;101:286-94.

83. Takaki, M, Nakayama, S, Misawa, H, Nakagawa, T and Kuniyasu, H. In vitro formation of enteric neural network structure in a gut-like organ differentiated from mouse embryonic stem cells. Stem Cells. 2006;24:1414-22.

84. Yamada, G, Kioussi, C, Schubert, FR, Eto, Y, Chowdhury, K, Pituello, F and Gruss, P. Regulated expression of Brachyury(T), Nkx1.1 and Pax genes in embryoid bodies. Biochem Biophys Res Commun. 1994;199:552-63.

85. Kang, SM, Cho, MS, Seo, H, Yoon, CJ, Oh, SK, Choi, YM and Kim, DW. Efficient induction of oligodendrocytes from human embryonic stem cells. Stem Cells. 2007;25:419-24.

86. Bruce, SJ, Gardiner, BB, Burke, LJ, Gongora, MM, Grimmond, SM and Perkins, AC. Dynamic transcription programs during ES cell differentiation towards mesoderm in serum versus serum-freeBMP4 culture. BMC Genomics. 2007;8:365.

87. ten Berge, D, Koole, W, Fuerer, C, Fish, M, Eroglu, E and Nusse, R. Wnt signaling mediates self-organization and axis formation in embryoid bodies. Cell Stem Cell. 2008;3:508-18.

88. Bain, G, Ray, WJ, Yao, M and Gottlieb, DI. Retinoic acid promotes neural and represses mesodermal gene expression in mouse embryonic stem cells in culture. Biochem Biophys Res Commun. 1996;223:691-4.

89. Okada, Y, Shimazaki, T, Sobue, G and Okano, H. Retinoic-acid-concentration-dependent acquisition of neural cell identity during in vitro differentiation of mouse embryonic stem cells. Dev Biol. 2004;275:124-42.

90. Fraichard, A, Chassande, O, Bilbaut, G, Dehay, C, Savatier, P and Samarut, J. In vitro differentiation of embryonic stem cells into glial cells and functional neurons. J Cell Sci. 1995;108:3181-8.

91. Rohwedel, J, Guan, K and Wobus, AM. Induction of cellular differentiation by retinoic acid in vitro. Cells Tissues Organs. 1999;165:190-202.

92. Lang, KJ, Rathjen, J, Vassilieva, S and Rathjen, PD. Differentiation of embryonic stem cells to a neural fate: a route to re-building the nervous system? J Neurosci Res. 2004;76:184-92.

93. Guan, K, Chang, H, Rolletschek, A and Wobus, AM. Embryonic stem cell-derived neurogenesis. Retinoic acid induction and lineage selection of neuronal cells. Cell Tissue Res. 2001;305:171-6.

94. De Luca, LM. Retinoids and their receptors in differentiation, embryogenesis, and neoplasia. Faseb J. 1991;5:2924-33.

95. Maden, M. Retinoic acid in the development, regeneration and maintenance of the nervous system. Nat Rev Neurosci. 2007;8:755-65.

96. Budhu, AS and Noy, N. Direct channeling of retinoic acid between cellular retinoic acid-binding protein II and retinoic acid receptor sensitizes mammary carcinoma cells to retinoic acid-induced growth arrest. Mol Cell Biol. 2002;22:2632-41.

97. Bastien, J and Rochette-Egly, C. Nuclear retinoid receptors and the transcription of retinoid-target genes. Gene. 2004;328:1-16.

98. Balmer, JE and Blomhoff, R. Gene expression regulation by retinoic acid. J Lipid Res. 2002;43:1773-808.

99. Schoorlemmer, J, van Puijenbroek, A, van Den Eijnden, M, Jonk, L, Pals, C and Kruijer, W. Characterization of a negative retinoic acid response element in the murine Oct4 promoter. Mol Cell Biol. 1994;14:1122-36.

100. Durston, AJ, van der Wees, J, Pijnappel, WW and Godsave, SF. Retinoids and related signals in early development of the vertebrate central nervous system. Curr Top Dev Biol. 1998;40:111-75.

101. Langston, AW, Thompson, JR and Gudas, LJ. Retinoic acid-responsive enhancers located 3' of the Hox A and Hox B homeobox gene clusters. Functional analysis. J Biol Chem. 1997;272:2167-75.

102. Martinez-Ceballos, E, Chambon, P and Gudas, LJ. Differences in gene expression between wild type and Hoxa1 knockout embryonic stem cells after retinoic acid treatment or leukemia inhibitory factor (LIF) removal. J Biol Chem. 2005;280:16484-98.

103. Simeone, A, Acampora, D, Arcioni, L, Andrews, PW, Boncinelli, E and Mavilio, F. Sequential activation of HOX2 homeobox genes by retinoic acid in human embryonal carcinoma cells. Nature. 1990;346:763-6.

104. Colbert, MC, Linney, E and LaMantia, AS. Local sources of retinoic acid coincide with retinoid-mediated transgene activity during embryonic development. Proc Natl Acad Sci U S A. 1993;90:6572-6.

105. Fraichard, A, Chassande, O, Bilbaut, G, Dehay, C, Savatier, P and Samarut, J. In vitro differentiation of embryonic stem cells into glial cells and functional neurons. J Cell Sci. 1995;108 (Pt 10):3181-8.

106. Pachernik, J, Bryja, V, Esner, M, Kubala, L, Dvorak, P and Hampl, A. Neural differentiation of pluripotent mouse embryonal carcinoma cells by retinoic acid: inhibitory effect of serum. Physiol Res. 2005;54:115-22.

107. Irioka, T, Watanabe, K, Mizusawa, H, Mizuseki, K and Sasai, Y. Distinct effects of caudalizing factors on regional specification of embryonic stem cell-derived neural precursors. Brain Res Dev Brain Res. 2005;154:63-70.

108. Goncalves, MB, Boyle, J, Webber, DJ, Hall, S, Minger, SL and Corcoran, JP. Timing of the retinoid-signalling pathway determines the expression of neuronal markers in neural progenitor cells. Dev Biol. 2005;278:60-70.

109. Gottlieb, DI and Huettner, JE. An in vitro pathway from embryonic stem cells to neurons and glia. Cells Tissues Organs. 1999;165:165-72.

110. Wobus, AM, Kaomei, G, Shan, J, Wellner, MC, Rohwedel, J, Ji, G, Fleischmann, B, Katus, HA, Hescheler, J and Franz, WM. Retinoic acid accelerates embryonic stem cell-derived cardiac differentiation and enhances development of ventricular cardiomyocytes. J Mol Cell Cardiol. 1997;29:1525-39.

111. Hidaka, K, Lee, JK, Kim, HS, Ihm, CH, Iio, A, Ogawa, M, Nishikawa, S, Kodama, I and Morisaki, T. Chamber-specific differentiation of Nkx2.5-positive cardiac precursor cells from murine embryonic stem cells. FASEB J. 2003;17:740-2.

112. Dani, C, Smith, AG, Dessolin, S, Leroy, P, Staccini, L, Villageois, P, Darimont, C and Ailhaud, G. Differentiation of embryonic stem cells into adipocytes in vitro. J Cell Sci. 1997;110 (Pt 11):1279-85.

113. Micallef, SJ, Janes, ME, Knezevic, K, Davis, RP, Elefanty, AG and Stanley, EG. Retinoic acid induces Pdx1-positive endoderm in differentiating mouse embryonic stem cells. Diabetes. 2005;54:301-5.

114. Metallo, CM, Ji, L, de Pablo, JJ and Palecek, SP. Retinoic acid and bone morphogenetic protein signaling synergize to efficiently direct epithelial differentiation of human embryonic stem cells. Stem Cells. 2008;26:372-80.

115. Metallo, CM, Ji, L, de Pablo, JJ and Palecek, SP. Directed differentiation of human embryonic stem cells to epidermal progenitors. Methods Mol Biol. 585:83-92.

116. Metallo, CM, Azarin, SM, Moses, LE, Ji, L, de Pablo, JJ and Palecek, SP. Human embryonic stem cell-derived keratinocytes exhibit an epidermal transcription program and undergo epithelial morphogenesis in engineered tissue constructs. Tissue Eng Part A. 16:213-23.

117. Honda, M, Hamazaki, TS, Komazaki, S, Kagechika, H, Shudo, K and Asashima, M. RXR agonist enhances the differentiation of cardiomyocytes derived from embryonic stem cells in serum-free conditions. Biochem Biophys Res Commun. 2005;333:1334-40.

118. Otero, JJ, Fu, W, Kan, L, Cuadra, AE and Kessler, JA. Beta-catenin signaling is required for neural differentiation of embryonic stem cells. Development. 2004;131:3545-57.

119. Santini, MT and Rainaldi, G. Three-dimensional spheroid model in tumor biology. Pathobiology. 1999;67:148-57.

120. Lin, RZ and Chang, HY. Recent advances in three-dimensional multicellular spheroid culture for biomedical research. Biotechnol J. 2008;3:1172-84.

121. Casciari, JJ, Sotirchos, SV and Sutherland, RM. Glucose diffusivity in multicellular tumor spheroids. Cancer Res. 1988;48:3905-9.

122. Goodman, TT, Chen, J, Matveev, K and Pun, SH. Spatio-temporal modeling of nanoparticle delivery to multicellular tumor spheroids. Biotechnol Bioeng. 2008;101:388-99.

123. Hu, G and Li, D. Three-dimensional modeling of transport of nutrients for multicellular tumor spheroid culture in a microchannel. Biomed Microdevices. 2007;9:315-23.

124. Sutherland, RM. Cell and environment interactions in tumor microregions: the multicell spheroid model. Science. 1988;240:177-84.

125. West, GW, Weichselbaum, R and Little, JB. Limited penetration of methotrexate into human osteosarcoma spheroids as a proposed model for solid tumor resistance to adjuvant chemotherapy. Cancer Res. 1980;40:3665-8.

126. Kwok, TT and Twentyman, PR. The response to cytotoxic drugs of EMT6 cells treated either as intact or disaggregated spheroids. Br J Cancer. 1985;51:211-8.

127. Kerr, DJ, Wheldon, TE, Hydns, S and Kaye, SB. Cytotoxic drug penetration studies in multicellular tumour spheroids. Xenobiotica. 1988;18:641-8.

128. Saitou, M, Fujimoto, K, Doi, Y, Itoh, M, Fujimoto, T, Furuse, M, Takano, H, Noda, T and Tsukita, S. Occludin-deficient embryonic stem cells can differentiate into polarized epithelial cells bearing tight junctions. J Cell Biol. 1998;141:397-408.

129. Guillemot, L, Hammar, E, Kaister, C, Ritz, J, Caille, D, Jond, L, Bauer, C, Meda, P and Citi, S. Disruption of the cingulin gene does not prevent tight junction formation but alters gene expression. J Cell Sci. 2004;117:5245-56.

130. Wartenberg, M, Finkensieper, A, Hescheler, J and Sauer, H. Confrontation cultures of embryonic stem cells with multicellular tumor spheroids to study tumor-induced angiogenesis. Methods Mol Biol. 2006;331:313-28.

131. Burdick, JA and Vunjak-Novakovic, G. Engineered microenvironments for controlled stem cell differentiation. Tissue Eng Part A. 2009;15:205-19.

132. Dawson, E, Mapili, G, Erickson, K, Taqvi, S and Roy, K. Biomaterials for stem cell differentiation. Adv Drug Deliv Rev. 2008;60:215-28.

133. Lund, AW, Yener, B, Stegemann, JP and Plopper, GE. The natural and engineered 3D microenvironment as a regulatory cue during stem cell fate determination. Tissue Eng Part B Rev. 2009;15:371-80.

134. Hwang, NS, Varghese, S and Elisseeff, J. Controlled differentiation of stem cells. Adv Drug Deliv Rev. 2008;60:199-214.

135. Anderson, DG, Levenberg, S and Langer, R. Nanoliter-scale synthesis of arrayed biomaterials and application to human embryonic stem cells. Nat Biotechnol. 2004;22:863-6.

136. Derda, R, Musah, S, Orner, BP, Klim, JR, Li, L and Kiessling, LL. High-throughput discovery of synthetic surfaces that support proliferation of pluripotent cells. J Am Chem Soc. 132:1289-95.

137. Flaim, CJ, Chien, S and Bhatia, SN. An extracellular matrix microarray for probing cellular differentiation. Nat Methods. 2005;2:119-25.

138. Flaim, CJ, Teng, D, Chien, S and Bhatia, SN. Combinatorial signaling microenvironments for studying stem cell fate. Stem Cells Dev. 2008;17:29-39.

139. Benoit, DS, Schwartz, MP, Durney, AR and Anseth, KS. Small functional groups for controlled differentiation of hydrogel-encapsulated human mesenchymal stem cells. Nat Mater. 2008;7:816-23.

140. Jongpaiboonkit, L, King, WJ and Murphy, WL. Screening for 3D Environments That Support Human Mesenchymal Stem Cell Viability Using Hydrogel Arrays. Tissue Eng Part A. 2008;

141. Randle, WL, Cha, JM, Hwang, YS, Chan, KL, Kazarian, SG, Polak, JM and Mantalaris, A. Integrated 3-dimensional expansion and osteogenic differentiation of murine embryonic stem cells. Tissue Eng. 2007;13:2957-70.

142. Li, YJ, Chung, EH, Rodriguez, RT, Firpo, MT and Healy, KE. Hydrogels as artificial matrices for human embryonic stem cell self-renewal. Journal of Biomedical Materials Research A. 2006;79:1-5.

143. Hwang, NS, Kim, MS, Sampattavanich, S, Baek, JH, Zhang, Z and Elisseeff, J. Effects of three-dimensional culture and growth factors on the chondrogenic differentiation of murine embryonic stem cells. Stem Cells. 2006;24:284-91.

144. Hwang, NS, Varghese, S, Theprungsirikul, P, Canver, A and Elisseeff, J. Enhanced chondrogenic differentiation of murine embryonic stem cells in hydrogels with glucosamine. Biomaterials. 2006;27:6015-23.

145. Hwang, NS, Varghese, S and Elisseeff, J. Cartilage tissue engineering: Directed differentiation of embryonic stem cells in three-dimensional hydrogel culture. Methods Mol Biol. 2007;407:351-73.

146. Magyar, JP, Nemir, M, Ehler, E, Suter, N, Perriard, JC and Eppenberger, HM. Mass production of embryoid bodies in microbeads. Ann N Y Acad Sci. 2001;944:135-43.

147. Shive, MS and Anderson, JM. Biodegradation and biocompatibility of PLA and PLGA microspheres. Adv Drug Deliv Rev. 1997;28:5-24.

148. Freiberg, S and Zhu, XX. Polymer microspheres for controlled drug release. Int J Pharm. 2004;282:1-18.

149. Choi, Y, Kim, SY, Kim, SH, Yang, J, Park, K and Byun, Y. Inhibition of tumor growth by biodegradable microspheres containing all-trans-retinoic acid in a human head-and-neck cancer xenograft. Int J Cancer. 2003;107:145-8.

150. Jeong, YI, Song, JG, Kang, SS, Ryu, HH, Lee, YH, Choi, C, Shin, BA, Kim, KK, Ahn, KY and Jung, S. Preparation of poly(DL-lactide-co-glycolide) microspheres encapsulating all-trans retinoic acid. Int J Pharm. 2003;259:79-91.

151. Giordano, GG, Refojo, MF and Arroyo, MH. Sustained delivery of retinoic acid from microspheres of biodegradable polymer in PVR. Invest Ophthalmol Vis Sci. 1993;34:2743-51.

152. Xu, AS and Reid, LM. Soft, porous poly(D,L-lactide-co-glycotide) microcarriers designed for ex vivo studies and for transplantation of adherent cell types including progenitors. Ann N Y Acad Sci. 2001;944:144-59.

153. Chun, KW, Yoo, HS, Yoon, JJ and Park, TG. Biodegradable PLGA microcarriers for injectable delivery of chondrocytes: effect of surface modification on cell attachment and function. Biotechnol Prog. 2004;20:1797-801.

154. Simmons, CA, Alsberg, E, Hsiong, S, Kim, WJ and Mooney, DJ. Dual growth factor delivery and controlled scaffold degradation enhance in vivo bone formation by transplanted bone marrow stromal cells. Bone. 2004;35:562-9.

155. Choi, YS, Park, SN and Suh, H. Adipose tissue engineering using mesenchymal stem cells attached to injectable PLGA spheres. Biomaterials. 2005;26:5855-63.

156. Mahoney, MJ and Saltzman, WM. Transplantation of brain cells assembled around a programmable synthetic microenvironment. Nat Biotechnol. 2001;19:934-9.

157. Newman, KD and McBurney, MW. Poly(D,L lactic-co-glycolic acid) microspheres as biodegradable microcarriers for pluripotent stem cells. Biomaterials. 2004;25:5763-71.

158. Tatard, VM, Venier-Julienne, MC, Benoit, JP, Menei, P and Montero-Menei, CN. In vivo evaluation of pharmacologically active microcarriers releasing nerve growth factor and conveying PC12 cells. Cell Transplant. 2004;13:573-83.

159. Tatard, VM, Sindji, L, Branton, JG, Aubert-Pouessel, A, Colleau, J, Benoit, JP and Montero-Menei, CN. Pharmacologically active microcarriers releasing glial cell line - derived neurotrophic factor: Survival and differentiation of embryonic dopaminergic neurons after grafting in hemiparkinsonian rats. Biomaterials. 2007;28:1978-1988.

160. Wiese, C, Kania, G, Rolletschek, A, Blyszczuk, P and Wobus, AM. Pluripotency: capacity for in vitro differentiation of undifferentiated embryonic stem cells. Methods Mol Biol. 2006;325:181-205.

161. Yoon, BS, Yoo, SJ, Lee, JE, You, S, Lee, HT and Yoon, HS. Enhanced differentiation of human embryonic stem cells into cardiomyocytes by combining hanging drop culture and 5-azacytidine treatment. Differentiation. 2006;74:149-59.

162. Guo, XM, Zhao, YS, Chang, HX, Wang, CY, E, LL, Zhang, XA, Duan, CM, Dong, LZ, Jiang, H, Li, J, Song, Y and Yang, XJ. Creation of engineered cardiac tissue in vitro from mouse embryonic stem cells. Circulation. 2006;113:2229-37.

163. Yan, Y, Yang, D, Zarnowska, ED, Du, Z, Werbel, B, Valliere, C, Pearce, RA, Thomson, JA and Zhang, SC. Directed differentiation of dopaminergic neuronal subtypes from human embryonic stem cells. Stem Cells. 2005;23:781-90.

164. Schroeder, M, Niebruegge, S, Werner, A, Willbold, E, Burg, M, Ruediger, M, Field, LJ, Lehmann, J and Zweigerdt, R. Differentiation and lineage selection of mouse embryonic stem cells in a stirred bench scale bioreactor with automated process control. Biotechnol Bioeng. 2005;92:920-33.

165. Wang, X, Wei, G, Yu, W, Zhao, Y, Yu, X and Ma, X. Scalable producing embryoid bodies by rotary cell culture system and constructing engineered cardiac tissue with ES-derived cardiomyocytes in vitro. Biotechnol Prog. 2006;22:811-8.

166. Moreira, JL, Santana, PC, Feliciano, AS, Cruz, PE, Racher, AJ, Griffiths, JB and Carrondo, MJ. Effect of viscosity upon hydrodynamically controlled natural aggregates of animal cells grown in stirred vessels. Biotechnol Prog. 1995;11:575-83.

167. Kallos, MS and Behie, LA. Inoculation and growth conditions for high-cell-density expansion of mammalian neural stem cells in suspension bioreactors. Biotechnol Bioeng. 1999;63:473-83.

168. Fok, EY and Zandstra, PW. Shear-controlled single-step mouse embryonic stem cell expansion and embryoid body-based differentiation. Stem Cells. 2005;23:1333-42.

169. Maniotis, AJ, Chen, X, Garcia, C, DeChristopher, PJ, Wu, D, Pe'er, J and Folberg, R. Control of melanoma morphogenesis, endothelial survival, and perfusion by extracellular matrix. Lab Invest. 2002;82:1031-43.

170. Moscona, A. Rotation-mediated histogenetic aggregation of dissociated cells. A quantifiable approach to cell interactions in vitro. Exp Cell Res. 1961;22:455-75.

171. Hamilton, GA, Westmorel, C and George, AE. Effects of medium composition on the morphology and function of rat hepatocytes cultured as spheroids and monolayers. In Vitro Cell Dev Biol Anim. 2001;37:656-67.

172. Dai, W, Belt, J and Saltzman, WM. Cell-binding peptides conjugated to poly(ethylene glycol) promote neural cell aggregation. Biotechnology (N Y). 1994;12:797-801.

173. Zweigerdt, R, Burg, M, Willbold, E, Abts, H and Ruediger, M. Generation of confluent cardiomyocyte monolayers derived from embryonic stem cells in

suspension: a cell source for new therapies and screening strategies. Cytotherapy. 2003;5:399-413.

174. Pfaffl, MW. A new mathematical model for relative quantification in real-time RT-PCR. Nucleic Acids Res. 2001;29:e45.

175. Maltsev, VA, Rohwedel, J, Hescheler, J and Wobus, AM. Embryonic stem cells differentiate in vitro into cardiomyocytes representing sinusnodal, atrial and ventricular cell types. Mech Dev. 1993;44:41-50.

176. Kurosawa, H, Imamura, T, Koike, M, Sasaki, K and Amano, Y. A simple method for forming embryoid body from mouse embryonic stem cells. J Biosci Bioeng. 2003;96:409-11.

177. Konno, T, Akita, K, Kurita, K and Ito, Y. Formation of embryoid bodies by mouse embryonic stem cells on plastic surfaces. J Biosci Bioeng. 2005;100:88-93.

178. Sakai, Y, Furukawa, K and Suzuki, M. Immobilization and long-term albumin secretion of hepatocyte spheroids rapidly formed by rotational tissue culture methods. Biotechnology Techniques. 1992;6:527-532.

179. Goodwin, TJ, Jessup, JM and Wolf, DA. Morphologic differentiation of colon carcinoma cell lines HT-29 and HT-29KM in rotating-wall vessels. In Vitro Cell Dev Biol. 1992;28A:47-60.

180. Martin, GR. Isolation of a pluripotent cell line from early mouse embryos cultured in medium conditioned by teratocarcinoma stem cells. Proceedings of the National Academy of Sciences of the United States of America. 1981;78:7634-8.

181. Thomson, JA, Kalishman, J, Golos, TG, Durning, M, Harris, CP, Becker, RA and Hearn, JP. Isolation of a primate embryonic stem cell line. Proc Natl Acad Sci U S A. 1995;92:7844-8.

182. Thomson, JA, Kalishman, J, Golos, TG, Durning, M, Harris, CP and Hearn, JP. Pluripotent cell lines derived from common marmoset (Callithrix jacchus) blastocysts. Biol Reprod. 1996;55:254-9.

183. Reubinoff, BE, Pera, MF, Fong, CY, Trounson, A and Bongso, A. Embryonic stem cell lines from human blastocysts: somatic differentiation in vitro. Nature Biotechnology. 2000;18:399-404.

184. Jia, F, Wilson, KD, Sun, N, Gupta, DM, Huang, M, Li, Z, Panetta, NJ, Chen, ZY, Robbins, RC, Kay, MA, Longaker, MT and Wu, JC. A nonviral minicircle vector for deriving human iPS cells. Nat Methods.

185. Gonzalez, F, Barragan Monasterio, M, Tiscornia, G, Montserrat Pulido, N, Vassena, R, Batlle Morera, L, Rodriguez Piza, I and Izpisua Belmonte, JC. Generation of mouse-induced pluripotent stem cells by transient expression of a single nonviral polycistronic vector. Proc Natl Acad Sci U S A. 2009;106:8918-22.

186. Ying, QL, Stavridis, M, Griffiths, D, Li, M and Smith, A. Conversion of embryonic stem cells into neuroectodermal precursors in adherent monoculture. Nature Biotechnology. 2003;21:183-6.

187. Nakano, T, Kodama, H and Honjo, T. Generation of lymphohematopoietic cells from embryonic stem cells in culture. Science. 1994;265:1098-101.

188. Brophy, CM, Luebke-Wheeler, JL, Amiot, BP, Khan, H, Remmel, RP, Rinaldo, P and Nyberg, SL. Rat hepatocyte spheroids formed by rocked technique maintain differentiated hepatocyte gene expression and function. Hepatology. 2009;49:578-86.

189. Curcio, E, Salerno, S, Barbieri, G, De Bartolo, L, Drioli, E and Bader, A. Mass transfer and metabolic reactions in hepatocyte spheroids cultured in rotating wall gas-permeable membrane system. Biomaterials. 2007;28:5487-97.

190. Choi, SC, Yoon, J, Shim, WJ, Ro, YM and Lim, DS. 5-azacytidine induces cardiac differentiation of P19 embryonic stem cells. Exp Mol Med. 2004;36:515-23.

191. Marikawa, Y, Tamashiro, DA, Fujita, TC and Alarcon, VB. Aggregated P19 mouse embryonal carcinoma cells as a simple in vitro model to study the molecular regulations of mesoderm formation and axial elongation morphogenesis. Genesis. 2009;47:93-106.

192. Paquin, J, Danalache, BA, Jankowski, M, McCann, SM and Gutkowska, J. Oxytocin induces differentiation of P19 embryonic stem cells to cardiomyocytes. Proc Natl Acad Sci U S A. 2002;99:9550-5.

193. Wang, W, Itaka, K, Ohba, S, Nishiyama, N, Chung, UI, Yamasaki, Y and Kataoka, K. 3D spheroid culture system on micropatterned substrates for improved differentiation efficiency of multipotent mesenchymal stem cells. Biomaterials. 2009;30:2705-15.

194. Arufe, MC, De la Fuente, A, Fuentes-Boquete, I, De Toro, FJ and Blanco, FJ. Differentiation of synovial CD-105(+) human mesenchymal stem cells into chondrocyte-like cells through spheroid formation. J Cell Biochem. 2009;108:145-55.

195. Laywell, ED, Kukekov, VG and Steindler, DA. Multipotent neurospheres can be derived from forebrain subependymal zone and spinal cord of adult mice after protracted postmortem intervals. Exp Neurol. 1999;156:430-3.

196. Piao, JH, Odeberg, J, Samuelsson, EB, Kjaeldgaard, A, Falci, S, Seiger, A, Sundstrom, E and Akesson, E. Cellular composition of long-term human spinal cord- and forebrain-derived neurosphere cultures. J Neurosci Res. 2006;84:471-82.

197. Bez, A, Corsini, E, Curti, D, Biggiogera, M, Colombo, A, Nicosia, RF, Pagano, SF and Parati, EA. Neurosphere and neurosphere-forming cells: morphological and ultrastructural characterization. Brain Res. 2003;993:18-29.

198. Yuhas, JM, Li, AP, Martinez, AO and Ladman, AJ. A simplified method for production and growth of multicellular tumor spheroids. Cancer Res. 1977;37:3639-43.

199. Shweiki, D, Neeman, M, Itin, A and Keshet, E. Induction of vascular endothelial growth factor expression by hypoxia and by glucose deficiency in multicell spheroids: implications for tumor angiogenesis. Proc Natl Acad Sci U S A. 1995;92:768-72.

200. Hauptmann, S, Denkert, C, Lohrke, H, Tietze, L, Ott, S, Klosterhalfen, B and Mittermayer, C. Integrin expression on colorectal tumor cells growing as monolayers, as multicellular tumor spheroids, or in nude mice. Int J Cancer. 1995;61:819-25.

201. Shield, K, Ackland, ML, Ahmed, N and Rice, GE. Multicellular spheroids in ovarian cancer metastases: Biology and pathology. Gynecol Oncol. 2009;113:143-8.

202. Fujiwara, T, Grimm, EA, Mukhopadhyay, T, Cai, DW, Owen-Schaub, LB and Roth, JA. A retroviral wild-type p53 expression vector penetrates human lung cancer spheroids and inhibits growth by inducing apoptosis. Cancer Res. 1993;53:4129-33.

203. Helmlinger, G, Netti, PA, Lichtenbeld, HC, Melder, RJ and Jain, RK. Solid stress inhibits the growth of multicellular tumor spheroids. Nat Biotechnol. 1997;15:778-83.

204. Kunz-Schughart, LA. Multicellular tumor spheroids: intermediates between monolayer culture and in vivo tumor. Cell Biol Int. 1999;23:157-61.

205. Gottfried, E, Kunz-Schughart, LA, Andreesen, R and Kreutz, M. Brave little world: spheroids as an in vitro model to study tumor-immune-cell interactions. Cell Cycle. 2006;5:691-5.

206. Venkatasubramanian, R, Henson, MA and Forbes, NS. Incorporating energy metabolism into a growth model of multicellular tumor spheroids. J Theor Biol. 2006;242:440-53.

207. Wartenberg, M, Donmez, F, Ling, FC, Acker, H, Hescheler, J and Sauer, H. Tumor-induced angiogenesis studied in confrontation cultures of multicellular tumor spheroids and embryoid bodies grown from pluripotent embryonic stem cells. FASEB J. 2001;15:995-1005.

208. Minchinton, AI and Tannock, IF. Drug penetration in solid tumours. Nat Rev Cancer. 2006;6:583-92.

209. Jain, RK. Barriers to drug delivery in solid tumors. Sci Am. 1994;271:58-65.

210. Tunggal, J, Wartenberg, M, Paulsson, M and Smyth, N. Expression of the nidogen-binding site of the laminin gamma1 chain disturbs basement membrane formation and maintenance in F9 embryoid bodies. J Cell Sci. 2003;116:803-12.

211. Thurber, GM and Wittrup, KD. Quantitative spatiotemporal analysis of antibody fragment diffusion and endocytic consumption in tumor spheroids. Cancer Res. 2008;68:3334-41.

212. Bain, G, Kitchens, D, Yao, M, Huettner, JE and Gottlieb, DI. Embryonic stem cells express neuronal properties in vitro. Dev Biol. 1995;168:342-57.

213. Theodosiou, M, Laudet, V and Schubert, M. From carrot to clinic: an overview of the retinoic acid signaling pathway. Cell Mol Life Sci.

214. Ashe, HL and Briscoe, J. The interpretation of morphogen gradients. Development. 2006;133:385-94.

215. Dessaud, E, McMahon, AP and Briscoe, J. Pattern formation in the vertebrate neural tube: a sonic hedgehog morphogen-regulated transcriptional network. Development. 2008;135:2489-503.

216. Wobus, AM and Boheler, KR. Embryonic stem cells: prospects for developmental biology and cell therapy. Physiol Rev. 2005;85:635-78.

217. Keller, G. Embryonic stem cell differentiation: emergence of a new era in biology and medicine. Genes Dev. 2005;19:1129-55.

218. Gorba, T and Allsopp, TE. Pharmacological potential of embryonic stem cells. Pharmacol Res. 2003;47:269-78.

219. Hwang, YS, Polak, JM and Mantalaris, A. In vitro direct chondrogenesis of murine embryonic stem cells by bypassing embryoid body formation. Stem Cells Dev. 2008;17:971-8.

220. Schuldiner, M, Yanuka, O, Itskovitz-Eldor, J, Melton, DA and Benvenisty, N. Effects of eight growth factors on the differentiation of cells derived from human embryonic stem cells. Proc Natl Acad Sci U S A. 2000;97:11307-12.

221. Ivascu, A and Kubbies, M. Diversity of cell-mediated adhesions in breast cancer spheroids. Int J Oncol. 2007;31:1403-13.

222. Davies Cde, L, Berk, DA, Pluen, A and Jain, RK. Comparison of IgG diffusion and extracellular matrix composition in rhabdomyosarcomas grown in mice versus in vitro as spheroids reveals the role of host stromal cells. Br J Cancer. 2002;86:1639-44.

223. Carpenedo, RL, Bratt-Leal, AM, Marklein, RA, Seaman, SA, Bowen, NJ, McDonald, JF and McDevitt, TC. Homogeneous and organized differentiation within embryoid bodies induced by microsphere-mediated delivery of small molecules. Biomaterials. 2009;30:2507-15.

224. Ferreira, L, Squier, T, Park, H, Choe, H, Kohane, DS and Langer, R. Human embryoid bodies containing nano- and microparticulate delivery vehicles. Advanced Materials. 2008;20:2285-2291.

225. Falconnet, D, Csucs, G, Grandin, HM and Textor, M. Surface engineering approaches to micropattern surfaces for cell-based assays. Biomaterials. 2006;27:3044-63.

226. Hui, EE and Bhatia, SN. Microscale control of cell contact and spacing via three-component surface patterning. Langmuir. 2007;23:4103-7.

227. Kane, RS, Takayama, S, Ostuni, E, Ingber, DE and Whitesides, GM. Patterning proteins and cells using soft lithography. Biomaterials. 1999;20:2363-76.

228. Li, N, Tourovskaia, A and Folch, A. Biology on a chip: microfabrication for studying the behavior of cultured cells. Crit Rev Biomed Eng. 2003;31:423-88.

229. Khademhosseini, A, Ferreira, L, Blumling, J, 3rd, Yeh, J, Karp, JM, Fukuda, J and Langer, R. Co-culture of human embryonic stem cells with murine embryonic fibroblasts on microwell-patterned substrates. Biomaterials. 2006;27:5968-77.

230. Khademhosseini, A, Suh, KY, Yang, JM, Eng, G, Yeh, J, Levenberg, S and Langer, R. Layer-by-layer deposition of hyaluronic acid and poly-L-lysine for patterned cell co-cultures. Biomaterials. 2004;25:3583-92.

231. Bhatia, SN, Balis, UJ, Yarmush, ML and Toner, M. Microfabrication of hepatocyte/fibroblast co-cultures: role of homotypic cell interactions. Biotechnology Progress. 1998;14:378-87.

232. Bhatia, SN, Balis, UJ, Yarmush, ML and Toner, M. Probing heterotypic cell interactions: hepatocyte function in microfabricated co-cultures. Journal of Biomaterials Science. Polymer Edition. 1998;9:1137-60.

233. Jinno, S, Moeller, HC, Chen, CL, Rajalingam, B, Chung, BG, Dokmeci, MR and Khademhosseini, A. Microfabricated multilayer parylene-C stencils for the generation of patterned dynamic co-cultures. J Biomed Mater Res A. 2008;86:278-88.

234. Lee, LH, Peerani, R, Ungrin, M, Joshi, C, Kumacheva, E and Zandstra, P. Micropatterning of human embryonic stem cells dissects the mesoderm and endoderm lineages. Stem Cell Res. 2009;2:155-62.

235. Peerani, R, Rao, BM, Bauwens, C, Yin, T, Wood, GA, Nagy, A, Kumacheva, E and Zandstra, PW. Niche-mediated control of human embryonic stem cell self-renewal and differentiation. EMBO J. 2007;26:4744-55.

236. Anderson, DG, Levenberg, S and Langer, R. Nanoliter-scale synthesis of arrayed biomaterials and application to human embryonic stem cells. Nature Biotechnology. 2004;22:863-6.

237. Flaim, CJ, Chien, S and Bhatia, SN. An extracellular matrix microarray for probing cellular differentiation. Nature Methods. 2005;2:119-25.

238. Chin, VI, Taupin, P, Sanga, S, Scheel, J, Gage, FH and Bhatia, SN. Microfabricated platform for studying stem cell fates. Biotechnology and Bioengineering. 2004;88:399-415.

239. Kim, L, Vahey, MD, Lee, HY and Voldman, J. Microfluidic arrays for logarithmically perfused embryonic stem cell culture. Lab on a Chip. 2006;6:394-406.

240. Yamamoto, K, Sokabe, T, Watabe, T, Miyazono, K, Yamashita, JK, Obi, S, Ohura, N, Matsushita, A, Kamiya, A and Ando, J. Fluid shear stress induces differentiation of Flk-1-positive embryonic stem cells into vascular endothelial cells in vitro. American Journal of Physiology. Heart and Circulatory Physiology. 2005;288:H1915-24.

241. Chung, BG, Flanagan, LA, Rhee, SW, Schwartz, PH, Lee, AP, Monuki, ES and Jeon, NL. Human neural stem cell growth and differentiation in a gradient-generating microfluidic device. Lab on a Chip. 2005;5:401-6.

242. McDonald, JC, Duffy, DC, Anderson, JR, Chiu, DT, Wu, H, Schueller, OJ and Whitesides, GM. Fabrication of microfluidic systems in poly(dimethylsiloxane). Electrophoresis. 2000;21:27-40.

243. Sia, SK and Whitesides, GM. Microfluidic devices fabricated in poly(dimethylsiloxane) for biological studies. Electrophoresis. 2003;24:3563-76.

244. Takayama, S, Ostuni, E, LeDuc, P, Naruse, K, Ingber, DE and Whitesides, GM. Selective chemical treatment of cellular microdomains using multiple laminar streams. Chemical Biology. 2003;10:123-30.

245. Takayama, S, Ostuni, E, LeDuc, P, Naruse, K, Ingber, DE and Whitesides, GM. Subcellular positioning of small molecules. Nature. 2001;411:1016.

246. Gerecht-Nir, S, Cohen, S and Itskovitz-Eldor, J. Bioreactor cultivation enhances the efficiency of human embryoid body (hEB) formation and differentiation. Biotechnology and Bioengineering. 2004;86:493-502.

247. Magyar, JP, Nemir, M, Ehler, E, Suter, N, Perriard, JC and Eppenberger, HM. Mass production of embryoid bodies in microbeads. Annals of the New York Academy of Sciences. 2001;944:135-43.

248. Maguire, T, Novik, E, Schloss, R and Yarmush, M. Alginate-PLL microencapsulation: effect on the differentiation of embryonic stem cells into hepatocytes. Biotechnology and Bioengineering. 2006;93:581-91.

249. Desai, MP, Labhasetwar, V, Amidon, GL and Levy, RJ. Gastrointestinal uptake of biodegradable microparticles: effect of particle size. Pharm Res. 1996;13:1838-45.

250. Desai, MP, Labhasetwar, V, Walter, E, Levy, RJ and Amidon, GL. The mechanism of uptake of biodegradable microparticles in Caco-2 cells is size dependent. Pharm Res. 1997;14:1568-73.

251. Sung, HJ, Meredith, C, Johnson, C and Galis, ZS. The effect of scaffold degradation rate on three-dimensional cell growth and angiogenesis. Biomaterials. 2004;25:5735-42.

252. Battista, S, Guarnieri, D, Borselli, C, Zeppetelli, S, Borzacchiello, A, Mayol, L, Gerbasio, D, Keene, DR, Ambrosio, L and Netti, PA. The effect of matrix composition of 3D constructs on embryonic stem cell differentiation. Biomaterials. 2005;26:6194-207.

253. Ding, S and Schultz, PG. A role for chemistry in stem cell biology. Nat Biotechnol. 2004;22:833-40.

254. Bratt-Leal, AM, Carpenedo, RL and McDevitt, TC. Engineering the embryoid body microenvironment to direct embryonic stem cell differentiation. Biotechnol Prog. 2008;in press:

255. Brennan, J, Lu, CC, Norris, DP, Rodriguez, TA, Beddington, RS and Robertson, EJ. Nodal signalling in the epiblast patterns the early mouse embryo. Nature. 2001;411:965-9.

256. Niederreither, K, Vermot, J, Schuhbaur, B, Chambon, P and Dolle, P. Retinoic acid synthesis and hindbrain patterning in the mouse embryo. Development. 2000;127:75-85.

257. Chiang, C, Litingtung, Y, Lee, E, Young, KE, Corden, JL, Westphal, H and Beachy, PA. Cyclopia and defective axial patterning in mice lacking Sonic hedgehog gene function. Nature. 1996;383:407-13.

258. Winnier, G, Blessing, M, Labosky, PA and Hogan, BL. Bone morphogenetic protein-4 is required for mesoderm formation and patterning in the mouse. Genes Dev. 1995;9:2105-16.

259. Richardson, TP, Peters, MC, Ennett, AB and Mooney, DJ. Polymeric system for dual growth factor delivery. Nat Biotechnol. 2001;19:1029-34.

260. Tusher, VG, Tibshirani, R and Chu, G. Significance analysis of microarrays applied to the ionizing radiation response. Proc Natl Acad Sci U S A. 2001;98:5116-21.

261. Niederreither, K, Subbarayan, V, Dolle, P and Chambon, P. Embryonic retinoic acid synthesis is essential for early mouse post-implantation development. Nat Genet. 1999;21:444-8.

262. Pfister, S, Steiner, KA and Tam, PP. Gene expression pattern and progression of embryogenesis in the immediate post-implantation period of mouse development. Gene Expr Patterns. 2007;7:558-73.

263. Bielinska, M, Narita, N and Wilson, DB. Distinct roles for visceral endoderm during embryonic mouse development. Int J Dev Biol. 1999;43:183-205.

264. Dufort, D, Schwartz, L, Harpal, K and Rossant, J. The transcription factor HNF3beta is required in visceral endoderm for normal primitive streak morphogenesis. Development. 1998;125:3015-25.

265. Lawson, KA, Meneses, JJ and Pedersen, RA. Clonal analysis of epiblast fate during germ layer formation in the mouse embryo. Development. 1991;113:891-911.

266. Burdsal, CA, Damsky, CH and Pedersen, RA. The role of E-cadherin and integrins in mesoderm differentiation and migration at the mammalian primitive streak. Development. 1993;118:829-44.

267. Ciruna, BG, Schwartz, L, Harpal, K, Yamaguchi, TP and Rossant, J. Chimeric analysis of fibroblast growth factor receptor-1 (Fgfr1) function: a role for FGFR1 in morphogenetic movement through the primitive streak. Development. 1997;124:2829-41.

268. Palmieri, SL, Peter, W, Hess, H and Scholer, HR. Oct-4 transcription factor is differentially expressed in the mouse embryo during establishment of the first two

extraembryonic cell lineages involved in implantation. Dev Biol. 1994;166:259-67.

269. Rivera-Perez, JA and Magnuson, T. Primitive streak formation in mice is preceded by localized activation of Brachyury and Wnt3. Dev Biol. 2005;288:363-71.

270. Ishikawa, T, Yagyu, K and Seguchi, H. A scanning electron microscopic study of the surface morphology of visceral endoderm and ectoderm in postimplantation mouse embryos. J Electron Microsc (Tokyo). 1986;35:185-94.

271. Li, M, Pevny, L, Lovell-Badge, R and Smith, A. Generation of purified neural precursors from embryonic stem cells by lineage selection. Curr Biol. 1998;8:971-4.

272. O'Shea, KS. Neuronal differentiation of mouse embryonic stem cells: lineage selection and forced differentiation paradigms. Blood Cells Mol Dis. 2001;27:705-12.

273. Quinn, G, Ochiya, T, Terada, M and Yoshida, T. Mouse flt-1 promoter directs endothelial-specific expression in the embyroid body model of embryogenesis. Biochem Biophys Res Commun. 2000;276:1089-99.

274. White, RJ, Nie, Q, Lander, AD and Schilling, TF. Complex regulation of cyp26a1 creates a robust retinoic acid gradient in the zebrafish embryo. PLoS Biol. 2007;5:e304.

275. Vallier, L, Reynolds, D and Pedersen, RA. Nodal inhibits differentiation of human embryonic stem cells along the neuroectodermal default pathway. Dev Biol. 2004;275:403-21.

276. Cao, Z, Flanders, KC, Bertolette, D, Lyakh, LA, Wurthner, JU, Parks, WT, Letterio, JJ, Ruscetti, FW and Roberts, AB. Levels of phospho-Smad2/3 are sensors of the interplay between effects of TGF-beta and retinoic acid on monocytic and granulocytic differentiation of HL-60 cells. Blood. 2003;101:498-507.

277. Pendaries, V, Verrecchia, F, Michel, S and Mauviel, A. Retinoic acid receptors interfere with the TGF-beta/Smad signaling pathway in a ligand-specific manner. Oncogene. 2003;22:8212-20.

278. Toh, WS, Yang, Z, Heng, BC and Cao, T. Differentiation of human embryonic stem cells toward the chondrogenic lineage. Methods Mol Biol. 2007;407:333-49.

279. Adelman, CA, Chattopadhyay, S and Bieker, JJ. The BMP/BMPR/Smad pathway directs expression of the erythroid-specific EKLF and GATA1 transcription factors during embryoid body differentiation in serum-free media. Development. 2002;129:539-49.

280. Tran, TH, Wang, X, Browne, C, Zhang, Y, Schinke, M, Izumo, S and Burcin, M. Wnt3a-induced mesoderm formation and cardiomyogenesis in human embryonic stem cells. Stem Cells. 2009;27:1869-78.

281. Takahashi, T, Lord, B, Schulze, PC, Fryer, RM, Sarang, SS, Gullans, SR and Lee, RT. Ascorbic acid enhances differentiation of embryonic stem cells into cardiac myocytes. Circulation. 2003;107:1912-6.

282. Kong, XB and Zhang, C. Dickkopf (Dkk) 1 promotes the differentiation of mouse embryonic stem cells toward neuroectoderm. In Vitro Cell Dev Biol Anim. 2009;45:185-93.

283. Frank-Kamenetsky, M, Zhang, XM, Bottega, S, Guicherit, O, Wichterle, H, Dudek, H, Bumcrot, D, Wang, FY, Jones, S, Shulok, J, Rubin, LL and Porter, JA. Small-molecule modulators of Hedgehog signaling: identification and characterization of Smoothened agonists and antagonists. J Biol. 2002;1:10.

284. Wichterle, H, Lieberam, I, Porter, JA and Jessell, TM. Directed differentiation of embryonic stem cells into motor neurons. Cell. 2002;110:385-97.

285. Konuma, N, Wakabayashi, K, Matsumoto, T, Kusumi, Y, Masuko, T, Iribe, Y, Mitsumata, M, Okano, H, Kusafuka, T and Mugishima, H. Mouse Embryonic Stem Cells Give Rise to Gut-like Morphogenesis, Including Intestinal Stem Cells, in the Embryoid Body Model. Stem Cells Dev. 2008;

286. Arceci, RJ, King, AA, Simon, MC, Orkin, SH and Wilson, DB. Mouse GATA-4: a retinoic acid-inducible GATA-binding transcription factor expressed in endodermally derived tissues and heart. Mol Cell Biol. 1993;13:2235-46.

287. Jacobsen, CM, Narita, N, Bielinska, M, Syder, AJ, Gordon, JI and Wilson, DB. Genetic mosaic analysis reveals that GATA-4 is required for proper differentiation of mouse gastric epithelium. Dev Biol. 2002;241:34-46.

288. Lobo, MV, Arenas, MI, Alonso, FJ, Gomez, G, Bazan, E, Paino, CL, Fernandez, E, Fraile, B, Paniagua, R, Moyano, A and Caso, E. Nestin, a neuroectodermal stem cell marker molecule, is expressed in Leydig cells of the human testis and in some specific cell types from human testicular tumours. Cell Tissue Res. 2004;316:369-76.

289. Wiese, C, Rolletschek, A, Kania, G, Blyszczuk, P, Tarasov, KV, Tarasova, Y, Wersto, RP, Boheler, KR and Wobus, AM. Nestin expression--a property of multi-lineage progenitor cells? Cell Mol Life Sci. 2004;61:2510-22.

APPENDIX A

DERIVATION OF SPHEROID DIFFUSION EQUATIONS

The diffusion of solutes into spheroids is governed by Fick's second law:

$$\frac{\partial C_{ext}(r)}{\partial t} = D_1 \nabla^2 C_{ext}$$
$$\frac{\partial C_{\text{int}}(r)}{\partial t} = D_2 \nabla^2 C_{int} + q$$

where C_{ext} and C_{int} are the concentration outside and inside the spheroid, respectively, D_1 and D_2 are the respective diffusion coefficients, ∇^2 is the Laplacian operator, and q is the rate of consumption (q<0). Assuming spherical symmetry, constant consumption and steady state, this system of equations becomes:

$$\frac{d^2 C_{ext}(r)}{dt^2} + \frac{2}{r}\frac{dC_{ext}(r)}{dt} = 0$$
$$\frac{d^2 C_{\text{int}}(r)}{dt^2} + \frac{2}{r}\frac{dC_{\text{int}}(r)}{dt} - Q = 0$$

where $Q = -q/D_2$. Integration of these equations twice yields:

$$C_{ext}(r) = \frac{C_1}{r} + C_2$$
$$C_{\text{int}}(r) = \frac{C_3}{r} + C_4 + \frac{1}{6}Qr^2$$

The constants are solved for by applying boundary conditions. Two cases are described; in the first case, diffusion throughout the spheroid occurs, and in the second case, depletion occurs within the interior of the spheroid.

Case 1. No depletion

As r approaches ∞, $C_{ext}=C\infty$

For a spheroid of radius R:

$$Cext(R) = C\,\mathrm{int}(R)$$
$$\frac{dC_{ext}(r)}{dr_{r=R}} = \frac{dC_{\mathrm{int}}(r)}{dr_{r=R}}$$

$0 \le C_{int}(0) < \infty$ (that is, the concentration at the spheroid center is finite and non-negative).

These four boundary conditions allow the constants to be solved for:

$$C_{ext}(r) = C_{\infty} - \frac{QR^3}{3r}$$
$$C_{\mathrm{int}}(r) = C_{\infty} - \frac{QR^2}{2} + \frac{1}{6}Qr^2$$

The final boundary condition ($0 \le C_{int}(0) < \infty$) is only true when

$$C_{\infty} \ge \frac{QR^2}{2}$$
or,
$$R \le \sqrt{\frac{2C_{\infty}}{Q}} \equiv R_0$$

For $R>R_0$, depletion within the spheroid occurs, and the second case applies.

Case 2. Depletion within the spheroid.

Let R_1 equal the radius of the depletion zone.

As r approaches ∞, $C_{ext}=C\infty$

For a spheroid of radius R:

$$Cext(R) = C\,\mathrm{int}(R)$$
$$\frac{dC_{ext}(r)}{dr_{r=R}} = \frac{dC_{\mathrm{int}}(r)}{dr_{r=R}}$$

$$C_{\mathrm{int}}(R_1) = \frac{dC_{\mathrm{int}}(r)}{dr_{r=R}} = 0$$

$Q=0$ and $C_{int}(r)=0$ for $r \leq R_1$

This set of boundary conditions allows the integration constants to be solved for and yields:

$$C_{ext}(r) = C_{\infty} + \frac{Q(R^2 - {R_0}^2) - R^3}{3r}$$
$$C_{\mathrm{int}}(r) = C_{\infty} + \frac{Q(R^2 - {R_0}^2)^{3/2}}{3r} - \frac{1}{2}QR^2 + \frac{1}{6}Qr^2$$